PHOTO-DEFINABLE DIELECTRICS WITH IMPROVED LITHOGRAPHIC, MECHANICAL, AND ELECTRICAL PROPERTIES

A Dissertation
Presented to
The Academic Faculty

by

Brennen Karl Mueller

In Partial Fulfillment
of the Requirements for the Degree
Doctor of Philosophy in the
School of Chemical and Biomolecular Engineering

Georgia Institute of Technology
May 2015

PHOTO-DEFINABLE DIELECTRICS WITH IMPROVED LITHOGRAPHIC, MECHANICAL, AND ELECTRICAL PROPERTIES

Approved by:

Dr. Paul A. Kohl, Advisor
School of Chemical and Biomolecular Engineering
Georgia Institute of Technology

Dr. Dennis W. Hess
School of Chemical and Biomolecular Engineering
Georgia Institute of Technology

Dr. Muhannad S. Bakir
School of Electrical and Computer Engineering
Georgia Institute of Technology

Dr. Pete J. Ludovice
School of Chemical and Biomolecular Engineering
Georgia Institute of Technology

Dr. David G. Bucknall
School of Materials Science and Engineering
Georgia Institute of Technology

Dr. J. Carson Meredith
School of Chemical and Biomolecular Engineering
Georgia Institute of Technology

Date Approved: December 5, 2014

ACKNOWLEDGMENTS

It is with incredible support from mentors, colleagues, labmates, friends, and family that this work has been undertaken. These people have my deepest gratitude and respect. Specifically, I would like to Prof. Paul Kohl for his guidance, encouragement, and insights. I am indebted to him for the knowledge and skills I have gained under his advisement.

I also thank those at Promerus LLC for supporting these projects through funding, materials, and very helpful discussions. In particular, Dr. Edmund Elce was pivotal for his help in pathfinding and his willingness to synthesize a library of materials.

Thank you to the Intel Foundation and Semiconductor Research Corporation Education Alliance for support through a fellowship. Thank you especially to Shirley Maier, Lee Ann Clewell, and MaryLisabeth Rich. Their continual support has undoubtedly impacted my future as a researcher.

At Georgia Tech I am grateful to have had a wonderful lab to brighten up the days in the Bunger Henry cave. Thank you Dr. Nathan Fritz, Dr. Mehrsa Raeis-Zadeh, Dr. Yu-Chun Chen, Dr. Rajarshi Saha, Dr. Sarah Kim, Dr. Johanna Stark, Erdal Uzunlar, John Ahlfield, and Dami Phillips for letting me distract you with crazy ideas and nonsense. Thank you Jared Schwartz for doing the same, but also for going through the ups and downs of this research with me. Jared's contributions to this work cannot be overstated, and I am lucky to have had such a great research partner.

While completing this work, I have had the pleasure of mentoring several incredibly talented undergraduate researchers. Thank you, in chronological order, Angelica Grillo, Christina Bins, Emily Korby, Sang Lee, Oluwatobi Fatunmbi, Jodie Simkoff, Ben Schmidt, Zachary Pritchard, Helen Li, Jane Ericksen, Jonathan Tuck, and

Alexis Sutlief. I hope they all achieve great success even if I could not convince them all to attend graduate school.

I would not have attended Georgia Tech if my undergraduate advisor had not pushed me to do so. I would like to thank Prof. C. Grant Willson for his encouragement to pursue a Ph.D. and his continued collaborations. Also from undergraduate research, I thank Dr. Jeffrey Strahan and Dr. Chris Bates for teaching me proper research methods that were enabling to many aspects of this work. Thank you Dr. William Bell and Colin Hayes for continuing to take my questions about chemistry and for being wonderful collaborators.

TABLE OF CONTENTS

LIST OF TABLES

LIST OF FIGURES

NOMENCLATURE

AC	alternating current
AIBN	azobisisobutyronitrile
ATR	attenuated total reflection
BCB	benzocyclobutene
BGA	ball grid array
BPADGE	bisphenol-A diglycidyl ether
ButylNB	butyl norbornene
CA	chemical amplification/chemically amplified
CBANB	carboxylic acid norbornene
CMP	chemical-mechanical polish
CPTX	1-chloro-4-propoxy-9H-thioxanthene-9-one
CPU	central processing unit
CTE	coefficient of thermal expansion
DNQ	diazonaphthoquionone
DSC	differential scanning calorimetry
DUV	deep ultraviolet
DVS-bis-BCB	divinylsiloxane bisbenzocyclobutene
FTIR	Fourier transfer infrared spectroscopy
GPC	gel permeation chromatography
HEMA	2-hydroxyethyl methacrylate
HFANB	hexafluoroisopropanol norbornene
HMDS	hexamethyl disilazane

IC	integrated circuit
ICA	indene carboxylic acid
MEMS	microelectromechanical systems
NMR	nuclear magnetic resonance spectroscopy
PAC	photoactive compound
PAG	photoacid generator
PBOCST	poly(tert-butoxycarbonyl styrene)
PCB	printed circuit board
PEB	post-exposure bake
PE	pentaerythritol
PEEO	pentaerythritol ethoxylate
PEGME	poly(ethylene glycol) dimethyl ether
PGMEA	propylene glycol monomethyl ether acetate
PHOST	poly(hydroxystyrene)
PI	polyimide
PNB	polynorbornene
QCM	quartz crystal microbalance
RAM	random access memory
RDL	redistribution layer
SAC	tin-gold-copper solder
SEM	scanning electron microscopy/micrograph
TBE	tert-butyl ester
TBENB	tert-butyl ester norbornene
TBMA	tert-butyl methacrylate
TBOC	tert-butoxycarbonyl

TGA	thermogravimetric analysis
THF	tetrahydrofuran
TMAH	tetramethylammonium hydroxide
TMP	trimethylolpropane
TMPEO	trimethylolpropane ethoxylate
TMPTGE	trimethylolpropane triglycidyl ether
TPV	through-package via
UV	ultraviolet
UV-Vis	ultraviolet-visible spectroscopy

LIST OF SYMBOLS

A	area
A_0	original peak area
A_n	peak area at time n
$A(h_c)$	projected area at contact depth
c_0	original concentration
c_n	concentration at time n
C	capacitance
C_e	edge capacitance
d_f	film thickness
d_s	substrate thickness
D_0	maximum dose for no solubility change
D_{100}	minimum dose for full solubility change
E_f	elastic modulus of film
E_i	elastic modulus of indenter tip
E_r	film reduced modulus
E_s	elastic modulus of substrate
f	frequency
f_o	resonant frequency
h_c	contact depth
h_{max}	maximum indent depth
H	hardness
k	reaction rate constant

m	mass
m_0	original film mass
m_t	swollen film mass
M_c	molecular weight between cross-links
M_n	number-average molecular weight
M_w	weight-average molecular weight
n	index of refraction
NA	numerical aperture
p	perimeter
P_{max}	maximum indent pressure
r	minimum feature size
R	change in radius of curvature
R_1	bare substrate radius of curvature
R_2	coated substrate radius of curvature
S	stiffness
SR_t	swelling ratio
t	time
T	temperature
T_d	decomposition temperature
T_g	glass transition temperature
$\alpha_{f,xy}$	in-plane CTE of film
$\alpha_{f,z}$	through-plane CTE of film
$\alpha_{s,xy}$	in-plane CTE of substrate
β	indentation geometrical constant
γ	contrast

δ	impedance vector angle
ε_r	relative permittivity
ε_r'	dielectric constant, real relative permittivity
ε_r''	dielectric loss, imaginary relative permittivity
ϵ	conversion
ζ	Oliver-Pharr geometrical constant
λ	wavelength
μ_q	shear modulus of quartz
ν_i	Poisson's ratio of indenter tip
ν_f	Poisson's ratio of film
ν_s	Poisson's ratio of substrate
ρ_q	density of quartz
σ	stress

SUMMARY

Permanent dielectric materials are integral to the fabrication of microelectronic devices and packaging. Dielectrics are used throughout devices to electrically and mechanically isolate conductive components. As such, they are required to have low electrical permittivity and robust mechanical properties. For packaging applications, dielectrics can be directly photo-definable. Dielectrics need to have excellent lithographic properties. These properties are pivotal for enabling high yield and low cost fabrication of reliable, energy efficient devices. The aim of this work was to develop new positive tone dielectrics which have improved or application-specific lithographic, mechanical, and electrical properties. To this end, several new dielectric polymers and chemistries were evaluated and characterized.

Initially, it was desired to develop a positive tone, polynorbornene (PNB) dielectric that utilizes diazonaphthoquinone (DNQ) photochemistry. Cross-linking was achieved with epoxy cross-linkers during a thermal cure. Several DNQ-containing compounds were evaluated, but only one had good miscibility with PNB. The dissolution characteristics of PNB were measured with respect to polymer composition, DNQ loading, and cross-linker loading. PNB films exhibited unique dissolution properties, and these measurements allowed for an optimum formulation to be developed. A formulation with 20 pphr DNQ and 10 pphr epoxy cross-linker had sufficient inhibition in unexposed regions and fast dissolution in exposed regions. The resulting dielectric was the first positive tone, DNQ-based PNB dielectric.

After achieving photo-definability, the cross-linking of the cured dielectric was evaluated by characterizing the mechanical properties. It was discovered that DNQ acted as a cross-linker in these films, and this insight was key to achieving good curing of the dielectric. Several experiments were performed to support this conclusions, and the

reaction kinetics of this cross-linking reaction were evaluated. This effort produced a functional, positive tone dielectric with a sensitivity of 408 mJ cm^{-2} and contrast of 2.3. The modulus was 2.0 to 2.6 GPa and the dielectric constant of 3.7 to 3.9, depending on the curing conditions.

The DNQ cross-linking results led to the investigation of other cross-linking chemistries for positive tone dielectrics. A chemically amplified (CA) photochemistry was utilized along with a Fischer esterification cross-linking reaction. Patterning and cross-linking were demonstrated with a methacrylate polymer. Successful positive tone lithography was demonstrated at a high sensitivity of 32.4 mJ cm^{-2} and contrast of 5.2. Cross-linking was achieved at 120°C as shown by residual stress and solubility measurements.

The CA photochemistry and Fischer esterification cross-linking were also demonstrated using a PNB dielectric, which was shown to have improved lithographic properties: a sensitivity of 8.09 mJ cm^{-2} and contrast of $\geq$ 14.2. Work was performed to evaluate the effect of the polymer composition on the mechanical and electrical properties. A polymer with 60 mol% hexafluoroisopropanol norbornene and 40 mol% tert-butyl ester norbornene exhibited a dielectric constant of 2.78, which is lower than existing positive tone dielectrics. It also outperformed existing dielectrics in several other categories, including dark erosion, volume change, cure temperature, and in-plane coefficient of thermal expansion. However, a limitation of this dielectric was cracking in thick films.

The final study was to improve the mechanical properties of this CA PNB dielectric specifically to enable 5 μm thick films. First, a terpolymer was tested that included a non-functional third monomer. The dielectric constant increased to 3.48 with 24 mol% of the third monomer. Second, low molecular weight additives were used to lower the modulus. Only one of the five tested additives enabled high quality, thick films. This additive did not significantly affect the dielectric constant at low loadings.

An optimized formulation was made, and processing parameters were studied. The additive decreased the lithographic properties, lowering the sensitivity to 175 mJ cm^{-2} and lowering the contrast to 4.36.

In all, this work produced three functional dielectrics with positive tone photo-definability and good lithographic properties. Each dielectric can serve a variety of purposes in microelectronics packaging.

CHAPTER 1

LOW-K DIELECTRICS FOR MICROELECTRONICS PACKAGING

The interaction between humans and electronics continues to evolve. In one respect, the continued increase in computing power enables ever more complex calculations and modeling to be performed. With new methods of analyzing and calculating data, many fields have seen dramatic shifts, not the least of which is scientific research. However, shear computing power has not been the only factor to change how humans interact with technology. Shrinking form factors, increased and diversified functionality, and lower power consumption have revolutionized how, when, where, and what kinds of data are collected.

1.1 Need for Advanced Microelectronics Packaging

Microelectronics packaging is integral for connecting multiple discrete components on one electronic device. Individually or together, the capabilities of devices are not useful unless they can communicate with each other and the user. The field of microelectronics packaging encompasses these connections chip-to-chip, chip-to-package, and package-to-package, where the package could be defined as any secondary substrate or molding to which the active chips are connected. Figure 1.1 shows Intel's 4^{th} and 5^{th} generation Core chips mounted to their respective packages.[1] Here, the package is the printed circuit board (PCB) that routes the electrical connections from the IC on the front side to the back side where it can be connected to the motherboard. Since length scales at the system and package level are orders of magnitude larger than at the IC level, improvements here dramatically affect the size of devices.[2] These dimensions are important in the x- and y-directions (area) as well as the z-direction (thickness).

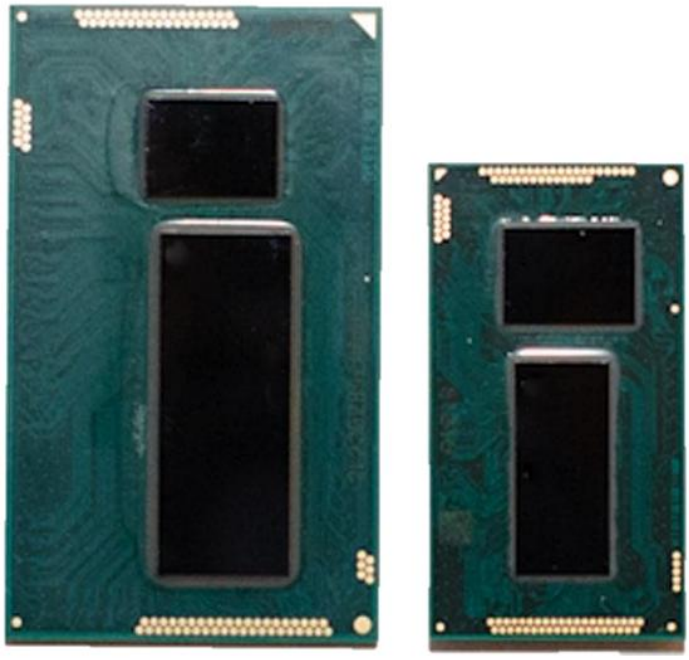

Figure 1.1: Evolution of Intel chip package from 4th (left) to 5th generation (right) © 2014 Intel Corporation. Used with permission [1]

The goal of packaging is to enable fast communication between active devices without adding size or cost. These associated costs come in many forms. First, smaller and denser wiring requires better lithographic equipment and materials. Second, denser wiring, and therefore smaller off-package connections are more expensive to test. This can be avoided by testing at a later stage in packaging with larger off-package connections. However, testing at a later stage introduces yield concerns, as it is also costly to package a chip and then determine it does not function. The packaging field considers a balance between cost, performance, and form factor. These design parameters must be evaluated for each new device.

1.2 Uses for Organic Low-k Dielectrics

Dielectric materials serve many vital roles in microelectronics packaging. These materials have low electrical permittivity and serve to separate conductive wiring. In this

role they prevent electrical cross-talk and losses between neighboring conductive traces.[3] Organic dielectrics are used in packaging applications because they are easily processed and often more cost-effective than inorganic dielectrics. These organic dielectrics are used in several places throughout the IC and packaging fabrication.

1.2.1 Stress Buffer

The coefficient of thermal expansion (CTE) and elastic modulus preclude the use of organic dielectrics in the interconnect stack on ICs. The high CTE of organic dielectrics can cause delamination of copper vias (Cu CTE = 17 ppm K^{-1}) and the modulus is not high enough to support the hard mask for pattern transfer (requires modulus of ~10 GPa). The last dielectric layer to be deposited on the IC, however, is a stress buffer meant to absorb stress so that the IC does not fail mechanically.[4], [5] Failures occur both in manufacturing and in operation from heating and cooling of the device. Since the device is composed of many materials with different CTEs, mechanical stresses build up and eventually plastically deform the materials. The specifics of this stress build up are covered in Chapter 2. The die-package interface is a region where large stresses can build up.[6] A layer termed the stress buffer is an organic dielectric layer deposited on the die that helps to absorb this stress. The stress buffer is also the layer that will accompany the fabrication of the metallization for contacting the packaging solder. At this level, the wiring pitch is important as it dictates how many electrical connections can be made to the package via solder bumps.

As seen in Figure 1.2, the stress buffer is composed of several layers.[4], [7] The previous metal/low-k dielectric layer is coated with a nitride as a passivation layer to prevent moisture or ionic particles from contaminating the interconnect stack.[7] The nitride is selectively removed above the metallization so that electrical contact can be made. Next, a dielectric layer is deposited and patterned, again opening a region for electrical contact. Metal is plated on top of this dielectric layer and subsequently

patterned to fabricate the traces. Another dielectric layer is then deposited and patterned. The under-bump metallization can be plated and patterned to form a landing pad for the solder ball. Finally, solder can be deposited, and the chip can be bonded to the packaging substrate with a solder ball grid array (BGA). There can be many variations of this process or the final structure. One useful variation is to selectively remove the nitride after depositing and patterning the dielectric. This lowers the number of processing steps but requires that the dielectric be resistant to the nitride etchant.

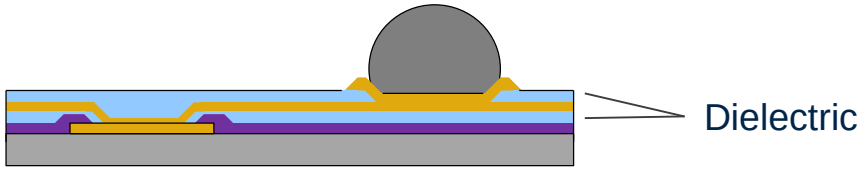

Figure 1.2: Stress buffer with two permanent dielectric layers (blue)

1.2.2 Ball Grid Arrays

BGAs are a critical technology for state-of-the-art packaging applications.[8] Previously, chips were connected to their packages via wire bonding. For wire bonding, connection pads were patterned on the top side of the silicon chip (i.e. side with transistors and interconnects). Gold wires were then attached in a serial process to connect the chip to the underlying substrate. Eventually, the length of these connections became limiting because of high RC delay, hindering device speed.[8] Additionally, connections were limited to the periphery of the silicon chip.

BGAs provide one solution to these problems. In the BGA scheme, solder connections are patterned on the package via photolithography. The silicon die is subsequently mounted with the top side facing the package so that the interconnect layer is aligned with these solder connections. The solder is reflowed to form an intimate electrical connection with both the package and the interconnect. This scheme has

several benefits over wire bonding. First, the solder is patterned in a bulk photolithographic process, so the speed at which bumps can be fabricated is higher than the serial wire bonding process. Second, more connections can be made to the package in a BGA scheme since these connections are not limited to the periphery. Finally, the BGA has shorter connections between the active die and the package, so RC delay is improved.

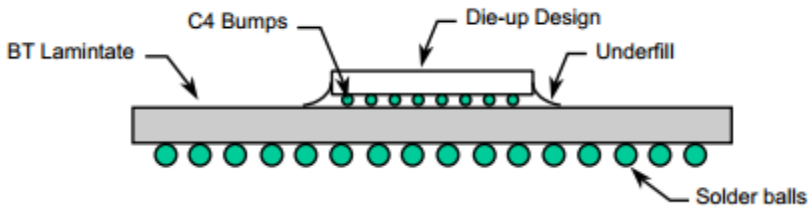

Figure 1.3: BGA package side view, © 2000, Intel Corporation. Used with permission[9]

The solder used to make electrical connections have high melting points, which has been a challenge for selecting dielectric materials that can survive the reflow and do not exhibit high residual stress after the thermal step. A popular Pb-free solder is a Sn-Au-Cu alloy, termed SAC.[10] The melting point for the solder is 217°C, and it is commonly reflowed around 265°C. This sets a critical temperature requirement for permanent dielectrics; dielectrics must be able to withstand this temperature excursion for solder reflow without degrading.

1.2.2 Redistribution/Fan Out

As was seen in Figure 1.1, the ICs are mounted on a PCB that has metal traces leading from the chip-to-package BGA to the backside of the package. Depending on the electronic device, the backside of the package will have a land grid array for mounting into a system board socket (e.g. LGA 1150), or the package may have a BGA for permanent mounting onto the system board. The metal traces that route the connections

from the chip to the subsequent board are considered a redistribution layer (RDL), redistributing the size and pitch of the connections.

This type of package usually begins as an epoxy/fiber glass composite core through which through-package vias (TPVs) are formed, commonly through laser ablation. Copper is plated inside the TPVs to form electrical connections from the front side of the package to the back. On both sides of the package, dielectric and metal layers are alternately deposited and patterned to form the RDL.[11] The connection arrays are patterned in a process similar to the stress layer/under-bump metallization process. The chip is finally aligned and placed on the package, and the solder is reflowed to bond them together.

1.3 Photosensitive Dielectrics

Two classes of permanent dielectrics exist: directly photosensitive and non-photosensitive. An advantage offered by non-photosensitive dielectrics is low electrical permittivity. The photosensitive compounds required for patterning are commonly polar and increase the permittivity. Non-photosensitive dielectrics are beneficial when paired with a low-permittivity substrate in high frequency applications. At high frequency operation, tanδ contributes to the electrical permittivity much more. This will be discussed in more detail in Chapter 2.

Photo-definability, on the other hand, is attractive from a fabrication perspective. For packaging applications, it can be desirable to use directly photo-definable dielectrics. The benefit of photosensitive dielectrics is the lower number of process steps, although the materials cost is often significantly higher.[7], [12] In comparison, non-photosensitive dielectrics often require many more processing steps. One processing scheme is given in Figure 1.4. In addition to the photoresist required for patterning non-photosensitive dielectrics, each process requires a dedicated tool that is a large capital cost.

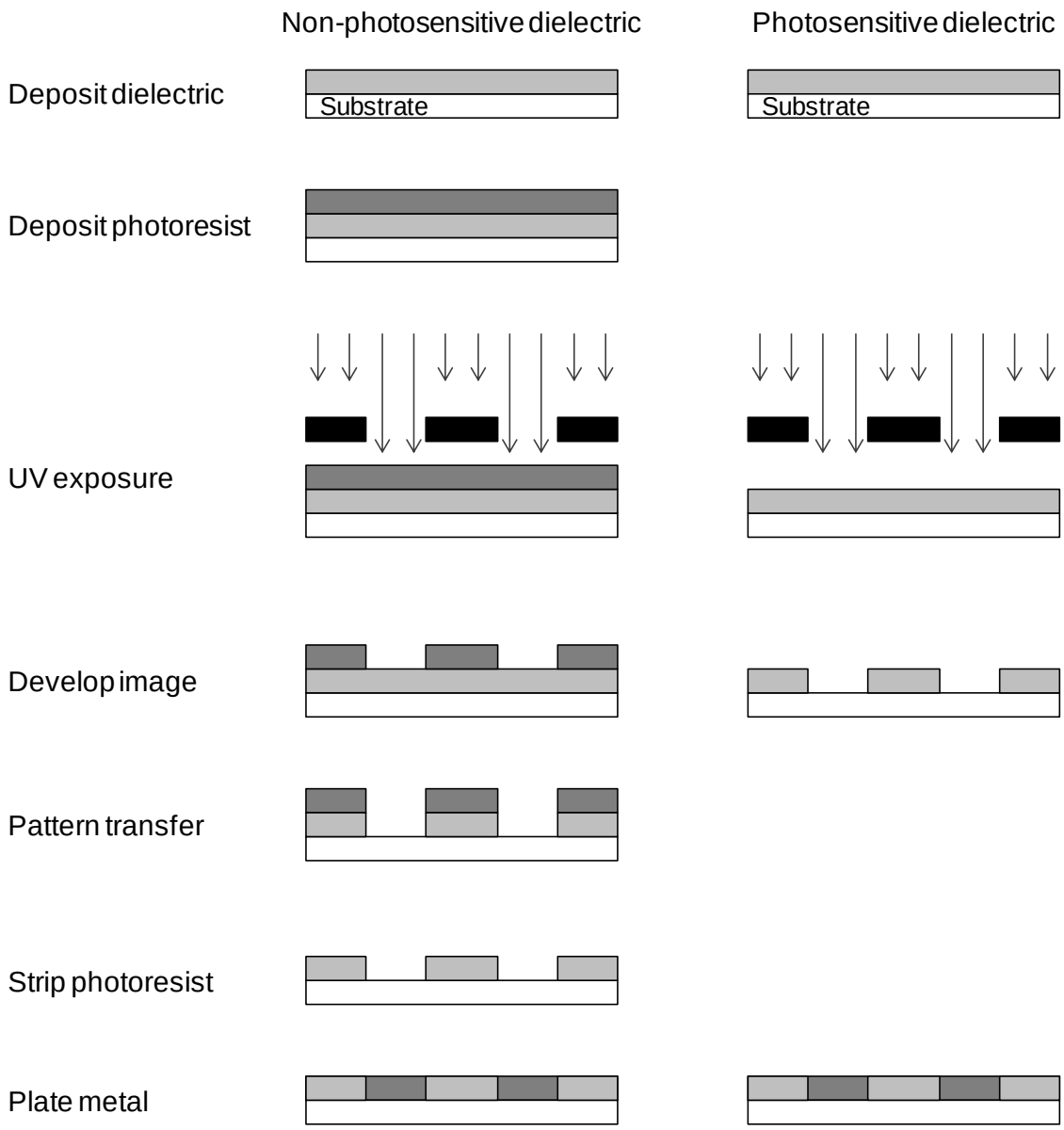

Figure 1.4: Fabrication process with non-photosensitive (left) and photosensitive dielectrics (right)

For non-photosenstive dielectrics, the processing starts with deposition of the dielectric material. Many dielectrics are spin coated, but others may be meniscus coated, laminated, or even vacuum deposited.[13], [14] After deposition of the dielectric, a photoresist is applied. This photoresist is taken through the photolithographic process, described later, to selectively remove portions of the resist and create a 3-D pattern. An

etching step is then required to transfer the pattern of the photoresist to the dielectric. This step can be harsh, requiring corrosive materials or plasma treatment., both of which can affect the material properties of the dielectric.[15], [16] Low etch resistance of the photoresist to the etchant is often a challenge.[17] Finally, the remaining photoresist is stripped from the dielectric surface, and copper is plated in the newly formed openings of the dielectric. This metallization will connect conductive traces below the dielectric to the traces in the subsequent layer.

For photosensitive dielectrics, this process is simpler than the photoresist-assisted process shown in Figure 1.4. Organic dielectric materials can be laminated, spin coated, or meniscus coated. No photoresist is required in this case, and the dielectric is patterned with the photolithographic process to selectively remove the regions in which the copper will be plated. Photo-definable dielectrics often require a thermal cure to impart good electrical and mechanical properties after photolithography. After the cure, the openings in the dielectric are plated with copper.

1.4 Photolithography

Photolithography has been used by the microelectronics industry to print small patterns to make functional devices.[18] Often, photo-definable materials are polymeric. Polymers can be spin coated to form transparent films, and their chemistry can easily be manipulated during synthesis for tunable properties. The basis of photolithography is that the solubility of a film can be changed via the exposure to radiation. Exposure through a photomask induces the solubility switch in the transparent regions of the mask. Depending on the tone of the photo-definable dielectric, exposure to UV light either increases solubility in developer (positive tone) or decreases solubility in developer (negative tone). Though the term ‘dielectric’ will be used to describe further photo-definable materials, photoresists are processed by the same methods. Photoresists are not incorporated in the final device.

1.4.1 Optical Considerations

Photolithographic exposure tools create radiation at a source, filter the radiation to a specific wavelength, and direct it toward the sample to be patterned. Historically, a Hg arc lamp has been used as the source because it is inexpensive and high intensity. G-line (436 nm) and i-line (365 nm) are commonly the wavelengths of choice due to their high intensities and the photochemistries used.[19] A Hg arc lamp produces these wavelengths, and its emission spectrum is shown in Figure 1.5.

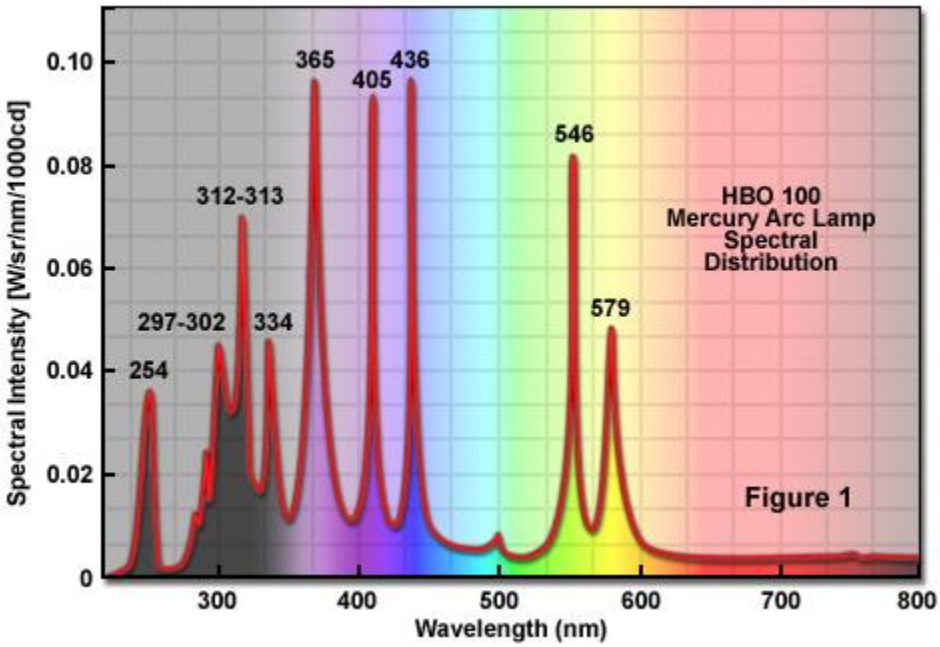

Figure 1.5: Emission spectrum of a Hg arc lamp. Image from www.zeiss.com/campus, ©Mike Davidson, FSU, Tallahassee[20]

The Rayleigh equation (Equation 1.1) describes the minimum feature size (r) that can be printed, where λ is the wavelength of light, NA is the numerical aperture, and k is a constant that depends on the photo-definable material.[21] This minimum size is proportional to the wavelength of light, so lower wavelengths are necessary for smaller features, keeping all else constant. At deep ultraviolet (DUV, 248 nm), the Hg arc lamp

was replaced with a KrF excimer laser because of its higher intensity at this wavelength. Most photosensitive dielectrics use photochemistries that are sensitive to i-line radiation.

$$r = \frac{k\lambda}{NA} \tag{1.1}$$

Three different methods can be used for the photolithographic exposure, each having issues and benefits. First, the photomask can be placed in contact with the dielectric, termed contact lithography, resulting in a one-to-one image of the photomask.[21], [22] In contact lithography, the repeated mechanical wear on the mask and films causes high defect rates, and masks have to be replaced often. Proximity lithography also produces a one-to-one image of the photomask, but the photomask is held slightly above the dielectric. The images printed in contact and proximity lithography are distorted by near-field (Fresnel) diffraction. An ideal intensity profile would be discontinuous, with the maximum intensity of light at any mask opening and zero intensity in all shaded regions. However, the diffraction of light results in an intensity profile similar to that in Figure 1.6. This can result in partial solubility conversion of the photo-definable dielectric, sloped sidewalls, or biased feature dimensions, which will be discussed later.

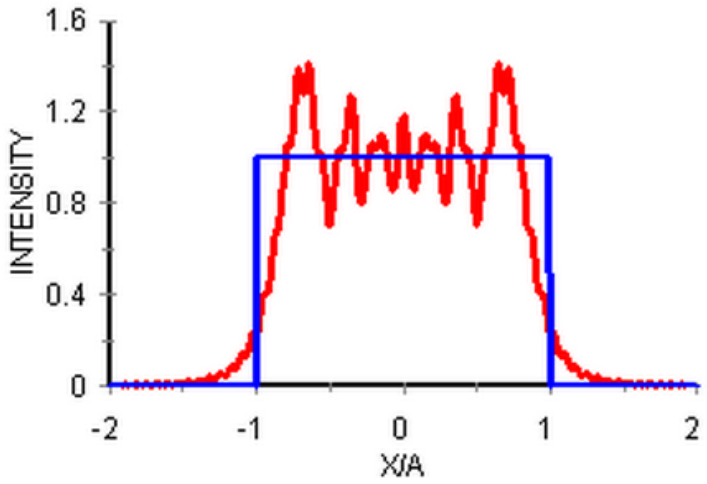

Figure 1.6: Spatial intensity profile under mask opening. Image from webtop.msstate.edu © Mississippi State University [23]

A third method, projection lithography puts the mask far away from the dielectric, but uses a lens to condition the far-field (Fraunhofer) diffracted image after passing through the mask. The projection system can also magnify the image so that feature sizes on the photomask are much smaller on the printed sample. Projection lithography is attractive to manufacturers due to its high quality patterns and low defect rates, but this is far more expensive than the other photolithography methods. Due to the cost sensitive nature of microelectronics packaging and the availability of exposure tools, contact and proximity lithography are often used for patterning permanent dielectrics.

1.4.2 Materials Processing

Photo-definable dielectrics can be deposited by a variety of methods. Spin coating uses a solvated polymer deposited at the center of a wafer, and the wafer is spun at speeds of 1000 to 5000 rpm to spread the liquid. During spinning, viscous and inertial forces of the fluid are balanced while the solvent evaporates, leaving a solid, thin film of uniform thickness.[24] To remove much of the residual solvent, the film is baked at a temperature below the boiling point of the solvent. This step is termed the “soft bake” or

"post-apply bake" and is typically 1-3 minutes at 80-150°C depending on the casting solvent. The bake should be performed at a temperature much lower than the boiling point of the casting solvent to prevent bubbling of the film. Both residual solvent and degradation of PACs can affect the lithographic properties of the film.[25] The soft bake temperature and time must be chosen to remove much of the solvent without prematurely degrading the PAC.

After the soft bake, the polymeric film is exposed through the photomask by one of the lithographic methods described previously. Photoactive compounds (PACs) in the film undergo a photoreaction during this step. Often, the exposure is all that is needed to shift the solubility, but some photochemistries require added energy after the exposure. For these chemistries, a post-exposure bake (PEB) is common. Finally, the film is immersed in or sprayed with developer solution that selectively dissolves either the exposed or unexposed regions. For photoresists, a pattern transfer step is required, typically by wet or dry etching, to pattern the underlying layer of interest. After the pattern transfer, the photoresist is stripped.

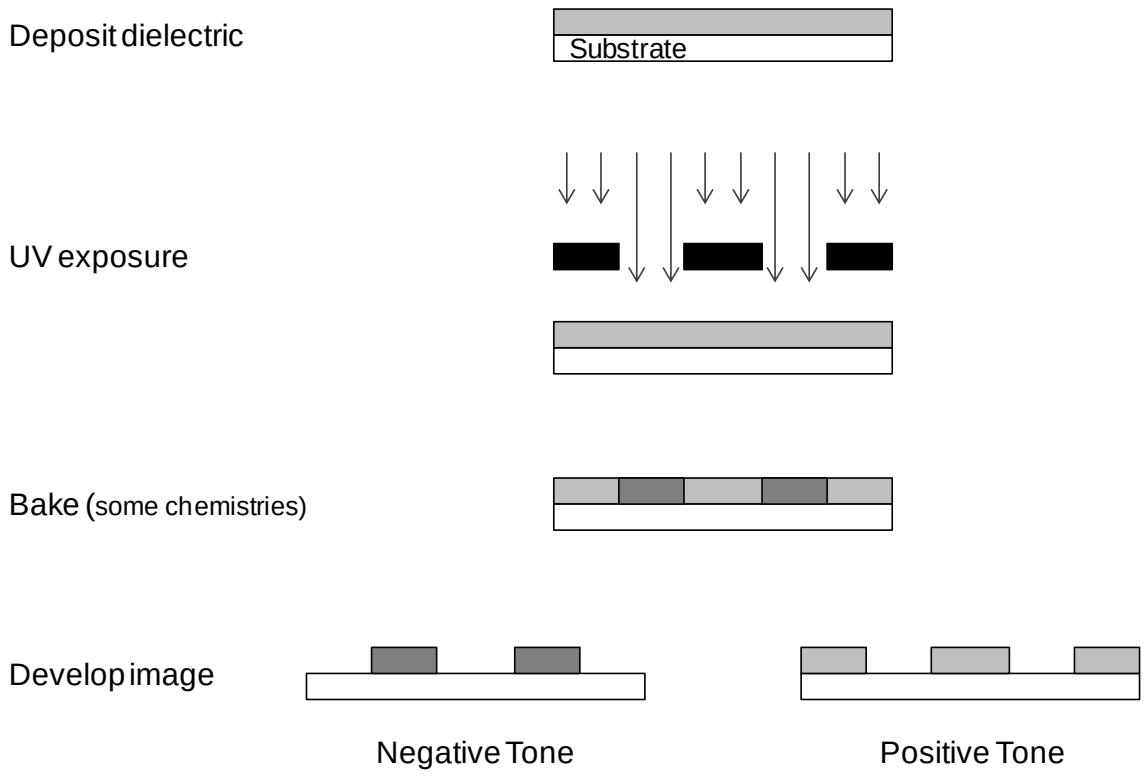

Figure 1.7: Photolithographic processing

Since permanent dielectric materials will remain in the device structure, they are thermally cured after patterning. The cure imparts good electrical and mechanical properties onto the film, discussed in Chapter 2. Additionally, the cure ensures that subsequent thermal processing will not result in degradation or dimensional changes in the dielectric.

1.4.3 Lithographic Tone

As shown in Figure 1.7, photo-definable dielectrics can be negative or positive tone. Negative tone dielectrics are initially soluble in developer, and UV exposure decreases their solubility. Thus, developing removes the unexposed regions. UV exposure of a positive tone dielectric must impart solubility upon a previously insoluble material.

Tone is important from a yield perspective, and this generally dictates when a negative or positive tone dielectric will be used.[26] One source of defects is the presence of dust particles in the path of the exposure beam. To lower the probability of a dust particle interfering with the final image, the mask for the dielectric should be as opaque as possible. If a mask is more opaque than transparent, it is more probable that the dust will overlap with the opaque region and no defect will result. For printing stand-alone features of low pattern density (often in MEMS), it is better to use a negative tone material, because the mask will be mostly opaque with transparency only where the features will be printed. On the other hand, positive tone dielectrics serve better for forming vias or interconnects in films for the same reason. Since most of microelectronics packaging consists of the latter case, positive tone dielectrics are preferred.

Another important factor is the slope of the sidewall of openings in the dielectric. After lithography, negative tone dielectrics can have undercut sidewalls as a result of diffraction, demonstrated in Figure 1.8.[26]–[29] This is unattractive for stress buffer or redistribution applications, because copper is plated in the open lines and vias. Conformal plating of copper in undercut structures can lead to voids in the copper. Positive tone materials exhibit a sloped sidewall, where the opening at the top is wider than at the substrate. This is better for achieving void-free plating of the copper lines and vias. It is noted, however, that sloped sidewalls can be fabricated with negative tone dielectrics. These rely on dark erosion of the dielectric in exposed regions or shrinkage of the dielectric during the thermal cure. These phenomena are discussed in Chapter 2.

Figure 1.8: Illustration of sidewall profiles of negative tone (left) and positive tone (right) materials

1.5 Positive Tone Solubility Switching Chemistries

The basis of photolithography is that the solubility of a film can be changed by exposing it to ultraviolet (UV) light. This requires that the film have a moiety that absorbs light at a specific wavelength and undergoes a chemical reaction as a result. Many types of chemical reactions can be considered to effect this solubility switch.

1.5.1 Diazonaphthoquinone-Based

A popular chemistry for positive tone photo-definability is the diazonaphthoquinone (DNQ) photochemistry along with an aqueous base develop. The discussion of this chemistry must first be approached by looking at appropriate resins. The base polymer, without the addition of DNQ, must be soluble in aqueous base. Novolac is a widely-studied example.[30]–[47] Novolac is a poly(phenol formaldehyde) or poly(cresol formaldehyde) backbone, which has pendent hydroxyl groups, as shown in Figure 1.9. When immersed in aqueous base, the anions deprotonate these acidic hydroxyl groups. The resulting phenolate is stabilized by the phenyl ring. Polar water molecules coordinate with the phenolate, and when enough of the hydroxyl groups have been deprotonated, the polymer dissolves.

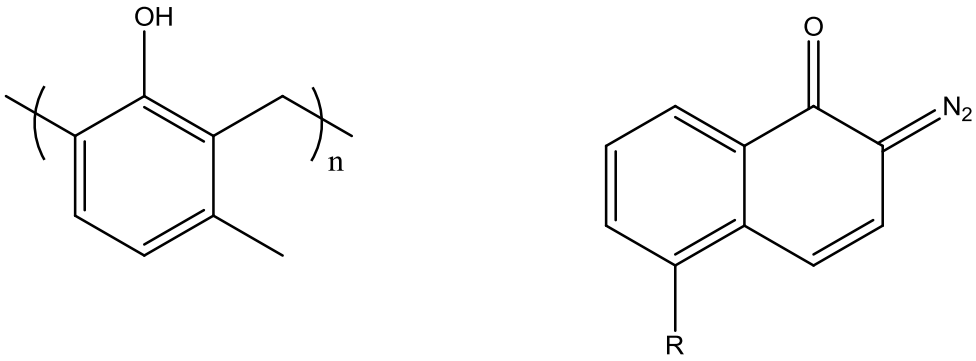

Figure 1.9: Chemical structures of novolac (left) and DNQ (right)

DNQ exhibits a large dipole with a partial negative charge on the carbonyl group. A hydrogen bond forms to a hydroxyl group on novolac, lowering the acidity of this proton and slowing the deprotonation of novolac by base.[48] Since hydroxyl groups are hydrogen bond donors and acceptors, a string of hydrogen bonds forms which begins at the DNQ molecule.[31] Thus, one DNQ molecule inhibits many hydroxyl groups from deprotonation.

DNQ absorbs light in the UV and visible parts of the spectrum. When DNQ is excited by irradiation, it expels gaseous nitrogen and undergoes the Wolff Rearrangment to form indene carboxylic acid (ICA), shown in Figure 1.10.[49] This reaction has several effects. First, the heat released during reaction provides energy to break up chains of hydrogen-bonded hydroxyl groups.[32] Second, the reaction changes the conjugation of DNQ lowering its optical absorbance and its dipole. Lowering the optical absorbance is known as photobleaching, and this is pivotal for exposure of thick films.[50] Third, ICA cannot induce the same hydrogen-bonded strings as the DNQ, leaving the phenolic alcohols uninhibited from deprotonation. Finally, ICA is soluble in aqueous base, whereas DNQ is not. The exposure of these films not only imparts solubility, but exposed films dissolve faster than the neat resin due to the presence of ICA.[51]

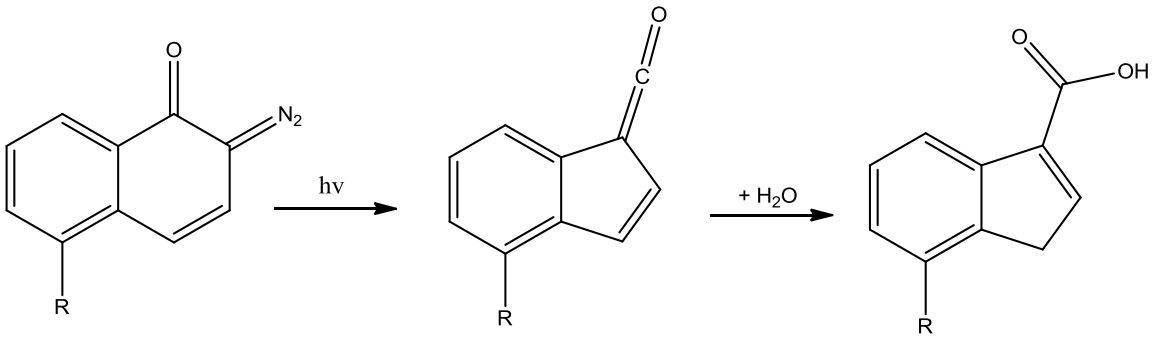

Figure 1.10: Wolff rearrangement of DNQ to ICA

Polymers that include an acidic group with a pK_a similar to the novolac hydroxyl group are inhibited by the same hydrogen bonding mechanism. Otherwise, enough DNQ must be added to change the solubility properties of the film without chemically interacting with the polymer. Non-interacting polymers require more DNQ to inhibit, which can impact the final properties of permanent dielectrics. Insufficient inhibition allows for dissolution of unexposed regions. This effect is termed dark erosion.

1.5.2 Chemical Amplification

The shift to 248 nm radiation for lithographic exposures created two problems. At 365 nm, DNQ photobleaches, decreasing its absorbance after reaction.[50] At 248 nm, however, this is not the case; ICA has high absorbance at 248 nm. This is bad from a sensitivity standpoint, as non-functional molecules (ICAs) are absorbing light. Second, the intensity of 248 nm light from Hg arc lamps is much less than the intensity at 365 nm.[20], [52] These limitations required a shift in the photoresist chemistry to achieve higher sensitivity.

A new chemistry, invented at IBM by Willson, Ito, and Frechet, was termed chemical amplification because it used a catalytic solubility shift reaction.[53]–[55] The novolac base polymer was replaced with a protected form of poly(hydroxystyrene)

(PHOST). PHOST is soluble in aqueous base, whereas the protected version, poly(tert-butoxycarbonyl styrene) (PBOCST) is not. These structures are shown in Figure 1.11.

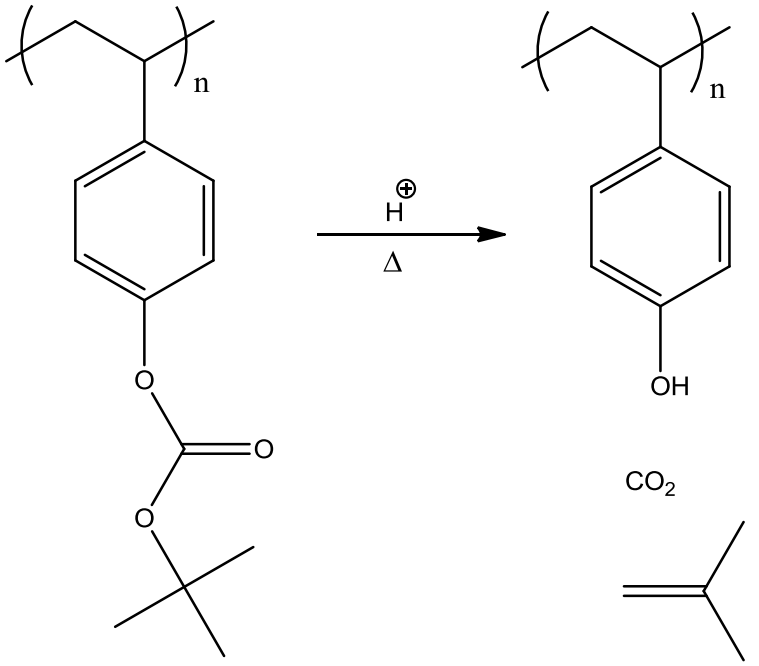

Figure 1.11: Acid-catalyzed deprotection of PBOCST to form PHOST

PBOCST can be thermally deprotected to form PHOST and acid acts as a catalyst for this reaction. A small amount of photoacid generator (PAG) is mixed into the formulations, and exposure to UV radiation produces the acid needed to catalyze the deprotection.[56] Since the deprotection reaction is catalytic, each photoreaction can produce 100s to 1000s of solubility switching reactions. The quantum efficiency of chemically amplified chemistries are much greater than 1, and these materials have much higher sensitivities and contrast than conventional novolac/DNQ resists.

Chemical amplification has several challenges. One challenge is the interdependence of resolution, line edge roughness, and sensitivity termed the "Triangle of Death".[57] Any effort to improve one of these properties causes degradation of the

other properties. For example, improving the sensitivity can be achieved by increasing the PEB time or temperature so that each acid moiety catalyzes more deprotection reactions. The increased energy also causes the acid catalyst to diffuse farther into the unexposed regions of the film and blur the printed features.[58] Many efforts have been made to overcome the limitations. These include studying acid diffusion in chemically amplified (CA) materials, studying the kinetics of the deprotection reaction, dosing CA materials with a background level of base, and developing photodefinable materials that exhibit lithographic gain without bias.[52], [56], [59]–[63]

Another challenging aspect of CA materials is the selection of the protecting groups. For example, the TBOC group in Figure 1.11 can be replaced with a tert-butyl ester (TBE) functional group. This change raises the deprotection temperature approximately 30°C and produces a carboxylic acid rather than an alcohol.[63] Other carboxylic acid protecting groups have been evaluated, some of which are shown in Figure 1.12. These changes impact the solubility, sensitivity, contrast, etch resistance, shrinkage, and thermal stability of the material.[64]–[67]

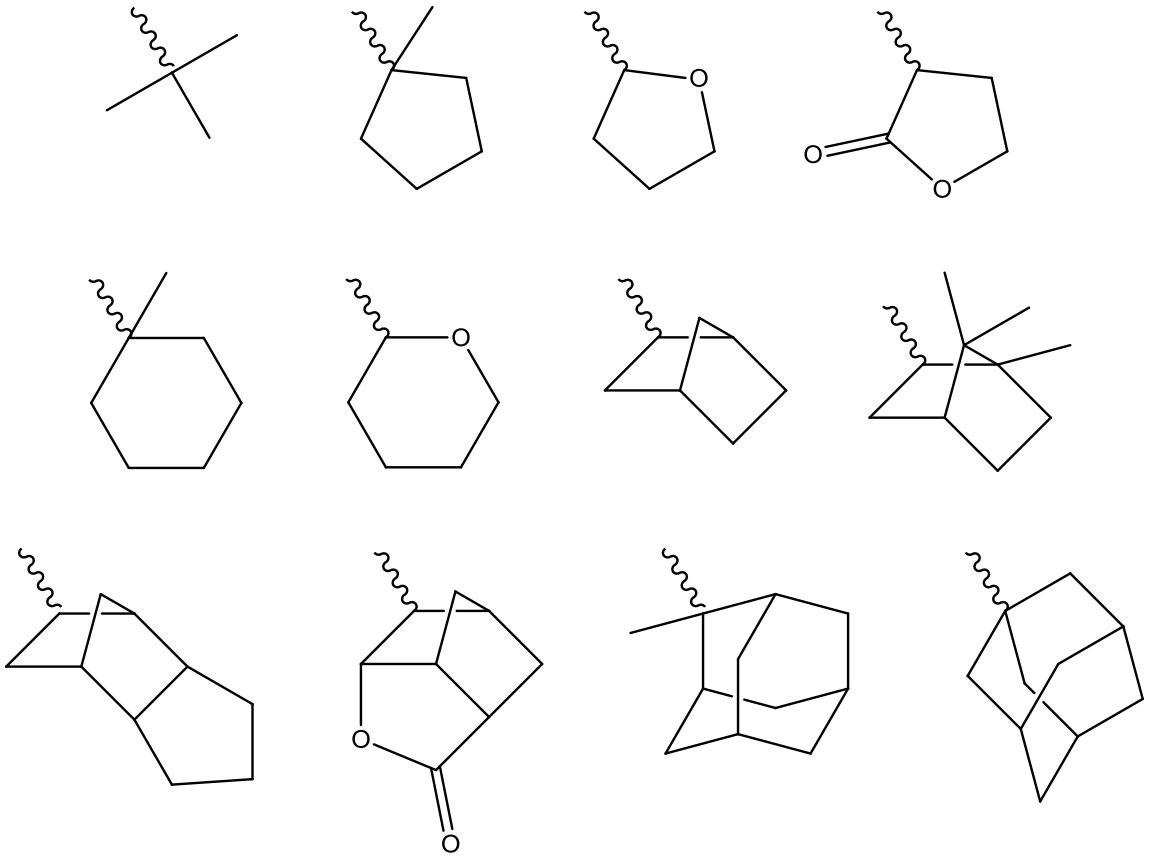

Figure 1.12: Previously studied carboxylic acid protecting groups

Another challenge with CA chemistry is its sensitivity to atmospheric base. Amines in the atmosphere at parts per billion levels can absorb into the film and react with the strong acid to form ammonium compounds, which will not catalyze the deprotection reaction. This can lead to a phenomenon known as T-topping, where a small lip of exposed but insoluble material remains at the top of the printed opening.[68] In extreme cases, atmospheric base can result in an insoluble skin on top of the desired features. To remedy this, chemically amplified (CA) resists must be used in an environment free of atmospheric bases. Activated carbon filtering of the circulated air can remove base. A low level of basic species can also be added to the film, which sets the threshold acid concentration for conversion at a higher level. While this can solve T-topping issues, it also lowers the sensitivity.

CHAPTER 2

PROPERTY REQUIREMENTS AND CURRENT MATERIALS

2.1 Properties for Permanent Dielectrics

Photo-definable, permanent dielectrics can be used in microelectronic devices and packages. In addition to good lithographic properties, these materials must exhibit excellent mechanical and electrical properties for reliability and energy efficiency. Some applications have different property requirements. In many cases, improvement of one property leads to degradation of another property, so tradeoffs must be carefully considered.

2.1.1 Lithographic Properties

Sensitivity – Sensitivity refers to the amount of energy (in the form of photons at a given wavelength) required to pattern a dielectric. More sensitive dielectrics require less energy to pattern which can lead to higher throughput. Figure 2.1 depicts typical negative and positive tone contrast curves, where the normalized residual thickness after develop is plotted against the logarithmic dose. The dose is a measure of energy per area, with units mJ cm^{-2}. D_{100} refers to the minimum amount of areal energy required to effect complete solubility change of the material. Since dose is the product of intensity and time, and since intensity is fixed, D_{100} dictates the minimum amount of time a dielectric must be exposed. For negative tone materials, the dielectric may still swell with developer above the D_{100}, which is depicted in Figure 2.1. Often, dielectrics are exposed at D_{150}, or 1.5x the D_{100}. Higher sensitivity is better for throughput so long as the material is not too sensitive to ambient light during formulating and transferring.

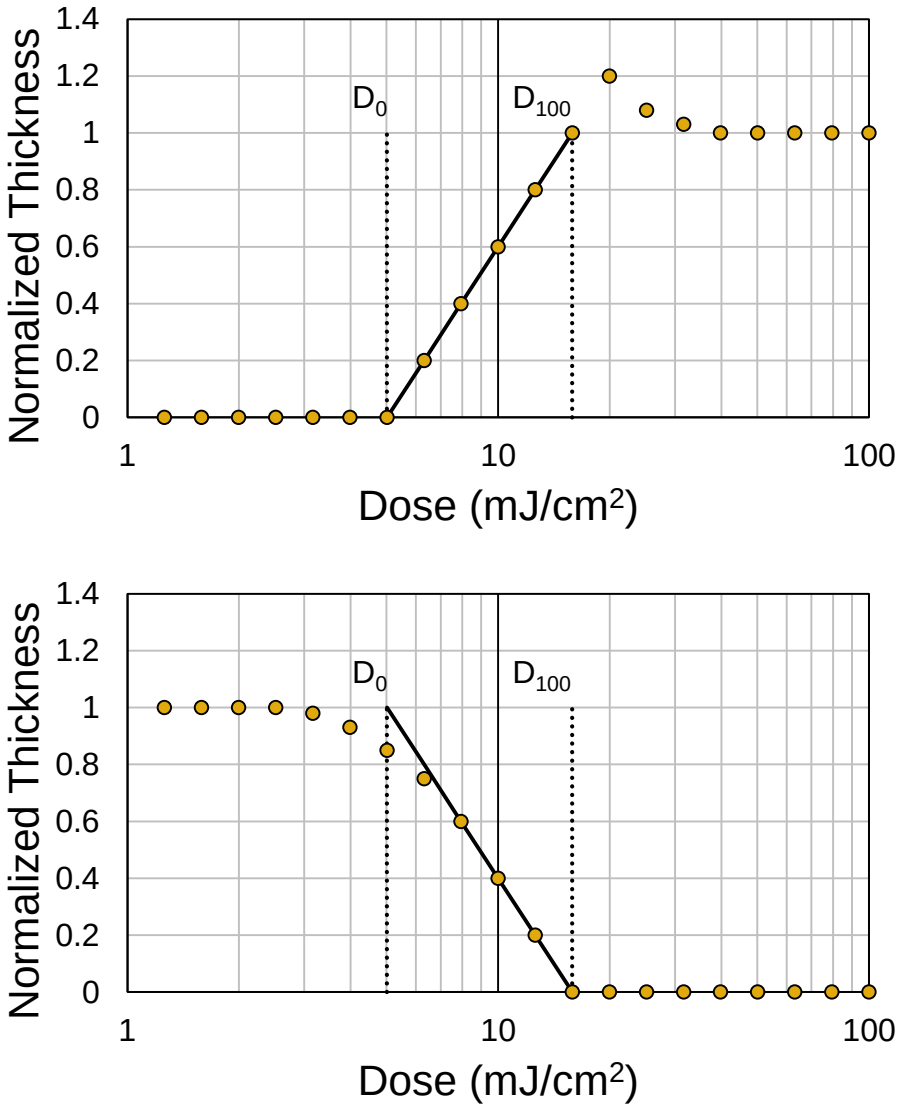

Figure 2.1: Typical negative tone (top) and positive tone (bottom) contrast curves

Contrast – Contrast is a measure of the sharpness of solubility change, denoted by γ. Contrast is defined in Equation 2.1, and it is exactly the slope of the contrast curve nearest D_{100}. As discussed in Chapter 1.4.1, light will diffract through the exposure mask and there will be a gradient in intensity from the dark to light regions. Low and high contrast dielectrics are affected by this to a different degree. Low contrast dielectrics may exhibit considerable solubility change in the diffracted regions, resulting in sloped

sidewalls. A sharper sidewall can be achieved by increasing the total exposure dose and thus increasing the intensity gradient, but this requires longer exposures, sacrificing throughput. High contrast dielectrics may have almost vertical sidewalls, because their transition from insoluble to soluble is a small change in dose. However, diffraction shifts the spatial coordinate at which D_{100} is reached, so the dimensions and shape of the pattern may not match that of the mask for high contrast dielectrics. Optical proximity correction can be used to bias the mask openings so that the desired feature is printed.[69]

$$\gamma = \frac{1}{\log\left({}^{D_{100}}/_{D_0}\right)} \tag{2.1}$$

Absorbance – For photo-definability, dielectric materials must absorb incident photons. Higher absorbance results in more photons absorbed, increasing the dielectric's sensitivity. However, as stated by the Beer-Lambert law, the intensity of light through an absorbing medium decreases exponentially with respect to the distance into that medium. The film near the substrate does not receive as much light as the top of the film, and this exponential decay is increased with higher absorbance. For patterning thick dielectrics, high absorbance can be an issue. These dielectrics require long exposure times to fully switch the solubility of film near the substrate if photobleaching does not mitigate the problem. This causes an inherent tradeoff in sensitivity and contrast. Increasing the absorbance increases sensitivity since more photons are absorbed, but this lowers the contrast since the dose required to expose deeper regions of the film is higher compared to that at the surface.

Developability – There are several important factors about the develop step. The first is the type of developer that can be used for each material. Solvent developers may be environmentally harmful and may require expensive disposal. It is more attractive to use an aqueous base developer for this reason. Another factor is the dissolution rate of

the dielectric. Slow-developing dielectrics present a throughput problem, so a higher dissolution rate is desirable. Finally, the dielectric must have adequate resistance to the developer in the regions that remain (exposed for negative tone, unexposed for positive tone). A measure of this resistance to developer is "dark erosion", which can be quantified as the amount of material dissolved as a percentage of the film thickness or the dissolution rate of the desired feature. Ideally, the dielectric would not be soluble at all in these regions, but often the photochemistry must rely on a finite solubility change. The DNQ photochemistry is one such chemistry.

Volume Change – Generally, volume shrinkage of the film due to loss of material or densification of the polymer molecules can occur. Two types of volume change are considered in the processing of a permanent dielectric. The first volume change is the shrinkage of the film during photochemical reactions, which can lead to biased feature dimensions. CA resists exhibit this type of volume change because the solubility switching reaction often produces gaseous products.[70], [71] Secondly, there is a volume change associated with the thermal curing reactions. Polyimide dielectrics are good examples of this phenomena. Polyimide dielectrics exhibit cure shrinkage as a result of the curing reaction which produces water and increases chain stacking. Since the film is constrained at the substrate, cure shrinkage changes the profile of patterned features, widening the opening at the top. This is highly desired when sloped sidewalls are needed for Cu electroplating or PVD coating. Stacking multiple dielectric layers can be challenging if they each have considerable volume change. Shrinkage could result in mechanical failure of the structure or dimensional changes in the hierarchical pattern.

2.1.2 Mechanical Properties

Coefficient of thermal expansion (CTE) – The dielectric's CTE is a measure of the expansion or contraction of the dielectric with respect to a temperature change, and is reported in ppm/K. A positive CTE value indicates that the dielectric expands as

temperature increases and vice versa. Dielectrics can be anisotropic, exhibiting direction-dependent values typically from molecular orientation of the material, such as a different CTE in the in-plane (xy) direction vs. the out-of-plane (z) direction. Since dielectrics for packaging applications are often continuous films with patterned lines and vias, there are advantages to matching the in-plane CTE to that of the underlying substrate, but this is often not possible. There are also advantages to matching the out-of-plane CTE to the material filling the layer-to-layer via connection, for example Cu. Unfortunately, the volumetric thermal expansion is usually conserved in polymers so that an exceptionally small value in one direction results in an exceptionally high value in other directions. The dependence of stress on temperature change is given in Equation 2.2, where σ is stress, T is temperature, E_f is the film's Young's modulus, ν_f is the film's Poisson's ratio, $\alpha_{f,xy}$ is the film's in-plane CTE, and $\alpha_{s,xy}$ is the substrate's in-plane CTE.

$$\frac{\partial \sigma}{\partial T} = \left(\frac{E_f}{1-\nu_f}\right)\left(\alpha_{f,xy} - \alpha_{s,xy}\right) \tag{2.2}$$

If in-plane CTE mismatch occurs, heating or cooling of the device will result in warping of the substrate. It is desirable to match the out-of-plane CTE to copper, 17 ppm K^{-1} because of the stress put on copper vias during thermal cycling. For polymer dielectrics, the out-of-plane CTE is often too high due to in-plane orientation of the polymer strands, which can cause delamination of the inter-layer copper connections. This property can limit the use of polymers in many applications.

Modulus – Elastic modulus (E), also known as Young's Modulus, is the relationship between stress and strain. Figure 2.2 shows a typical stress vs. strain curve. The elastic modulus is taken as the slope of this curve in the elastic region, or before any plasticization has occurred. For packaging, a modulus greater than 1 GPa is desired due to the need to plate copper and deposit subsequent layers.[72] However, since the

thermal stress is proportional to elastic modulus (Equation 2.2), a low elastic modulus is desirable. Polymer dielectrics often have a modulus between 2 and 10 GPa.

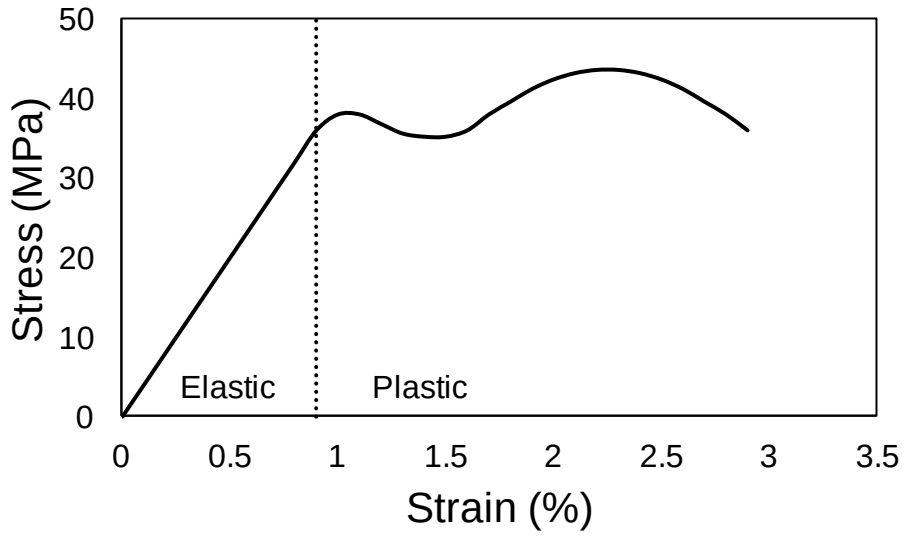

Figure 2.2: Typical stress vs. strain curve

Fracture Toughness – Toughness is the resistance to brittle fracture and is calculated as the integral under the stress vs. strain curve (Figure 2.2) until failure of the material. This value is the amount of energy per unit volume required to cause a fracture, so higher toughness is better for permanent dielectrics and can lead to higher reliability. The modulus, strain at plasticization, and strain at break are factors affecting toughness of materials. A low toughness can cause mechanical failures throughout the processing of the permanent dielectric, especially after bake steps. Cooling the film to room temperature from an elevated temperature induces strain that can crack the thin film. This cracking sets an upper limit on thickness for the dielectric film.

Cross-Link Density – Cross-link density is evaluated by measuring the molecular weight between cross-links (M_c), and it is inversely proportional to the cross-link density

where the density of the film (ρ) is the proportionality constant. Cross-link density critically affects many other properties, including elastic modulus, fracture toughness, solvent resistance, electrical permittivity, and glass transition temperature. As given in Equation 2.3, elastic modulus is proportional to the cross-link density where R is the gas constant and T is the temperature. This means that increasing cross-link density also increases the film stress for stresses originating from a CTE mismatch between a film and its substrate.

$$E_f = \frac{3RT}{2}\nu = \frac{3RT}{2}\frac{\rho}{M_c} \tag{2.3}$$

Even though increased cross-link density increases elastic modulus, it can often increase fracture toughness and decrease dielectric constant (discussed in Section 2.1.4) if the polarity of the cross-linked bonds are lower than the uncross-linked bonds and the densification of the film does not off-set the effects. Generally, higher cross-link densities are desired. In applications with stacked dielectric layers, achieving a high cross-link density is critical. The casting solvent of subsequent dielectric layers can partially dissolve or swell low cross-link density films. The amount of solvent that can swell the film is inversely proportional to the cross-link density. This effect also enables the measurement of cross-link density by solvent swelling, assuming dissolution does not occur.

It is noted that not all permanent dielectrics are heavily cross-linked. Polyimides, for example, can have good mechanical and electrical properties even though the final structures have only light cross-linking or no cross-linking. For these dielectrics, the curing reaction makes the polymer insoluble in most solvents. The degree of cure is an equivalent metric used to describe these uncross-linked systems. The degree of cure is

the percentage of poly(amic acid) moieties that have undergone the imidization reaction. This chemistry is discussed in Chapter 2.2.

2.1.3 Thermal Properties

Glass Transition Temperature – The glass transition temperature (T_g) of a dielectric is the temperature above which the dielectric transitions to a glassy state. In the glassy state, the polymer can flow. This can cause issues if any of the lithographic bake steps (soft bake or PEB) are above the T_g, because the patterned features can be distorted. However, below the T_g, mobility of the polymer chains is low, and curing reactions proceed slowly. Additionally, as cross-linking density increases, so does the T_g, so the dielectric will likely have a higher cross-link density if cured above the T_g. These limitations require that the T_g of the starting polymer be higher than lithographic bake steps, but low enough to allow for a reasonable cure temperature.

Decomposition Temperature – The decomposition temperature (T_d) is the temperature at which the film begins to degrade. This can occur via the decomposition of the polymer backbone or the decomposition of the cross-links. It is desired that these bonds be as thermally stable as possible to allow for high temperature processing. For example, solder reflow is performed for flip-chip packaging at 265°C.[10]

Cure Temperature – The optimal cure temperature and time are dictated by previously mentioned properties of the dielectric, such as the curing kinetics, T_g, T_d, CTE, cross-link density, and modulus. To minimize equipment load and maximize throughput, it is desired to have the lowest cure temperature and shortest cure time that the dielectric will allow. The cure temperature is often the stress-free temperature of the dielectric since it is free to flow before cross-linking. Cooling the film induces thermal stress, which is a function of the temperature change. The ability to cure at a low temperature decreases the resulting thermal stress. Permanent dielectrics are often cured

at temperatures well above their T_g, so that polymer mobility and curing reaction rates are increased.

2.1.4 Electrical Properties

Permittivity – An electrical field applied to a dielectric results in a net polarization of the dielectric and a complimentary electric field in the dielectric. The magnitude by which the external electric field can affect the dielectric material is known as the electrical permittivity. Often the permittivity is referenced as a relative permittivity (ε_r) to the vacuum permittivity. The vacuum permittivity is the lowest possible permittivity, so ε_r must be ≥ 1. The electrical signals in microelectronics packaging are high frequency alternating current (AC) signals. Since the energy is not perfectly recoverable, the relative permittivity is comprised of real (ε_r', in-phase) and imaginary (ε_r'', out-of-phase) parts, as given in Equation 2.3. The real part of the relative permittivity is termed the dielectric constant, which is the recoverable portion of the energy stored. The imaginary part (or dielectric loss) is unrecoverable, and can be reported as dissipation factor or tanδ, where δ is the angle between the impedance vector and the negative reactive axis on the impedance plane.

$$\varepsilon_r = \varepsilon_r' + i\varepsilon_r'' \tag{2.3}$$

ε_r' and ε_r'' are frequency dependent, as illustrated in Figure 2.3. At low frequency, the polarization events in the dielectric can switch at the same rate as the applied electric field, so the dielectric constant is high. At higher frequency, the inertia of the particles being polarized causes the internal polarization to lag behind the applied electric field. This is highly resistive, and the dissipation factor is high. At high frequency, the inertia of the polar particle is too large to be influenced by the applied electric field. The contributions to the permittivity can be ionic, dipolar, atomic, or

electronic as illustrated in Figure 2.3. Dielectrics for packaging applications are subject to circuits that operate in the GHz range, so both parts of the permittivity are critical.

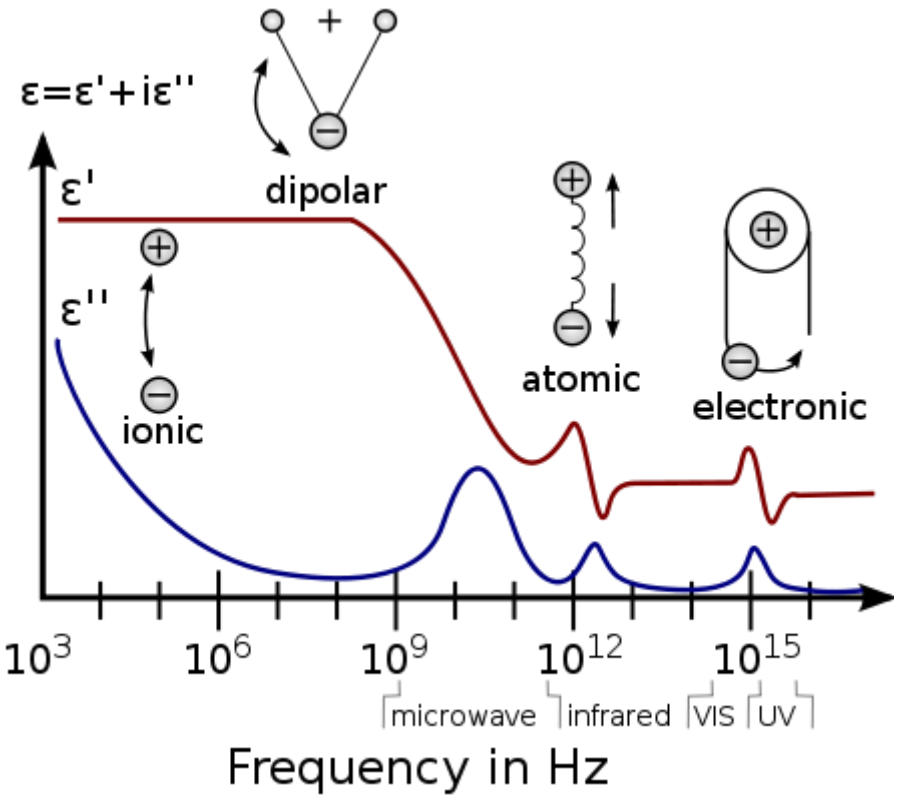

Figure 2.3: Frequency-dependent contributions to relative permittivity. Image by Beau Lambert, Dr. Kenneth A. Mauritz, University of Southern Mississippi [73]

Three main factors impact the permittivity of a dielectric. The first is the polarizability of a material. Lowering the amount of polarizable bonds or molecules will decrease the permittivity. This is often done by incorporating less polar bonds into the structure, or incorporating carbon-fluorine bonds (polar but not highly polarizable). A second factor affecting the permittivity is the porosity. Dielectrics can be deposited with porogens that leave pores after curing. Polyimides have high thermal stability and are well-suited for this. Third, minimizing water uptake also lowers a dielectric's

permittivity.[74] Water has a dielectric constant of ~80, so even a small amount of water can increase the effective dielectric constant of a film substantially.

2.2 Current Dielectric Polymers

As mentioned in Chapter 1, imparting a dielectric with positive tone photo-definability is challenging and often requires a high loading of additives. These light-absorbing additives can be polar, increasing the electrical permittivity. In this case, the process simplification of the photo-definable dielectric may not offset the performance decrease caused by its higher electrical permittivity. Due to this, few positive tone dielectrics have been developed with which to compare properties. This section summarizes the development of three popular polymeric dielectric materials with which positive tone photo-definability is possible.

2.2.1 Polyimide/Polybenzoxazole

One class of dielectrics being studied is that of polyimides (PI) and polybenzoxazoles (PBO).[7], [75], [76] The two materials are similar in both processing and final properties, so they are considered together. Both materials are synthesized by a step-growth polymerization of two difunctional precursors. For PI, dianhydrides and diamines are reacted to produce a poly(amic acid) chain. Imidization of the poly(amic acid) via a thermal cure results in the final PI. PBO is synthesized by the step-growth polymerization of 4,6-diaminoresorcinol (or similar diamine-dihydroxyl molecule) and terephthaloyl chloride (or other bis(acid chloride)) to produce a polyamide. Thermal curing closes the polyamide to produce PBO. The first commercial polyimide was Kapton, produced by DuPont, and it was made from 4,4'-oxydianiline (ODA) and pyromellitic dianhydride (PMDA). While it can be used in microelectronics for a variety of applications, it is not inherently photosensitive and suffers from a modestly high dielectric constant of 3.4 to 3.5 and water uptake of 1.8%.[77], [78] Though only a few

PI and PBO variations are discussed here, the library of precursors to make PI and PBO is large. The selection of these precursors largely dictates the final material properties, affecting the linearity and polarizability of the final polymer.[79]

The first photosensitive PI was reported in 1971, but the first stable photosensitive PI was reported in 1979 by Rubner, et al.[80] In order to achieve negative tone photosensitivity, the poly(amic acid) was replaced with a poly(amic acid ester) that was esterified with 2-hydroxyethyl methacrylate (HEMA). This polymer had pendent methacrylate groups that were radically cross-linked during UV exposure. Unexposed regions were developed with an organic solvent, and after photolithography, the polymer was cured at 400°C, forming the PI. Since this successful demonstration, a library of other working synthesis schemes and negative tone photochemistries have been developed.[81], [82] Many of these include variations on the poly(amic acid ester)-type material. Others have used a poly(amic acid) and an inter-penetrating network of cross-linkable polymer to achieve negative tone photo-definability. Later it was discovered that basic compounds catalyze the ring-closing imidization reaction, and photobase generators were employed to impart the negative tone photo-definability.[77]

To impart positive tone photo-definability and aqueous base developability, PI dielectrics were formulated with DNQ as a PAC. Since DNQ does not inhibit the poly(amic acid) from deprotonation by the aqueous base, these materials suffer from high dark erosion. The inclusion of DNQ also made these films brittle, limiting the thickness of films and limiting their use in packaging applications. PIs also suffer from high shrinkage during cure from the increased packing of the linear PI compared to the poly(amic acid). Finally, high cure temperatures (often 300 to 400°C) can result in high thermal stresses after the cure. Fortunately, some PIs are anisotropic, exhibiting in-plane CTEs that are low and well-matched to Si or Cu.

The most recent positive tone dielectrics are the HD-8800 and HD-8900 series, which are PBO dielectrics produced by HD Microsystems.[83] Both are limited to

maximum thicknesses between 10 and 14 μm. Little is reported on HD-8900, but technical notes show that it can be cured at temperatures as low as 200°C.[84] The HD-8800 series is cured at temperatures > 250°C and the optimal curing temperature is 320°C. The properties of this dielectric and another positive tone dielectric are presented later in Table 2.1. Notable properties of this dielectric are its low dielectric constant of 2.94 and high T_d of 399°C.

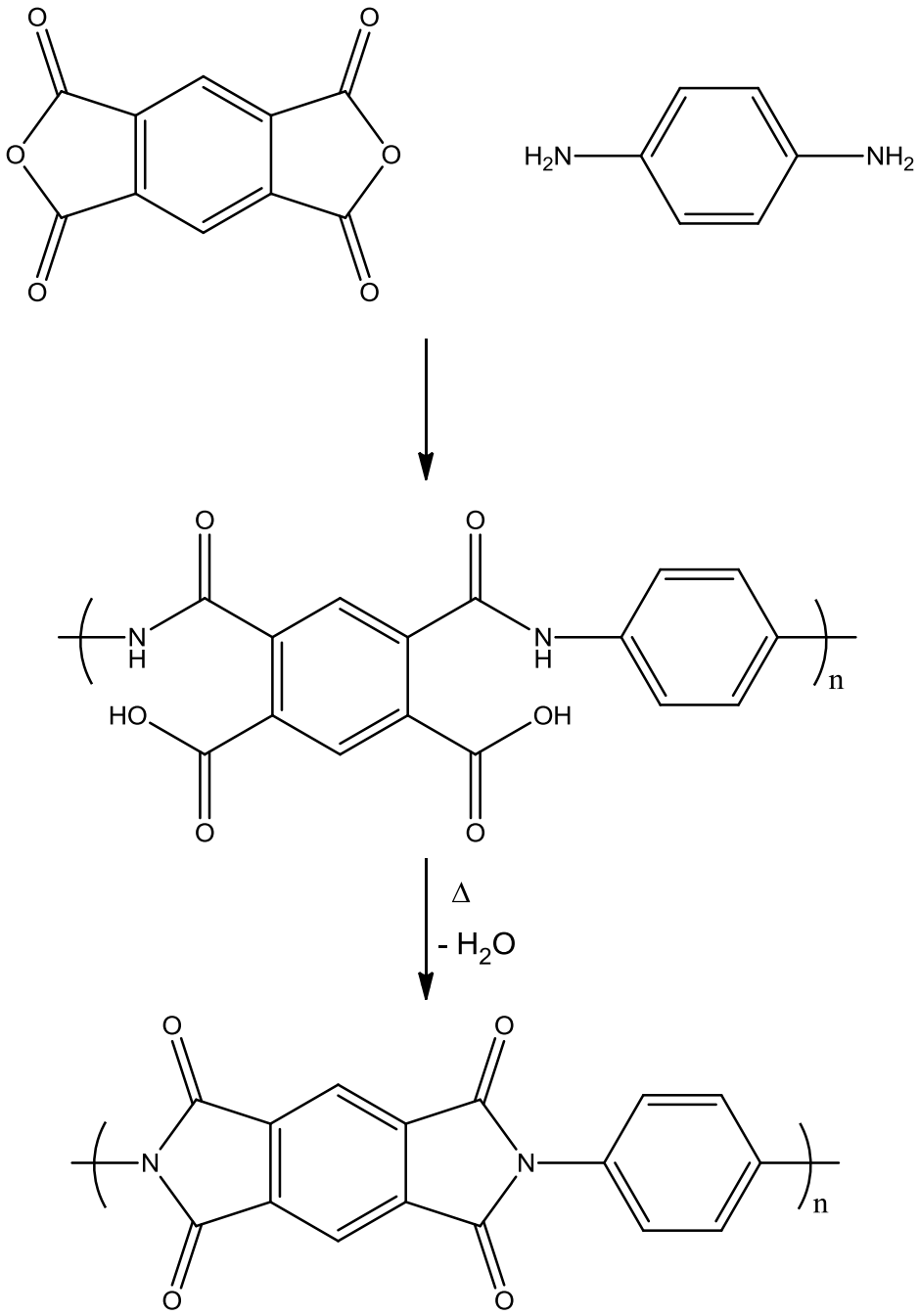

Figure 2.4: Polyimide polymerization and curing reactions

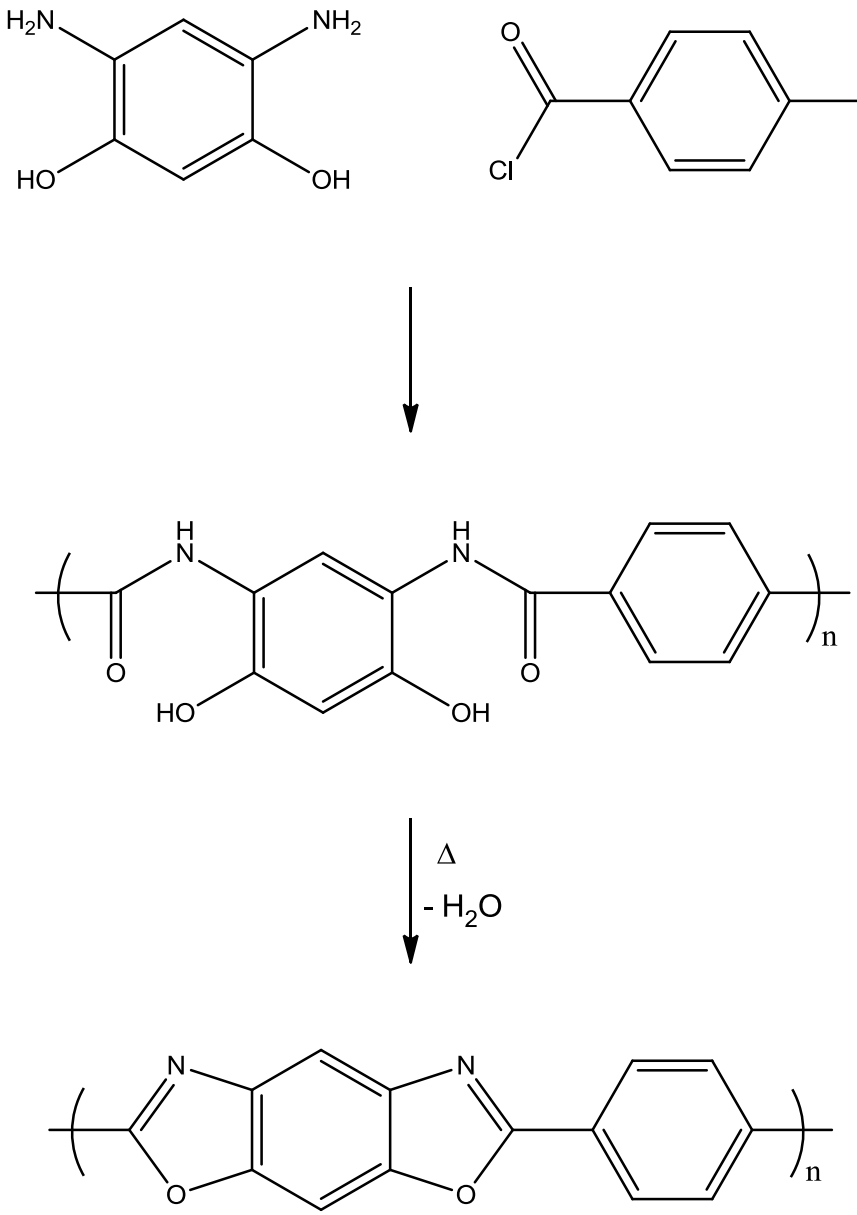

Figure 2.5: Polybenzoxazole polymerization and curing reactions

2.2.2 Benzocyclobutene-Based Dielectric

Benzocyclobutene (BCB) is another popular dielectric, which is produced under the tradename Cyclotene by The Dow Chemical Company. The structure of this dielectric was first described in a US Patent #4,812,588 in 1989.[85] These BCB dielectrics start as the monomer divinylsiloxane bisbenzocyclobutene (DVS-bis-BCB).

This difunctional monomer, is partially cured (i.e. B-staged) so that it can be spin-cast. The B-staging reaction proceeds by thermally ring-opening the BCB moiety to form a diene. The diene can react with another diene or a carbon-carbon double bond via a Diels-Alder reaction, increasing the molecular weight until a desired composition is achieved. After photolithographic processing, the films are fully cured by the same chemical reaction. One attractive quality of this dielectric is that no volatile products are formed from the cross-linking reaction.

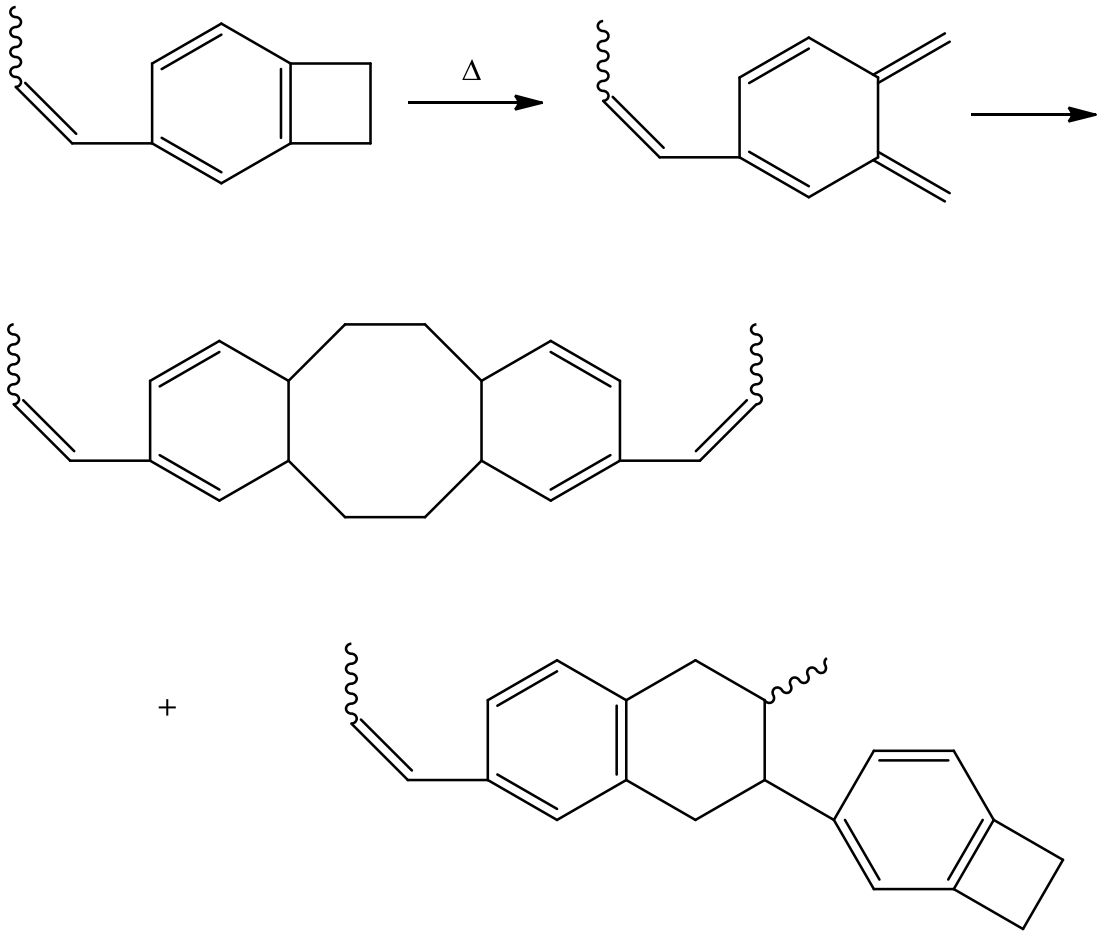

Figure 2.6: Thermal B-staging and curing reaction of BCB

Another BCB-type dielectric was produced by copolymerizing styrene and 4-vinylBCB.[86] Without the presence of carbon-carbon double bonds, the curing reaction

proceeds by the diene-diene reaction. It was found that just 22 mol% 4-vinylBCB was enough to produce a material with a T_g above 350°C, even though polystyrene has a T_g of 100°C. A dielectric with 26 mol% of 4-vinylBCB had a dielectric constant of 2.58 and only 0.12% water uptake.

A negative tone, photo-definable version of the DVS-bis-BCB dielectric was formulated by adding a bis(aryl azide) to cross-link the film upon exposure. The bis(aryl azide) is photoactive, and excitation by UV light results in the expulsion of gaseous nitrogen. The resulting nitrene is very reactive and will readily cross-link to carbon-carbon double bonds to form aziridines. An example bis(aryl azide), 2,6-Bis((4-azidophenyl)methylene)-4-ethylcyclohexanone is shown in Figure 2.7. Since each azide can only react once, the cross-linking density after exposure is fairly low, and this can result in swelling of exposed regions during the develop step. Negative tone Cyclotene can be cast from cyclohexanone, and the recommended developer is 1,3,5-triisopropylbenzene. The lightly cross-linked structure is much less soluble in this developer.

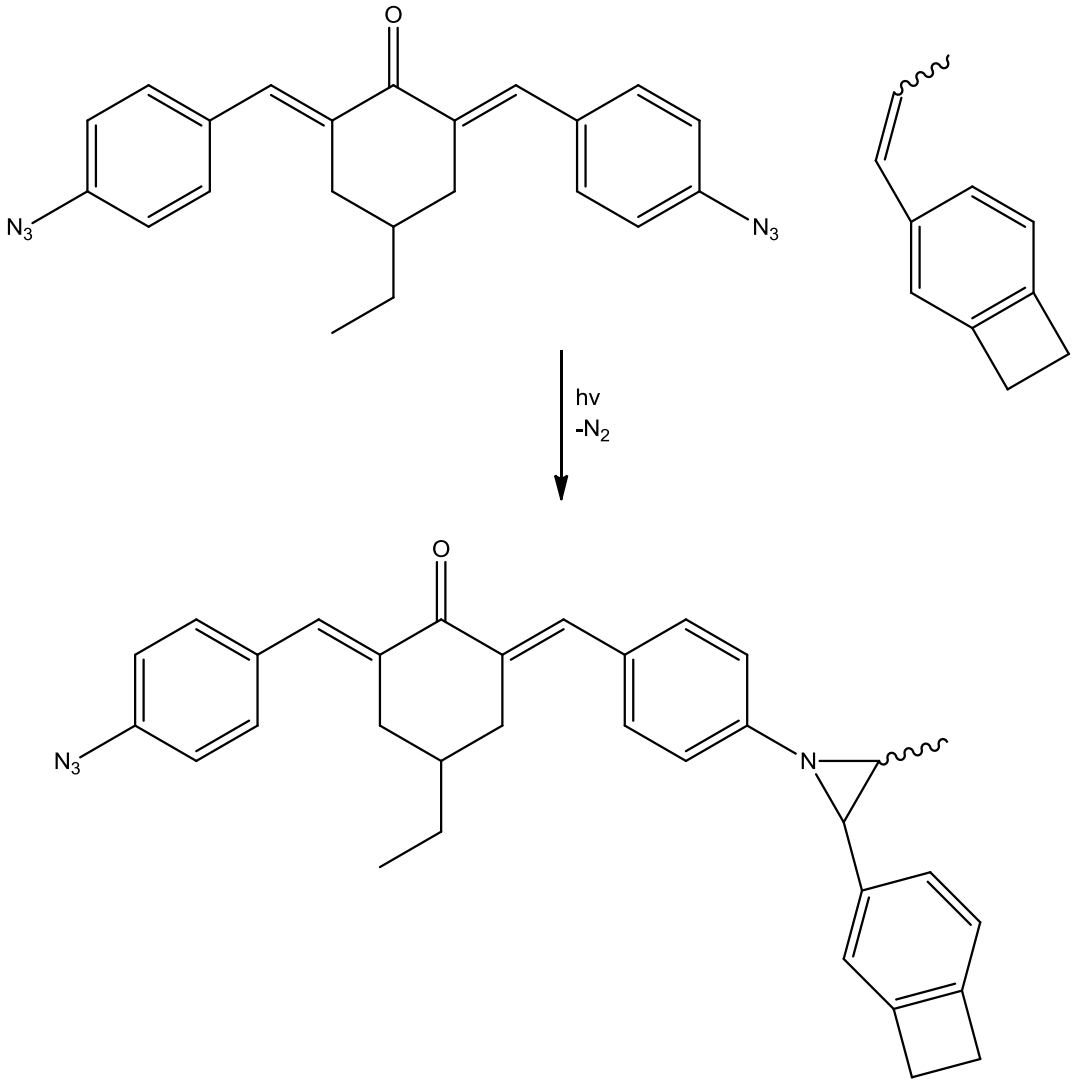

Figure 2.7: Cross-linking of a bis(aryl azide) with unsaturated group on BCB resin

In 2006, an aqueous base developable, positive tone version of BCB was reported in the literature.[87] Here, the authors also B-staged DVS-bis-BCB, but also included BCB-acrylic acid during B-staging so as to incorporate carboxylic acid moieties for aqueous base developability. Positive tone photo-definability was achieved with the addition of DNQ. A dielectric constant of 2.9 was achieved. This value is higher than non-photodefinable Cyclotene (ε_r' = 2.65) because of the polarizable carboxylic acids and DNQ. Unfortunately, a thick film (16.4 μm) required a dose of 810 mJ cm^{-2} to achieve

full solubility in TMAH developer (70 s). 2.5 μm films were patterned with 200 mJ cm^{-2} when developed for 120 s. Unfortunately, dark erosion is 19%, which is expected since DNQ does not inhibit carboxylic acid from deprotonation in TMAH. Commercially, the positive tone version of BCB is the Cyclotene 6000 series. The thicker version, Cyclotene 6505 has a dielectric constant of 3.2.

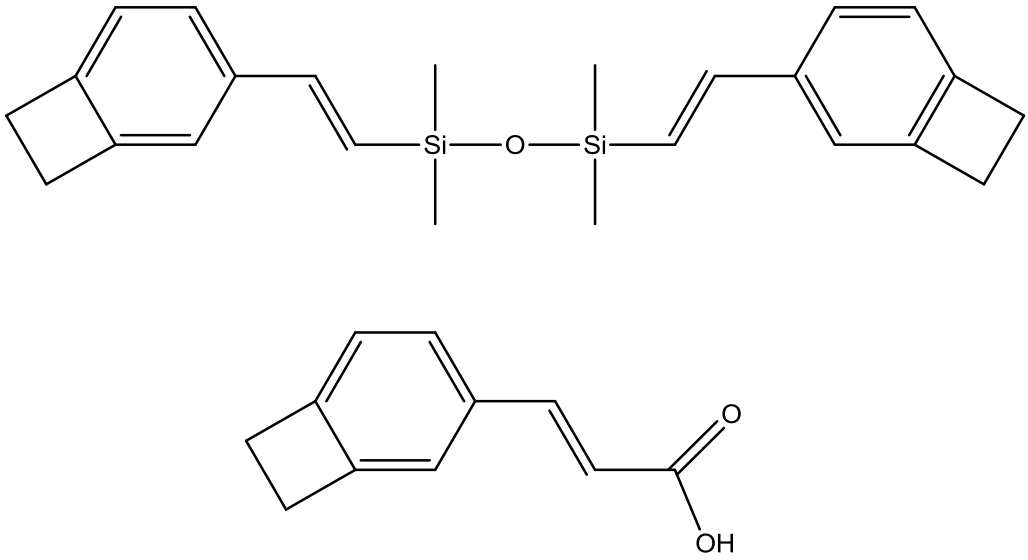

Figure 2.8: Chemical structures of DVS-bis-BCB (top) and BCB-acrylic acid (bottom)

2.2.3 Polynorbornene

The final class of dielectrics discussed here is polynorbornene (PNB). The precursor, norbornene, can be polymerized by free-radical polymerization, ring-opening metathesis polymerization, or vinyl addition polymerization. The latter method is achieved with a transition metal catalyst, such as Pd(II)-type or Ni(II)-type catalysts, and it results in a well-defined PNB structure. Commercially, PNB dielectrics have the tradename Avatrel and are produced by Promerus LLC. Non-functionalized PNB has a dielectric constant of 2.2, and is transparent to wavelengths as low as 200 nm.[88], [89] This transparency is a result of the lack of aromaticity in the cycloaliphatic structure.

PNB can also be functionalized to impart specific properties, including aqueous base solubility and photodefinability. These functional groups exist in both endo- and exo-configurations extending from the 5-position on norbornene.

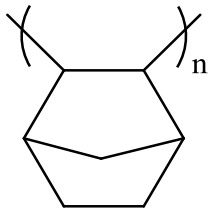

Figure 2.9: Chemical structure of PNB

PNB exists as a helical chain that is effectively linear. These linear chains are often insoluble in organic solvents since they are highly crystalline. However, one class of catalysts used to polymerize PNB has a low probability of producing a ~3° kink in the linear structure. Introducing these small kinks breaks up the crystallinity and imparts solvent solubility. The structure of PNB was modeled by Prof. Ludovice et al., where it was found that this kink occurs in approximately 0.2% of the monomeric connections.[90]–[92] This structure leads to an interesting phenomenon with respect to PNB's dissolution properties. Usually, increasing the molecular weight of a polymer lowers the dissolution rate because of increased chain entanglement.[34] However, it was shown that there are three regimes of dissolution for a polymer of hexafluoroisopropanol norbornene (HFANB).[93] At low molecular weights, each chain has a low probability of containing a kink in the structure, so the films are fairly crystalline and hydrogen-bonded. Dissolution of low molecular weight films is slow. Increasing the molecular weight introduces more kinks into the polymer structure, breaking up the crystallinity and increasing the dissolution rate. At even higher

molecular weights (~180 kg mol^{-1}), there are enough kinks per chain to induce entanglement and lower the dissolution rate.

Initial photo-definable versions on PNB were positive tone CA photoresists owing to the desire to move to shorter wavelengths for improved lithographic resolution.[65], [66], [89], [94] These were functionalized with appropriate protecting groups and were aqueous developable. The first permanent, photo-definable PNB materials were negative tone.[95], [96] There were copolymers of allyl glycidyl ether norbornene and decyl norbornene. Negative tone photo-definability was achieved by photo-induced acid catalyzed cross-linking of the epoxy groups. The final dielectric had low water uptake and a low dielectric constant between 2.7 and 3.2.

Radical changes to the negative tone, PNB dielectric were made to impart aqueous base developability.[29] Instead of the alkyl/epoxide functionalization, PNB was functionalized with hexafluoroisopropanol and carboxylic acid groups. Both of these groups can be deprotonated by TMAH, and the ratio of the two monomers controls dissolution properties. To achieve negative tone photo-definability, low molecular weight multifunctional epoxies were added. Generation of a strong acid by exposure of a PAG causes the epoxides to cross-link to the acidic functional groups on PNB, lowering solubility. This dielectric had a D_{100} of ~105 mJ cm^{-2}, a contrast of 9.04, and a dielectric constant of 3.8 to 4.0. The PNB had excellent adhesion to a number of substrates because of the included epoxy. Further work examined the addition of other epoxy cross-linkers and sensitizers.[28] Of the multifunctional epoxies, tetraphenylol ethane tetraglycidyl ether was found to increase the sensitivity of the dielectric by acting as a sensitizer to 365 nm radiation. The incorporation of this epoxy decreased the D_{100} to 18 mJ cm^{-2} and increased the contrast to 24.2. A feature height-to-width aspect ratio of 14:1 was achieved with this formulation. This dielectric could be cured at 160°C or lower and had a dielelctric constant between 3.9 and 4.4. The work discussed in Chapter 4 is the first attempt to create a positive tone version of PNB.

2.2.4 Property Benchmarks

In considering a material's use as a positive tone dielectric, it is important to compare the properties to commercially available dielectrics or other dielectrics reported in the literature. Table 2.1 lists reported properties for HD-8820, a positive tone polybenzoxazole dielectric, as well as a positive tone BCB dielectric reported in the literature. Both materials have comparable CTE, dielectric constant, and tanδ.

Table 2.1: Reported properties of positive tone dielectrics[83], [87] (**not reported)

Property	Unit	HD-8820	BCB
D_{100}	mJ/cm^2	280	810
Contrast	-	**	1.02
Dark Erosion	%	20 - 25	19
Volume Change	%	20	17.4
T_d (1% Loss)	°C	399	**
T_{cure}	°C	320	250
CTE (xy)	ppm/K	64	60
Modulus	GPa	2	3.6
Dielectric Constant	-	2.94	2.9
tanδ	-	0.0089	0.009
Water Uptake	%	< 0.5	1.2 @ 50% RH

CHAPTER 3

EXPERIMENTAL DESIGN AND PROCEDURES

3.1 Materials

PNB polymers and DNQ PACs were supplied by Promerus LLC (Brecksville, OH). Polymer compositions are listed in Table 3.1. These were all homopolymers, copolymers, or terpolymers of endo,exo-5-hexafluoroisopropanol norbornene (HFANB), endo,exo-5-propanoic acid norbornene (CBANB), endo,exo-5-tert-butyl ester norbornene (TBENB), and/or endo,exo-5-butyl norbornene (ButylNB).

Table 3.1: Experimental PNB polymer compositions

Polymer	Composition
PNB-A	75-25 HFANB-CBANB
PNB-B	90-10 HFANB-CBANB
PNB-C	HFANB
PNB-D	70-30 HFANB-TBENB
PNB-E	35-65 HFANB-TBENB
PNB-F	TBENB
PNB-G	50-50 HFANB-TBENB
PNB-H	43-47-10 HFANB-TBENB-ButylNB
PNB-I	38-38-24 HFANB-TBENB-ButylNB

Four DNQ PACs were used, identified as PAC1, PAC2, PAC3, and PAC4. All ballast portions of the PACs contained two or more hydroxyl groups which were esterified with 2,1,5-DNQ sulfonic acid. PAC1 was a 2,4-dihydroxybenzophenone-type ballast molecule with two hydroxyl groups, esterified at ~100% (i.e. two DNQ moieties per molecule). PAC2 and PAC3 were both made with a trisphenol-PA-type ballast molecule with three hydroxyl groups. PAC2 was esterified at 67%, and PAC3 was

esterified at 83%. PAC4 was a 4,4'-(2-methylpropylidiene)bis[2-cyclohexyl-5-methyl-phenol]-type ballast molecule containing two hydroxyl groups esterified at 100%. The only PAG used in this work was provided by Promerus LLC, and it is tetrakis-(pentafluorophenyl) borate-4-methylphenyl [4-(1-methylethyl)phenyl] iodonium (Rhodorsil FABA). AZ P4620 (AZ Electronic Materials) is a thick-film, novolac-based photoresist. MF-319 (Doe and Ingalls) is a 0.26 N TMAH developer.

Monomers tert-butyl methacrylate (TBMA) and 2-hydroxyethyl methacrylate (HEMA) were purchased from TCI America and Alfa Aesar, respectively, and were filtered through alumina before use to remove inhibitors. All other chemicals, including propylene glycol monomethyl ether acetate (PGMEA), tetrahydrofuran (THF), hexanes, trimethylolpropane triglycidyl ether (TMPTGE), trimethylolpropane (TMP), trimethylolpropane ethoxylate (TMPEO), pentaerythritol (PE), and pentaerythritol ethoxylate (PEEO) were purchased from Sigma Aldrich and used without further purification.

3.2 Procedures

3.2.1 Lithographic Measurements

Polymers were cast from PGMEA. Thin films were cast by spin-coating using a CEE 100CB spinner at speeds of 1500 to 3000 rpm for 60 seconds onto <100> Si wafers. Films were soft baked at temperatures between 100°C and 140°C for 60 to 120 s. Film thicknesses were measured on a Veeco Dektak profilometer. Samples were exposed using an Oriel Instruments flood exposure source with a 1000 W Hg(Xe) lamp filtered to provide 365 nm or 248 nm radiation. Films that required a PEB were baked at 140°C for various times. The films were developed with MF-319. Films were developed in an agitated puddle fashion. Contrast, sensitivity, and aspect ratio experiments were performed by exposing films in soft contact with a variable-density optical mask (Opto-line International Inc.).

Contrast (γ) values were obtained by plotting the normalized film thickness after an aqueous base develop against the logarithmic exposure dose and fitting the curve with a linear least squares fit at the points closest to D_{100}. D_{100} is defined as the minimum dose at which 100% of the film is removed for a positive tone resist. This point is the x-intercept of the contrast curve, where the film thickness is equal to zero. D_0 is theoretically defined as the minimum dose at which 100% of the film remains after development. Since positive resists have a finite solubility even in the unexposed regions, the value of D_0 was calculated by extrapolating the slope of the contrast curve to a normalized thickness of 1.

$$\gamma = \frac{1}{\log\left({}^{D_{100}}/_{D_0}\right)} \tag{3.1}$$

The aspect ratio is the ratio of the feature height-to-width for the smallest features that retained 100% of the unexposed film thickness. These widths and thicknesses were measured by scanning electron microscopy (SEM), using a Zeiss Ultra 60 SEM. The SEM samples were sputtered with 18 to 20 nm of gold using a Hummer 5 Gold Sputter tool to prevent charging of the film during examination.

Dissolution rate experiments were obtained using a QCM200 (Stanford Research Systems). Samples were spin-coated onto a 1" QCM with 5 MHz unloaded resonant frequency and 0.4 cm^2 active surface area. Coated QCMs were developed with MF-319 in a 125 μL flow cell connected to a ~800 μL min^{-1} peristaltic pump (Thermo Scientific). The flow path was equipped with a manual valve positioned ~5 cm from the inlet of the flow cell to control selection between water and MF-319. The polymer-coated QCM samples were first equilibrated in water before introduction of the aqueous base developer in order to minimize sharp frequency and resistance changes that result from immersion into a viscous medium from air. Mass changes (Δm) were obtained by

correlation of the resonant frequency change (Δf) using the Sauerbrey equation, Equation 3.2, where f_o is the resonant frequency of the unloaded quartz crystal, A is the active area between the gold electrodes, ρ_q is the density of quartz, and μ_q is the shear modulus of quartz. The thickness was calculated by taking the density of the polymer to be 1.3 +/- 0.05 g cm^{-3}, as obtained from measuring thickness and mass.

$$\Delta f = -\frac{2f_0^2}{A\sqrt{\rho_q \mu_q}}\Delta m \tag{3.2}$$

3.2.2 Thermal Curing

Films were cast by the same spin-coating method stated above. To thermally cure the films, samples were placed in a Lindberg quartz tube furnace and purged with nitrogen for 15 min at 5 LPM. The temperature was increased to a final cure temperature of 120°C to 250°C over a period of 65 to 90 min and held at the cure temperature for 2 hr under a nitrogen flow rate of 1 LPM. Finally, the samples were cooled under nitrogen (flow rate of 1 LPM in the furnace) to room temperature. The volume change was determined by measuring the thickness before and after cure.

3.2.3 Spectroscopy

^{1}H-NMR spectra were recorded on a Varian Mercury Vx 400 MHz instrument. Spectra were recorded in $CDCl_3$ and the protonated solvent peak at 7.26 ppm was used as an internal standard.

Ultraviolet-visible spectroscopy (UV-Vis) absorbance measurements were taken with a Hewlett Packard 8543 UV-Vis spectrophotometer. Films for UV-Vis measurements were spin coated on glass microscope slides. The background spectrum of the slide was subtracted from the sample spectrum. Absorbance values at 365 nm were

recorded, and film thicknesses were measured in order to calculate the absorption coefficient, α. FTIR measurements were obtained using a Magna 560 FTIR (Nicolet Instruments). FTIR samples were coated on a KBr disk. The absorbance data was averaged over 500 scans at a resolution of 2 cm^{-1}. FTIR spectra were automatically baseline corrected, and the peak areas were calculated by a least squares method, fitting Gaussian peaks.

Kinetic studies using IR were obtained using an attenuated total reflection (ATR) setup. FTIR samples were coated on a thallium bromide-iodide ATR crystal by doctor blading. The coated ATR crystal was mounted to a heated ATR temperature controller (Spectra Tech). Samples were heated to the desired temperature at a rate of 3°C min^{-1}. The absorbance data at each time point was averaged over 52 scans at a resolution of 2 cm^{-1}.

3.2.4 Mechanical Characterization

Elastic modulus and hardness were characterized with a Hysitron Triboindenter. Each sample was indented nine times or more at depths less than 10% of the film thickness.[97] For DNQ-PNB films, indents were performed with a Berkovich diamond tip. For CA-PNB films, indents were performed with a Northstar diamond tip because of the well-defined tip geometry. Tip geometry was calibrated against quartz and polycarbonate standards. The corrected tip geometry was defined by Equation 3.3, where h_c is the contact depth, $A(h_c)$ is the projected contact area at a specific h_c, and C_1-C_8 are fitted coefficients to account for tip imperfections. Step times for each indent were held constant, while the peak force was varied. The tip was loaded over a 10 s period of time, held at the peak force for 10 s to allow for time-dependent relaxations, and unloaded over a 4 s period of time.[97] Hardness, H, was calculated at the maximum load, P_{max}, divided by $A(h_c)$, Equation 3.4. The contact depth was estimated using the Oliver Pharr model in Equation 3.5, where h_{max} is the maximum indent depth, ζ, is a geometrical constant, and S

is the stiffness.[98] The stiffness was defined as the initial slope of the unloading curve, and the reduced modulus (E_r) was calculated using Equation 3.6, where β is a geometrical constant. The elastic modulus of the film (E_f) was calculated using Equation 3.7, where E_i is the elastic modulus of the diamond tip (1140 GPa), and ν_f and ν_i are the Poisson's ratios of the film and tip, respectively. ν_f was assumed to be 0.33, and ν_i was 0.07.

$$A(h_c) = 2.598h_c^2 + C_1h_c^1 + C_2h_c^{1/2} + \cdots + C_8h_c^{1/128} \tag{3.3}$$

$$H = \frac{P_{max}}{A(h_c)} \tag{3.4}$$

$$h_c = h_{max} - \frac{\zeta P_{max}}{S} \tag{3.5}$$

$$E_r = \frac{\sqrt{\pi}}{2\beta}\frac{S}{\sqrt{A(h_c)}} \tag{3.6}$$

$$\frac{1}{E_r} = \frac{(1-\nu_f^2)}{E_f} + \frac{(1-\nu_i^2)}{E_i} \tag{3.7}$$

Wafer curvature was measured with a Flexus Tencor Thin Film Stress Measurement System, Model F2320, equipped with a He-Ne laser. Deflection measurements were recorded over the middle 80 mm of a 100 mm Si wafer with 670 nm and 750 nm laser irradiation. The wavelength with the highest reflected intensity was used to prevent errors due to destructive interference. The thin film stress (σ) was calculated using Stoney's equation,

$$\sigma = \left(\frac{E_s}{1-\nu_s}\right)\frac{d_s^2}{6Rd_f} \tag{3.8}$$

where $E_s/1\text{-}\nu_s$ is the biaxial elastic modulus of the substrate, d_s is the substrate thickness, R is the effective radius of curvature of the substrate, and d_f is the film thickness. R is calculated by

$$\frac{1}{R} = \frac{1}{R_2} - \frac{1}{R_1} \tag{3.9}$$

where R_1 is the radius of curvature of the bare substrate and R_2 is the new radius of curvature after film deposition.

3.2.5 Thermal Characterization

The CTE was measured by measuring stress as a function of temperature. Ten measurements were taken every 10°C from 150°C to 200°C. The stress at each temperature was calculated by Stoney's equation, Equation 3.8. The stress as a function of temperature was fitted with a linear least squares fit to calculate $\partial\sigma/\partial T$. Equation 3.10 was then used to calculate the in-plane CTE of the film, $\alpha_{f,xy}$, where $\alpha_{s,xy}$ is the in-plane CTE of the substrate, and ν_f is the Poisson's ratio of the film, estimated to be 0.33.

$$\frac{\partial\sigma}{\partial T} = \left(\frac{E_f}{1-\nu_f}\right)[\alpha_{f,xy} - \alpha_{s,xy}] \tag{3.10}$$

Through-plane CTE was measured on a Woollam M-2000D ellipsometer equipped with a HCS 402 temperature-controlled stage with a liquid nitrogen pump. Ellipsometric measurements were made from 370 to 988.8 nm at an incident angle of 60 degrees. The sample was heated to 200°C and then ramped to room temperature at a rate of -5°C min^{-1}. The ellipsometric data was fit with an anisotropic model, with the in-plane and through-plane optical constants defined by Cauchy models, shown in Equation 3.11, where n is the refractive index, K_1, K_2, and K_3 are fitted coefficients, and λ is the wavelength. The temperature of the substrate was taken into account by modeling the Si wafer with the Si Temp JAW model. The as-collected values of polymer CTE, $\alpha_{f,z,measured}$, were corrected for expansion in the z-direction due to being constrained on the substrate by use of Equation 3.12, where $\alpha_{f,z}$ is the corrected through-plane CTE of the

polymer. This correction accounts for the in-plane contributions to the through-plane volume change due to the constraint of the Si wafer.

$$n(\lambda) = K_1 + K_2\lambda^{-2} + K_3\lambda^{-4} \tag{3.11}$$

$$\alpha_{f,z,measured} = \alpha_{f,z} + \left(\frac{2\nu_f}{1-\nu_f}\right)[\alpha_{f,xy} - \alpha_{s,xy}] \tag{3.12}$$

Glass transition temperatures (T_g) were measured by differential scanning calorimetry (DSC) with a TA Instruments DSC Q20 equipped with a Q-series DSC pressure cell. Measurements were taken under an unpressurized, nitrogen atmosphere. DSC samples were heated to 160°C at a rate of 10°C min^{-1} and then cooled to 60°C to remove the thermal history. Samples were again heated to 160°C at a rate of 10°C min^{-1} for T_g measurements. Thermogravimetric analysis (TGA) was performed with a TA Instruments TGA Q50. TGA samples were heated on a platinum pan at 3 to 5°C min^{-1} to a final temperature of 500°C.

3.2.6 Electrical Characterization

The electrical properties of the films were measured by fabricating parallel plate capacitors. Substrates were prepared by first growing 500 nm of thermal oxide on the silicon wafers for electrical insulation. Aluminum was deposited by electron beam evaporation using a Kurt Lesker PVD75 to a thickness of 300 nm as measured by a QCM. Films were spin-cast and cured by the same processes as stated above. Two different methods were used for fabricated the top aluminum pads. For samples in Chapter 6, aluminum was deposited by electron beam evaporation using a Kurt Lesker PVD75 to a thickness of 300 nm as measured by a QCM. Films were spin-cast and cured by the same process as stated above. Aluminum was deposited on the top of the cured films by the same process. The top layer of aluminum was patterned into circular pads

with a radius of 500 μm using photoresist, NR7-1500P, and the recommended processing. The photoresist pattern was transferred to the aluminum with a phosphoric acid/acetic acid/nitric acid wet etch for 210 s at room temperature. The remaining photoresist was stripped with acetone. In Chapter 7, this procedure was improved by using a shadow mask. To deposit the top aluminum pads, aluminum was evaporated onto the top of the sample through a molybdenum shadow mask with 500 μm radius holes.

Samples were dried at 150°C for 3 hr immediately prior to measuring the capacitance, C. The capacitance was measured at 200 kHz with a GW Instek LCR-800 on a Karl Suss probe station using a parallel RC model. The dielectric constant (i.e. real part of the complex permittivity), ε_r, was calculated from Equations 3.13 and 3.14, where ε_o is the permittivity of free space, d_f is the dielectric thickness, and A is the area of the aluminum pad. The dielectric constant was corrected for fringing fields with ASTM standard D150-11 by calculating an edge capacitance, C_e, based on the approximate dielectric constant, ε_r, film thickness, d_f, and perimeter, p.[99] The edge capacitance was then subtracted from the original capacitance, and a new dielectric constant was calculated. The imaginary, or unrecoverable portion of the permittivity is represented by tanδ, which is the tangent of the angle between the impendance vector and the negative imaginary axis on the complex impedance plane.

$$C = \frac{\varepsilon_o \varepsilon_r A}{d_f} \tag{3.13}$$

$$C_e = \left(0.0041\varepsilon_r' - 0.00334\ln\left(d_f\right) + 0.0122\right)p \tag{3.14}$$

3.2.7 Other Characterization

For swelling measurements, the masses of 100 mm Si wafers were measured prior to processing. Films were spun and cured as stated above. Initial mass of the films (M_0) was calculated as the sample mass after cure less the mass of the Si wafer. Samples were

placed in a bath of the swelling solvent and removed at regular time intervals to measure the masses. The time-dependent swelling ratio (SR_t) was calculated by Equation 3.15, where m_0 is the initial mass and m_t is the mass at a given time point.

$$SR_t = \frac{m_t - m_0}{m_0} \tag{3.15}$$

GPC was performed with a Waters 2690 separation module and a 2410 differential refractive index detector. These were connected to Waters Styragel columns (HP 1, HP 3, and HP 4), and THF was used as an eluent and solvent. Molecular weights were compared to polystyrene standards.

CHAPTER 4

DNQ-BASED POLYNORBORNENE DIELECTRIC: LITHOGRAPHY

Reproduced in part, with permission, from B. K. Mueller, E. Elce, A. M. Grillo, and P. A. Kohl, "Positive-tone, aqueous-developable, polynorbornene dielectric: Lithographic, and dissolution properties," J. Appl. Polym. Sci., vol. 127, no. 6, pp. 4653–4661, 2013.

4.1 Motivation and Critical Requirements

The goal of this project was to develop a positive tone dielectric based on the same polymer in the negative tone Avatrel 8000P. The base polymer in Avatrel 8000P is a random copolymer of hexafluoroisopropanol norbornene (HFANB) and carboxylic acid norbrnene (CBANB). Three polymers were donated by Promerus, LLC for this purpose. PNB-A and PNB-B were 75/25 and 90/10 mol% random copolymers of HFANB/CBANB, respectively. PNB-C was a homopolymer of HFANB. Since HFANB has a similar pK_a to novolac, it was hypothesized that these polymers could be inhibited by the addition of DNQ.[100] Since the DNQ would interact with the polymer through hydrogen bonding, this could enable lower loadings of DNQ than in other dielectric materials. It was first necessary to evaluate available PACs for their viability in this dielectric. Notably, miscibility and dissolution inhibition were key requirements. Photobleaching of the DNQ is also a requirement for exposure of thick films.

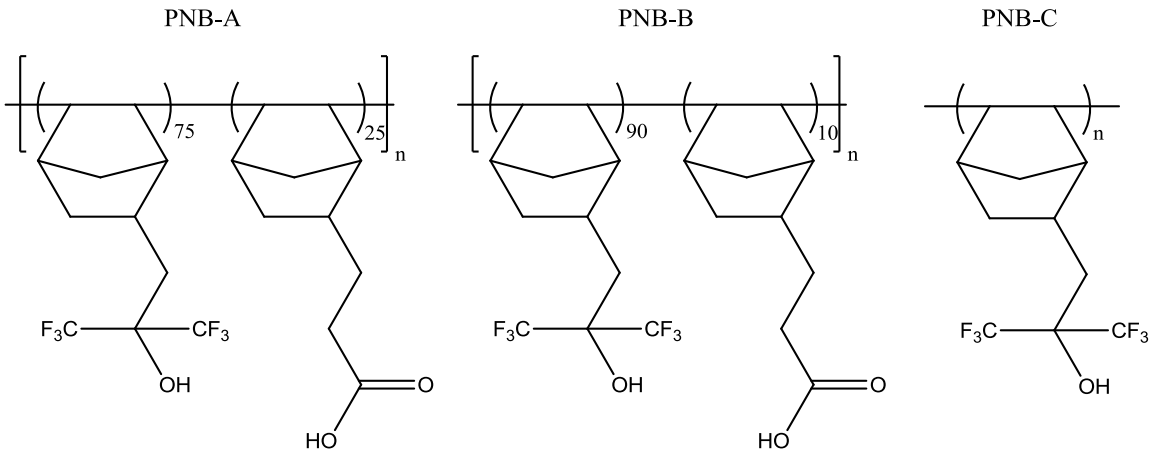

Figure 4.1: Structure and monomer ratios of PNB-A, B, and C

After selection of an appropriate photoactive compound (PAC), the dissolution properties of the PAC-loaded PNB polymers were desired. It was hypothesized that the monomer ratios in PNB-A, B, and C would substantially affect the dissolution characteristics, and therefore the lithographic properties. From these results, a leading PNB/PAC combination could be chosen with the best properties to move forward.

Unlike Avatrel 8000P, PAG could not be included in the positive tone formulations since it would initiate cross-linking in exposed regions. However, epoxy cross-linking was still desired for the curing reaction. After the best PNB/PAC combination was determined, it was then necessary to evaluate the effect of epoxy additives on the dissolution properties of the films. Finally, these results could be used to formulate a dielectric with excellent lithographic properties.

4.2 Effect of PAC Structure on Miscibility and Dissolution

To incorporate DNQ into the polymer film, the DNQ moiety was covalently bonded to a ballast molecule. The DNQ and ballast together make the PAC in this system. The PACs are synthesized by reacting a 2,1,5-DNQ sulfonic acid with a molecule containing phenolic hydroxyl groups to form a 2,1,5-DNQ sulfonic acid

ester.[35], [101] Generally, the ballast molecule is multifunctional, so more than one DNQ can be bound to it. This can also result in partial substitution of the phenolic hydroxyl groups.

Three different ballast molecules were used to make four different PACs. PAC1 had a ballast molecule of 2,4-dihydroxybenzophenone esterified at 100% with DNQ. PAC2 and PAC3 had a ballast molecule of trisphenol-PA, where PAC2 was substituted at 67% and PAC3 was substituted at 83%. PAC4 had a ballast molecule of 4,4'-(2-methylpropylidiene)bis[2-cyclohexyl-5-methyl-phenol] esterified at 100%. All PACs had an average of two DNQs per ballast molecule, except PAC3 which had an average of 2.5 DNQs per ballast molecule. Figure 4.2 depicts the ballast molecules of each PAC in the left column. In the right column of Figure 4.2, optical microscope images of PNB-A film with the respective PAC are shown.

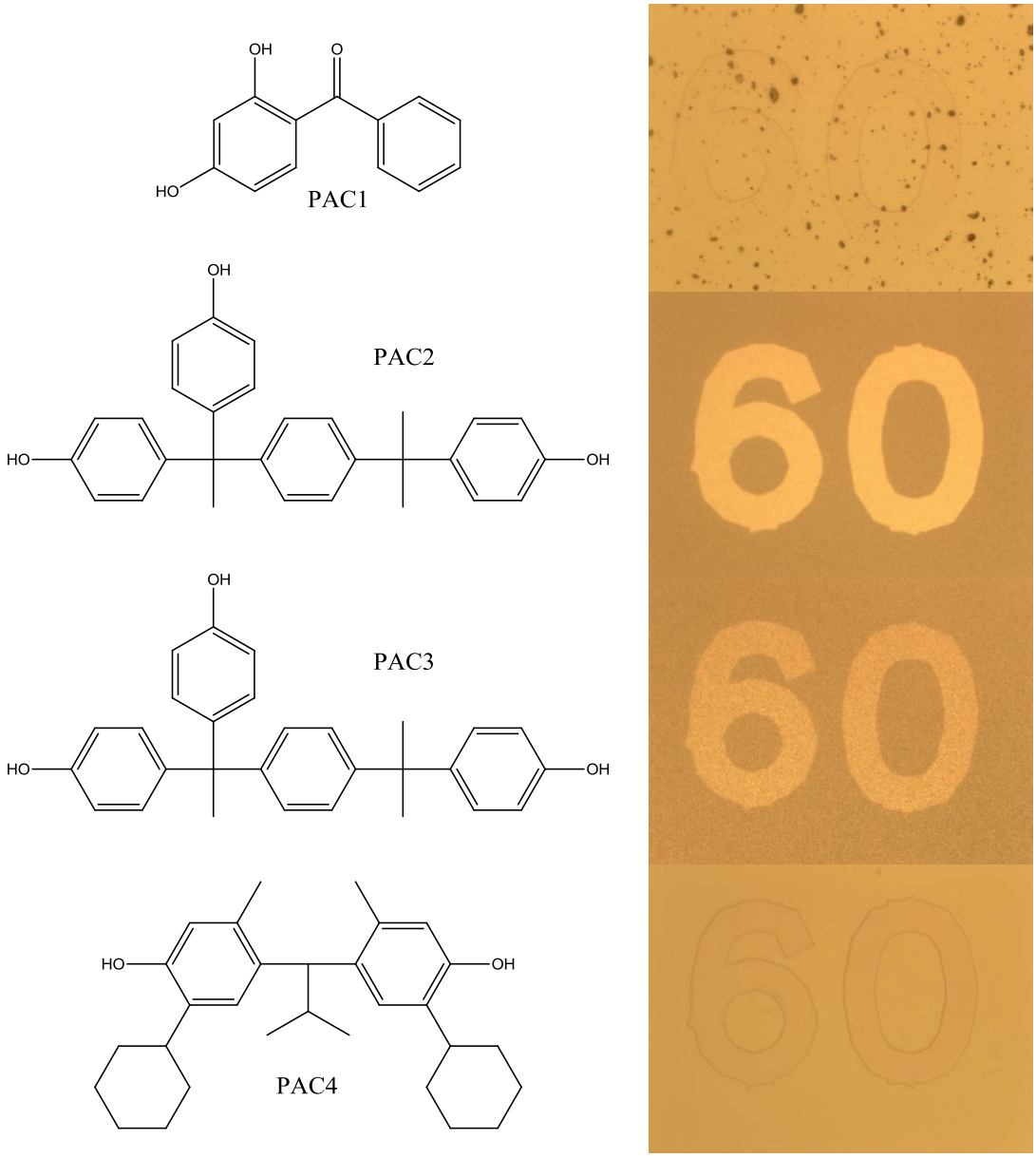

Figure 4.2: Chemical structures of PAC ballast molecules (left) and images of PAC-loaded PNB films (right)

4.2.1 Miscibility and Residues

Three PACs were initially investigated with the PNB-A polymer. The first, PAC1, a difunctional hydroxybenzophenone-type DNQ, is often used in novolac photoresists. All formulations containing PAC1 had poor miscibility resulting in visible precipitates

which were observed using an optical microscope after spin coating, as shown in Figure 4.2. The particle sizes ranged from 1 μm to more than 100 μm in diameter. A flaky brown film around exposed features was formed when the films were developed in 0.26 N TMAH. This brown film also formed in the light field region when large area films were exposed to UV radiation. The brown film appeared within the first few seconds of development when the exposure dose was low, 50 to 250 mJ cm^{-2}, for 15 μm thick films. It was also observed in a sample that received a gradient exposure dose that the brown film appeared during development when structures of varying exposure dose were developed across the same sample. The brown film took longer to appear at high exposure doses (>250 mJ cm^{-2} in 15 μm films). Finally, at a sufficiently high dose, the brown film did not appear in the light field region of the exposed films. However, the brown film still formed at feature edges when the exposure dose was high. This was because the optical dose at the transition region from the irradiated to unirradiated region at the edge of the features was less than the full exposure dose and within the values cited above for producing a brown film.

Formulations were made of PNB-C (i.e., HFANB) and PAC1. Films produced from these mixtures showed the same random precipitate. A similar brown color was observed during development, but it formed more slowly with time, compared to films made from PNB-A. It was also observed that the dissolution rate of PNB-C in base was much slower than that of PNB-A.

Mixtures of PNB-A and PAC2 in PGMEA appeared to be completely miscible after spin coating. However, the solvent-cast films became opaque almost immediately during soft baking at 100°C. Upon closer investigation with an optical microscope, it was seen that this opacity was a result of phase segregation. This effect was worse in formulations with higher PAC2 loading. These observations indicate that PAC2 has limited miscibility with PNB-A. Development of these films in 0.26 N TMAH produced the same brown color in the spin-cast film as previously noted. However, the brown film

formed in PNB-A with PAC2 was less flaky and more gel-like than the other brown films, causing it to smear over the sample. The brown film residue produced from PNB-A with both PAC1 and PAC2 are shown in Figure 4.3.

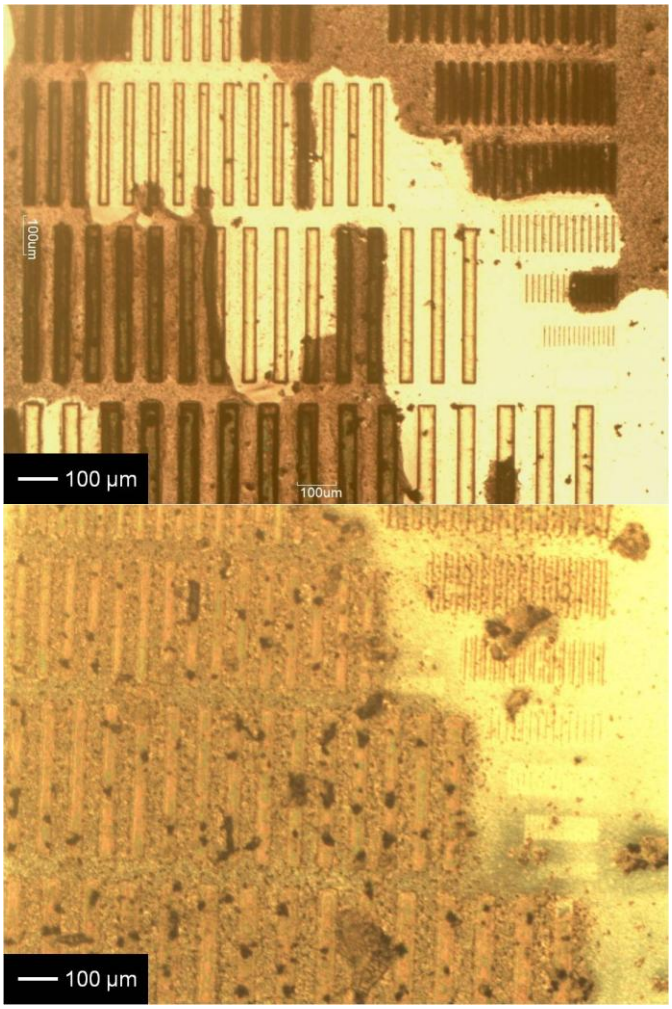

Figure 4.3: Brown residue from PNB-A with PAC1 (top) and PAC2 (bottom)

PNB-C/PAC2 formulations were also made. Films of these mixtures showed phase segregation to a greater extent than films with PNB-A. The brown color appeared more slowly in these formulations compared with the films made with PNB-A. The dissolution rate of the PNB-C/PAC2 films was very slow. The higher degree of phase segregation with PNB-C, compared to films made with PNB-A, implies that the CBANB

(25 mol% in PNB-A) increased the miscibility with PAC2. That is, the carboxylic acid functionality of the polymer improved the polymer/PAC miscibility and raised the dissolution rate. The increased miscibility between the PAC and PNB was likely caused by the increased polarity of the CBANB compared with the HFANB. The polar DNQ moiety was then more miscible with polymers that contained a higher content of polar CBANB. Formulations of PNB-A and PAC3 were also spin coated to form thin films. These samples, however, showed a greater degree of phase segregation than did formulations of PNB-A and PAC2. The greater degree of substitution from 67% to 83% worsened the miscibility of the PAC with PNB.

Finally, formulations were made with PNB-A and PAC4. As seen in Figure 4.2, these films were of excellent quality, and no particles or phase segregation were observed. Dissolution of these films appeared slower than formulations of PNB-A with other PACs. With this decrease in dissolution rate, the brown film observed with other PACs was also slightly, though not completely mitigated. The film formed more slowly and to a lesser degree.

4.2.2 Photobleaching of DNQ

UV–vis spectroscopy was used to understand the extent of DNQ photobleaching. PNB-A films with 27 mass parts DNQ per hundred mass parts resin (pphr) PAC1 were coated to a thickness of 16 to 17 μm. Figure 4.4 shows the absorption coefficient at 365 nm for the PNB-A/PAC1 formulation plotted against the exposure dose per micrometer of film thickness. The results show that the absorption coefficient at 365 nm for the unexposed film is 0.23, with a gradual decrease in the absorption coefficient of the film with exposure dose. This decrease in absorption coefficient continued until the dose reached ~95 mJ cm^{-2} μm^{-1} at which point the absorption coefficient became 0.04. Above ~95 mJ cm^{-2} μm^{-1}, there was little change in the absorption coefficient with UV dose. Initially, the optical dose deep in the film was low due to the high absorbance in the

upper regions of the film. As the upper layer of the film was exposed, its absorbance decreased which gave a higher UV intensity deep in the film. Hence, it is possible that the film consisted of two states during and after exposure: (i) fully exposed and (ii) underexposed. The fully exposed region was exposed to enough UV radiation to convert all DNQ to ICA, whereas the underexposed region was not fully exposed and thus contained both DNQ and ICA. A dose of 95 mJ cm^{-2} μm^{-1} was assumed to be the value at which the film was fully exposed in this experiment. This value is dependent on the PAC loading in the film.

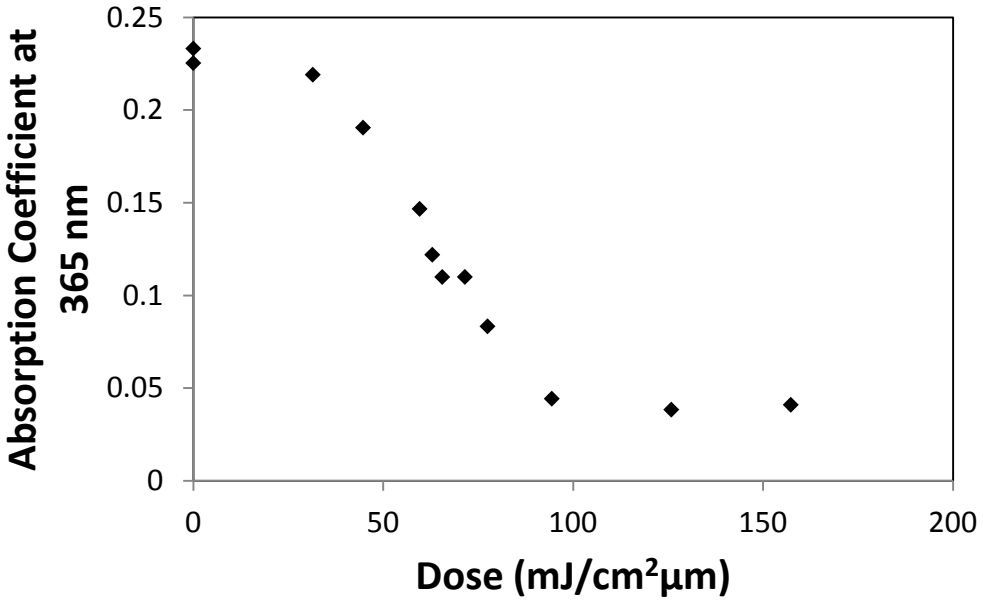

Figure 4.4: Photobleaching of PAC1 in PNB-A

The dose needed for full bleaching correlated well to the dose at which the brown film no longer formed during development in 0.26 N TMAH. From this result, it was concluded that the brown film was seen during the develop step only when both DNQ and ICA were present in the film. Others have shown that reactions of DNQ and ICA are possible, several of which may have little or no solubility in aqueous base.[102]–[104] It

was speculated that the brown film is the product of a reaction of DNQ and ICA, resulting in an insoluble, high molecular weight compound. This product would explain why no brown film was seen in fully exposed samples. Further, this explains why the brown film was more gel-like for formulations with PAC2. This was because the PAC2 ballast molecule initially had three hydroxyl groups but was only esterified with two 2,1,5-DNQ sulfonic acid groups on average. The nonesterified hydroxyl site on the ballast portion of the PAC2 molecule could react with base and make the brown film swell in aqueous base. From these results, the factors that most affect the lithographic properties of the PNB/PAC mixtures are PNB-PAC miscibility and degree of PAC substitution. The degree of immiscibility between PNB and the PAC caused film defects to occur that decreased product yield. It was also determined that PACs with 100% esterification performed better than the PACs with incomplete esterification due to the reactivity of unesterified hydroxyl groups with base.

The hypothesis that a DNQ/ICA reaction product occurs implies that the brown film can be formed in any DNQ-containing photoresist, as long as the dose is sufficiently low and the dissolution rate is sufficiently high. In an effort to investigate this effect, AZ P4620 was spin-coated to 14 μm thickness and processed by the same methods as the PNB formulations. AZ P4620 is a novolac/DNQ-based photoresist with a similar PAC to PAC1. At exposure doses of < 25 mJ cm^{-2}, the same brown color film was seen during the initial stages of development in 0.26 N TMAH. At this low dose, it was likely that the region of the film closest to the substrate contained both DNQ and ICA. The surface region was also exposed to the highest concentration of base during development.

4.2.3 DNQ Reaction

In an attempt to mitigate the formation of the brown film, an experiment was performed varying both the DNQ loading and the aqueous base developer normality. Formulations were made with PNB-A and PAC2 at three different loadings, 15.6, 20.0,

and 25.0 pphr. PAC2 was chosen over the other PACs because it did not form large precipitates like PAC1, and it was more miscible with PNB-A than was PAC3. To compensate for the varied PAC2 loading, each formulation was exposed to 0.833 mJ cm^{-2} um^{-2} per pphr PAC2. Films were then developed in 0.26, 0.195, and 0.13 N TMAH. Optical images of the resulting bright-field patterns are shown in Figure 4.5. It was observed that the formation of the brown film was worse at lower PAC2 loadings and higher TMAH normalities. The best image was formed with 25.0 pphr PAC2 developed with 0.13 N TMAH. This suggests that dissolution rate and aqueous base concentration in the film played a significant role in the formation of the brown film.

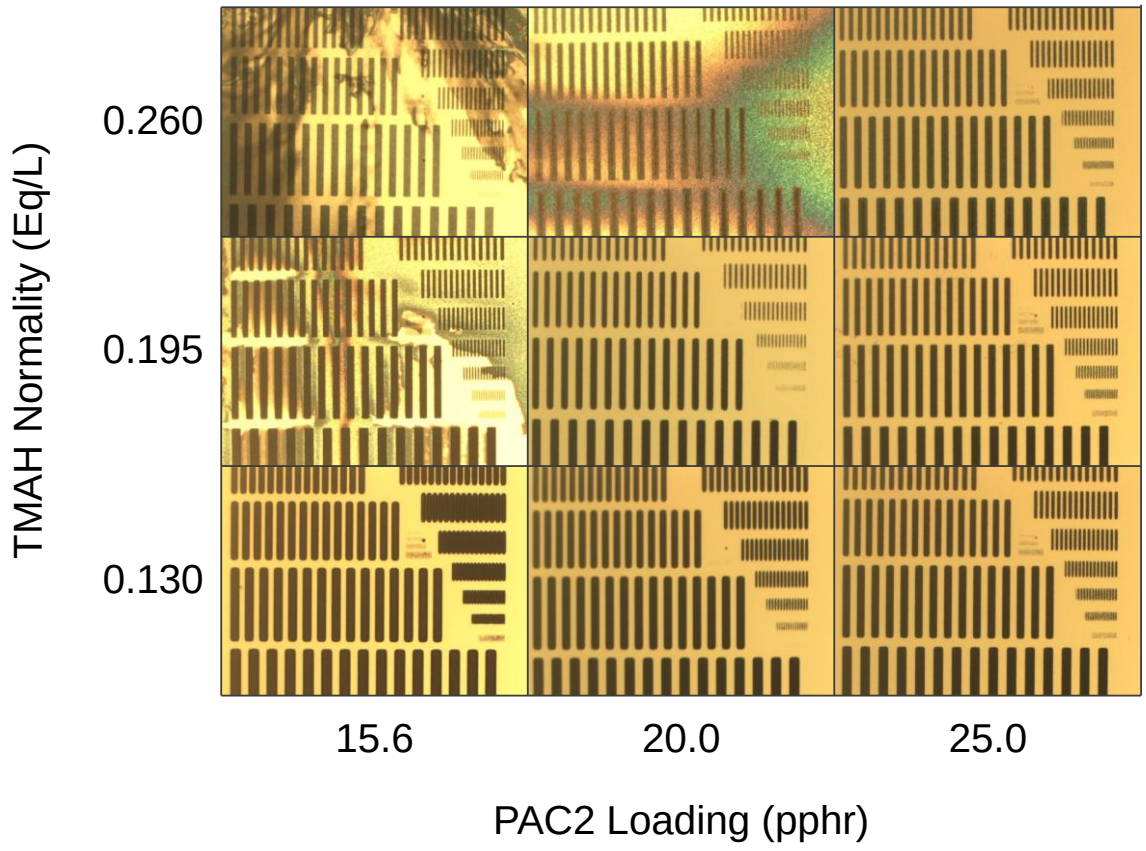

Figure 4.5: Effect of base normality (y-axis) and PAC2 loading (x-axis) on lithography

4.3 Effect of Copolymer Composition on Dissolution

The PNB copolymers studied in this work are composed of two monomers, each of which is susceptible to deprotonation by aqueous base. Carboxylic acids generally have a pKa value of 3 to 4, whereas the fluoroalcohol has a pKa of 9 to 10. Thus, it is expected that the deprotonation of CBANB occurs first (before HFANB) as base penetrates the film and the pH rises. However, since the molar percentage of CBANB in PNB-A is only 25 mol%, it is not expected that deprotonation of all CBANB moieties will result in dissolution of the polymer film.

The dissolution of PNB-A, PNB-B, and PNB-C mixtures were characterized using a quartz crystal microbalance (QCM) to monitor the sample mass as a function of time in the developer. At resonance, the frequency shift of the QCM is inversely proportional to the change in mass. Figure 4.6 shows the QCM responses for the three polymers, with the observed change in normalized mass plotted versus time. Measuring the slope of this curve during dissolution provides a mass dissolution rate. The bottom graph in Figure 4.6 shows the QCM resistance as a function of time for the same samples. This resistance is a measurement of the energy dissipated by the viscous layer on the solid polymer film on the quartz crystal.[105], [106] As the polymer takes up aqueous base, a gel layer is formed. The mechanical properties of this gel layer are different from that of the dry film. The magnitude and importance of the gel layer can be qualitatively understood by monitoring the resistance.

As seen in Figure 4.6, there is a period of several seconds where no effect of the TMAH was seen. This was due to the distance of tubing between the valve and the sample. Once TMAH reached the samples, the resistance increased for all three samples, indicating that a gel layer formed. For PNB-B and PNB-C, the resistance increased slightly but leveled off at a near-constant value, so the gel layer was of constant thickness throughout the dissolution. PNB-A, on the other hand, exhibited a gel layer that grew until it reached the QCM substrate. Unfortunately, since the rate of developer uptake and

rate of polymer dissolution did not match, the dissolution rate of PNB-A could not be calculated. The mass measurement is a convolution of aqueous base uptake and polymer decoupling from the QCM oscillation. It can be seen in the top graph of Figure 4.6, however, that the dissolution rate of PNB-B was higher than that of PNB-C. This was an expected result due to the increased CBANB content in PNB-B. The dissolution rates for PNB-B and PNB-C without additives were calculated to be 8.7, and 5.9 μm min^{-1}, respectively. The conversion of normalized mass to thickness was calculated with a density of 1.3 g cm^{-3}, found by mass and thickness measurements.

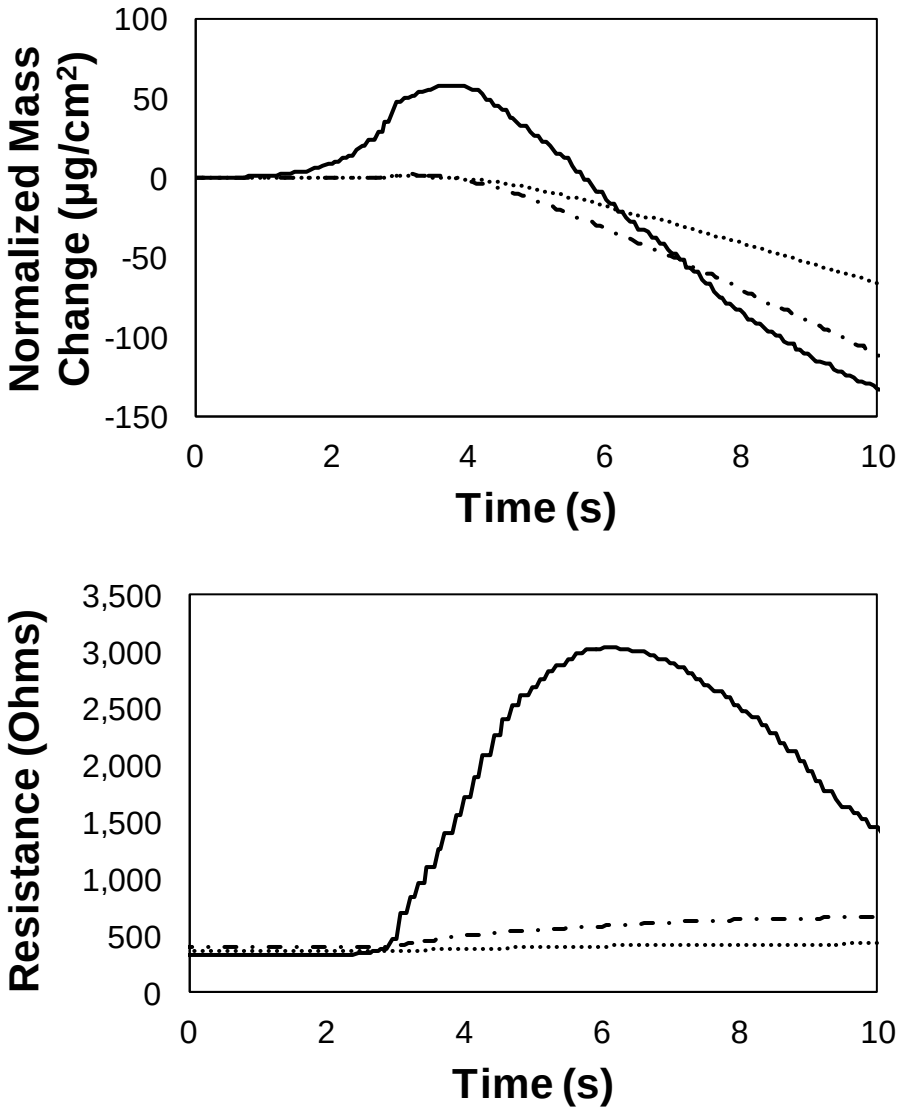

Figure 4.6: QCM traces of normalized mass change (top) and resistance (bottom) during dissolution. Legend: PNB-A (solid), PNB-B (dashed), PNB-C (dotted)

4.3.1 Meyerhofer Plots

The dissolution rate of polymer films was measured and the logarithmic rate was plotted versus PAC4 concentration in a Meyerhofer-type fashion. These plots are shown in Figure 4.7 for the three polymer mixtures. PNB-B and PNB-C exhibited a decrease in dissolution rate with increasing PAC4 loading, which is also expected and typical of

DNQ-type photoresists. However, these two polymers also showed a decrease in dissolution rate with increasing amounts of ICA (formed by exposure to UV radiation), which is not typical for positive tone, DNQ-based materials.[32] Generally, the dissolution rate of the exposed film remains constant or increases with ICA loading. In this regard, the dissolution of PNB films appeared to differ from the dissolution of novolac resists. This may be attributed to a large hydroxyl string reconnection efficiency after exposure originating at the PAC sulfonyl moieties. PNB-A appeared to show little change in dissolution rate with increasing PAC4 concentration between the exposed and unexposed films. However, the high resistance value indicated that a substantial gel layer formed during developing. The gel layer was soft enough so that it could not follow the QCM oscillations without significant energy loss. Thus, the film decoupled from the oscillator. This supports the conlcusion that the aqueous base penetration rate into the PNB-A film was faster than the dissolution rate of the film. This resulted in a net influx of aqueous base into the film causing the film to gel. The increase in resonant frequency of the QCM occured quickly once the sample is immersed into base. The frequency quickly reached a steady value; however, the resistance was slower to reach an equilibrium value. This higher resistance indicates that the physical presence of the film caused viscous energy loss even though the QCM frequency showed complete loss of mass.

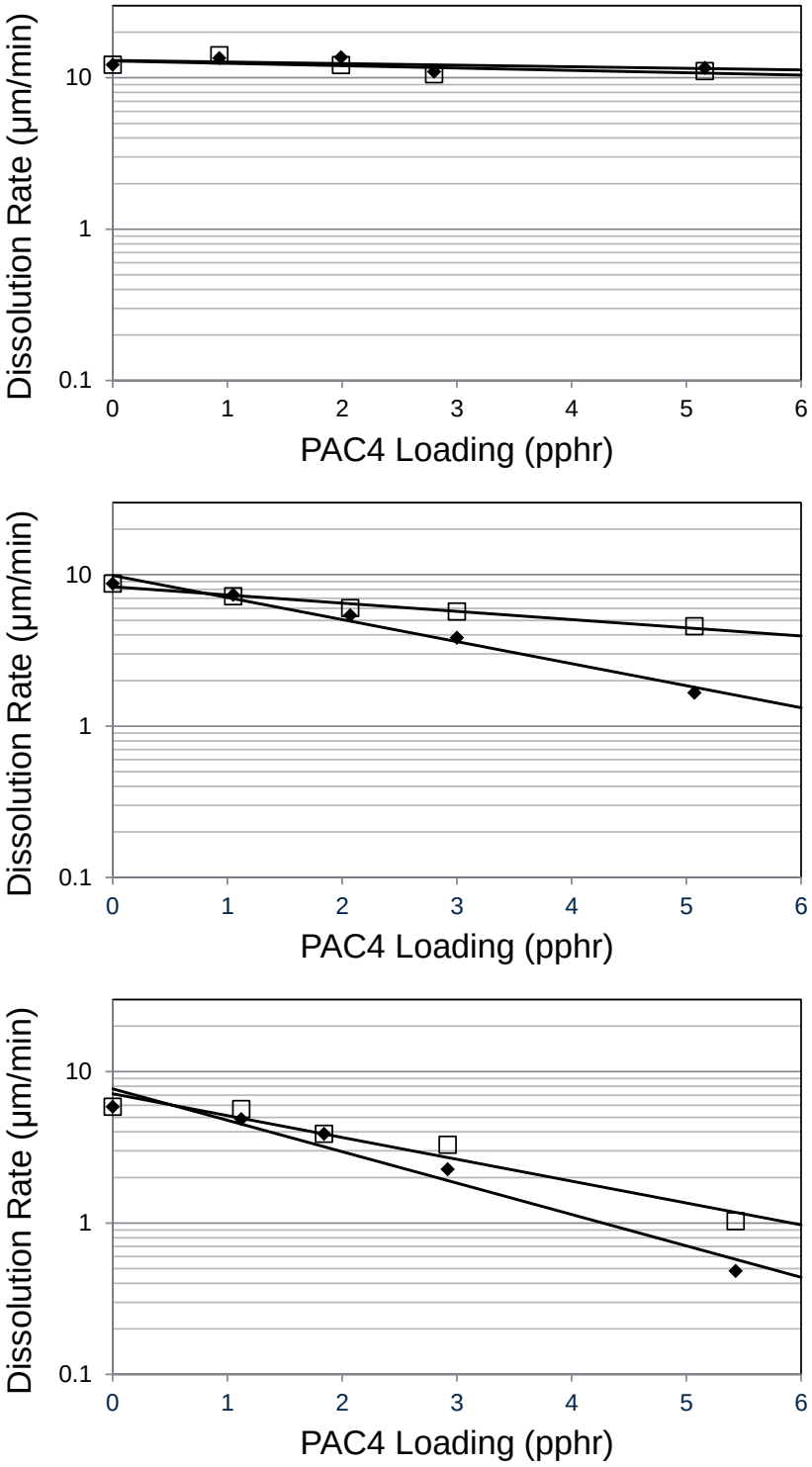

Figure 4.7: Meyerhofer plots of PNB-A (top), PNB-B (middle), and PNB-C (bottom) as a function of PAC4 loading. □ = unexposed, ♦ = exposed

The dissolution rate of the exposed and unexposed polymer films containing 20 pphr PAC4 were also measured by QCM. PNB-B and PNB-C were found to show similar characteristics. The unexposed films of each formulation showed no measureable change in mass indicating that these films were completely inhibited by the 20 pphr PAC4. After exposure to UV radiation, the films had a finite solubility that was almost two orders of magnitude less than the pure polymer films. Films of PNB-A with 20 pphr PAC4 showed a much different behavior. The observed dissolution rate of the UV-exposed films of PNB-A and 20 pphr PAC4 were calculated to be 8.4 μm min^{-1}. The dissolution rate of this formulation was confirmed by measuring the dissolution rate of films during puddle development.

4.3.2 Inhibited Formulation

Unexposed films of PNB-A with 20 pphr PAC4 displayed a different behavior from the similar mixtures with PNB-B or PNB-C. When exposed to aqueous base, the mass and resistance measurements rapidly increased. The resistance for films >200 nm increased to very high values and eventually the QCM stopped oscillating. For this reason, thinner films of PNB-A with 20 pphr PAC4 were cast (~185 nm thick or ~24 μg cm^{-2}). The QCM response of the thin films was monitored during development in aqueous base and is shown in Figure 4.8. Rapid increases in mass and resistance were again observed. These mass and resistance values peaked shortly after immersion in aqueous base and then fell. The final, steady-state frequency obtained in aqueous base would correspond to removal of most of the film; however, the final value of resistance was much higher than expected if this were the case. Water was then flowed into the QCM flow cell after the TMAH. If the film had dissolved, there would have been little change in frequency or resistance. Note, only a slight change in frequency and resistance was observed by changing the viscosity of the solution from water to aqueous base on a clean QCM. However, in the case of inhibited PNB-A, the change to water caused a large

decrease in frequency and increase in QCM resistance. After a long period of time where water flowed through the cell (much longer than the period shown in Figure 4.8), the frequency reached a value that corresponded to triple the initial mass. The resistance returned to a low value. Examination of the QCM after removal from the liquid cell indeed showed that undissolved polymer film was still present on the QCM surface. Taken together, these results show that the film swelled in aqueous base to the point of gelation with high energy loss so that the QCM response no longer reflected the correct mass. Once the film was immersed in pure water, the film returned to a rigid state with an increase in mass.

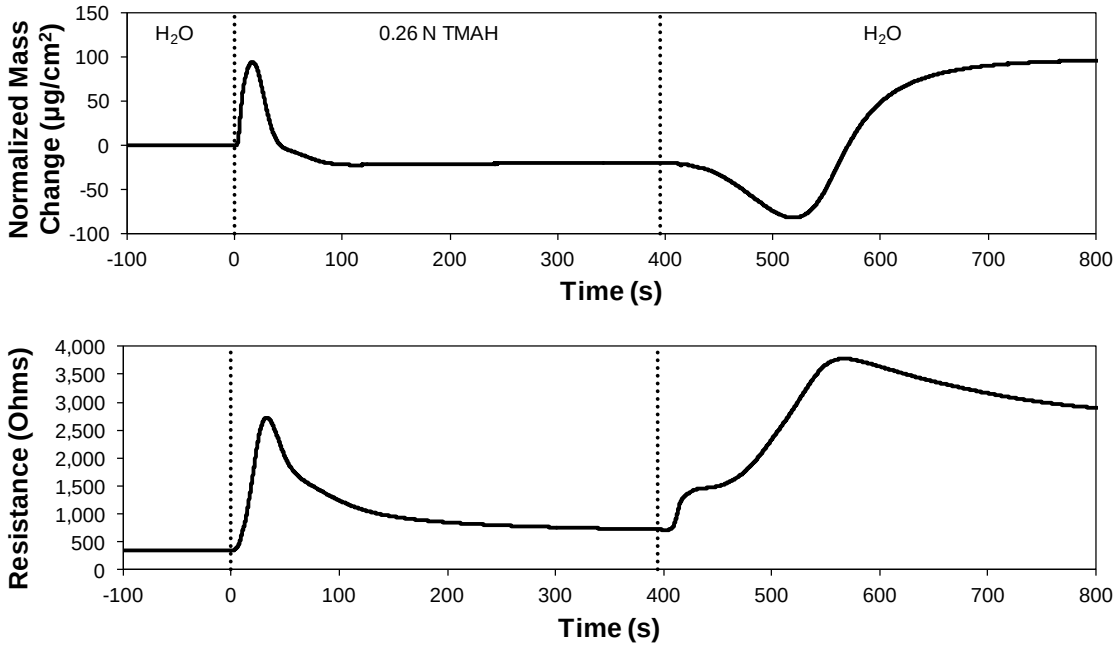

Figure 4.8: QCM traces of PNB-A inhibited with 20 pphr PAC4

4.3.3 Dissolution with Two Acidic Functional Groups

These PNB copolymers exhibit unique dissolution behavior that is attributed to the presence of two acidic functional groups on the PNB backbone. This is not the case

for other aqueous base developable dielectrics. The more acidic CBANB is deprotonated by TMAH much quicker than HFANB. However, 100% deprotonation of the CBANB would not be enough to solubilize any polymer molecule because only 25 mol% of PNB-A is CBANB. A large portion of the HFANB must also be deprotonated by TMAH before the polymer will dissolve. The formation of carboxylate anions in the film creates polar sites for water and TMAH to be absorbed. The absorbed TMAH can then either react with HFANB or penetrate deeper into the film by deprotonating another CBANB. This phenomenon causes PNB copolymers to swell quickly but dissolve more slowly. In contrast, PNB-C only has one acidic functional group and has a well-behaved dissolution. The formation of a gel layer by TMAH and the dissolution of PNB-C at the liquid interface occur at the same rate, so the thickness of the gel layer is constant during the bulk dissolution.

In inhibited films, the presence of the CBANB is substantial. Since the HFANB is inhibited by DNQ, it is not deprotonated by TMAH. However, the CBANB remains uninhibited, so polar pathways can be formed in which water and TMAH swell the film. If no other changes are made, this would result in a substantial amount of aqueous base present in the film before curing.

4.4 Hydrogen Bonding in DNQ-Loaded PNB Films

Studies of hydrogen bonding in HFANB-containing polymers have been previously reported.[93], [107] These studies showed that the ratio of free hydroxyl groups to hydrogen bonded hydroxyl groups could be measured by IR. Hydrogen bonding of the hydroxyl group raised its pK_a and lowered the dissolution rate of the films. Similar measurements were performed here to study the effect of PAC loading on the hydrogen bonding in the PNB-C film. Fourier transfer infrared spectroscopy (FTIR) measurements of PNB-C films containing 0, 5, and 20 pphr PAC4 were used to examine

the bonding environment and quantity of hydroxyl groups present. The hydroxyl stretching region occurs between 3000 and 3700 cm^{-1}. The peak associated with ‘‘free hydroxyl’’ occurs at 3600 cm^{-1}, whereas the hydrogen-bonded hydroxyl stretch has a broader peak between 3500 and 3300 cm^{-1}. The relative area associated with each peak was used to evaluate the fraction of hydroxyl groups associated with each state. Figure 4.9 is an FTIR spectrum of a PNB-C (i.e., HFANB homopolymer) film, which shows three possible hydroxyl peaks. The data from this study is shown in Table 4.1. In the PNB-C film with no additives only 10% of the hydroxyl groups were free. This concentration was smaller than in previous studies; however, the soft bake temperature used here was substantially lower than in the previous studies. The films in this work were soft baked at 100°C to avoid significant thermal activation of the DNQ. At this temperature, it was possible that residual solvents remained in the film which affected the hydrogen bonding of the fluoroalcohol groups.

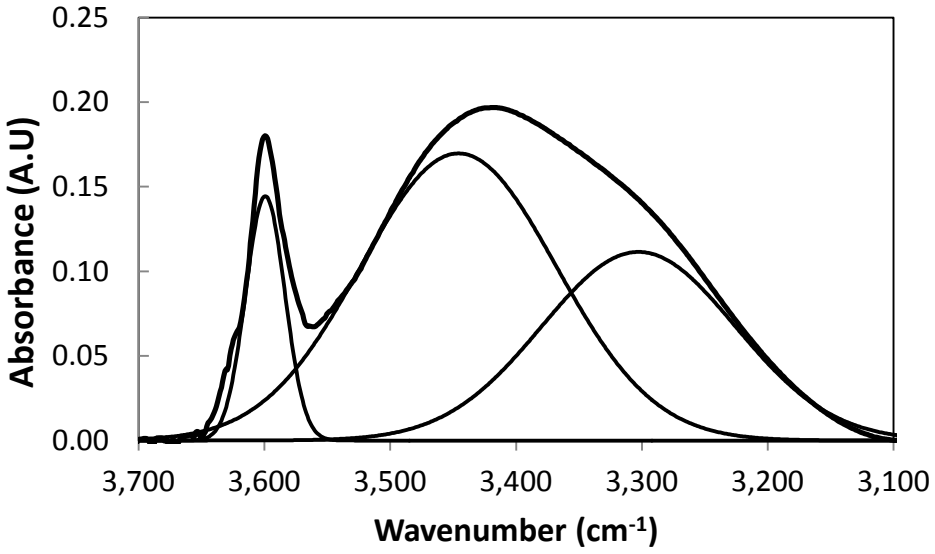

Figure 4.9: FTIR hydroxyl stretching regions of a PNB-C film

The addition of 5 pphr PAC4 resulted in a small increase in the free hydroxyl content to 12%. It was expected that a decrease in hydrogen bonding would cause an increase in the dissolution rate. However, the addition of 5 pphr PAC4 to PNB-C lowered the dissolution rate by a factor of 10 compared with films of pure PNB-C. An explanation for this may be that PNB-C had a large degree of hydrogen bonding without additives, and the introduction of large molecule, PACs disrupted the hydrogen bonding. The PAC lowered the dissolution rate of the film due to the insolubility of the high molecular weight, unexposed PAC in aqueous base. After complete UV exposure, the percentage of free hydroxyl groups remained the same at 12%. However, the dissolution rate more than doubleed after exposure. Further, increasing the PAC4 loading to 20 pphr caused the percentage of free hydroxyl groups to decrease to 7%. Again, exposure of this film caused no change in the free hydroxyl peak. In this case, the unexposed film was completely inhibited to development by aqueous base. Exposure of the film caused it to become soluble, although the dissolution rate was low. The first conclusion made from these results was that pure PNB-C had a large degree of hydrogen bonding without the addition of a PAC. In addition, the inclusion of a PAC did not change the hydrogen bonding to any appreciable extent. The result that UV exposure did not change the degree of hydrogen bonding was likely due to a number of factors. PNB-C already had extensive hydrogen bonding without the addition of DNQ, so the light-induced rearrangement of the carbonyl to a carboxylic acid may not have had a significant impact on the total hydrogen bonding effect. Furthermore, sulfonyl groups on the PAC remained unchanged after exposure. Reiser et al. found that the recombination of hydroxyl strings to these groups can be high.[32] It was then concluded that the largest effect of DNQ photolysis

on dissolution was the rearrangement of DNQ to be base-soluble. The presence of base-soluble ICA increased the dissolution rate compared with the unexposed state.

Table 4.1: FTIR hydroxyl peak percentages

PAC4 Loading	**3600 cm^{-1}**	**3450 cm^{-1}**	**3300 cm^{-1}**	**Dissolution Rate ($\mu m\ min^{-1}$)**
0 pphr	9%	55%	36%	5.8
5 pphr (unexposed)	12%	44%	44%	0.48
5 pphr (exposed)	12%	55%	33%	1.0
20 pphr (unexposed)	7%	30%	63%	~0
20 pphr (exposed)	7%	45%	48%	0.18

4.5 Effect of Additives on Dissolution

Permanent dielectric formulations are loaded with additives for a number of purposes.[108] Cross-linkers are incorporated to increase the cured T_g and to mechanically strengthen the material. Plasticizers are used to lower the modulus and increase plasticization so that thick, low stress films can be cast. Antioxidants increase the oxidative stability of the film during high temperature processing. Adhesion promoters increase the adhesion of the film to one or more surfaces by modifying the surface energy or by covalently reacting with the surface. PACs effect the lithographic solubility switching chemistry. Sensitizers increase the absorbance of the film at specific wavelengths useful for lithography.

4.5.1 Trimethylolpropane triglycidyl ether

Trimethylolpropane triglycidyl ether (TMPTGE) serves a number of purposes in DNQ-based PNB dielectrics. First, it acts as a plasticizer, enabling thick films > 10 μm in thickness. Additionally, TMPTGE has three glycidyl ether functional groups. These groups chemically react with the pendent carboxylic acid or alcohol pendent to the polymer backbone to form a covalently cross-linked film during cure. TMPTGE also increases the bonding strength to surfaces when they are modified with alcohols, carboxylic acids, or amines. Finally, the TMPTGE reaction with the carboxylic acid is expected to lower the permittivity, because the resulting alcohol is less polarizable than the carboxylic acid.

The dissolution rate of PNB-C was measured as a function of TMPTGE loading in the same manner that the Meyerhofer plots were created. This data is presented in Figure 4.10. Similar to the DNQ Meyerhofer plots, increased loading of TMPTGE decreased the dissolution rate of PNB-C logarithmically.

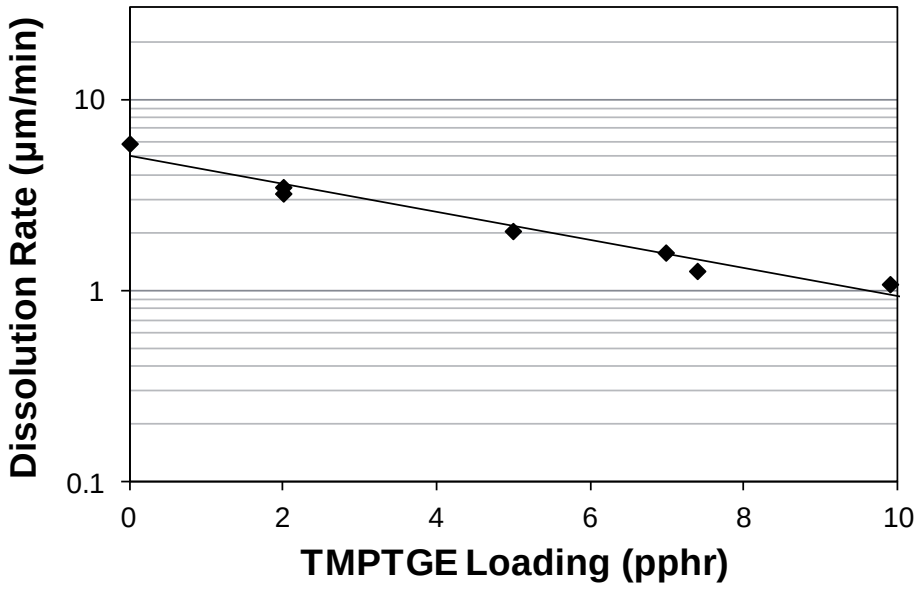

Figure 4.10: Effect of TMPTGE on PNB-C dissolution rate

This reduction in dissolution rate is generally favorable for PNB dielectrics, since it suggests that TMPTGE may lower the swelling of unexposed films. Final formulations would be made with PNB-A because the CBANB increased the overall film solubility in aqueous base developer. The CBANB is also more reactive than HFANB to the glycidyl ether on TMPTGE. This promotes the cross-linking of the film at lower cure temperatures.

Films of PNB-A with 20 pphr PAC4 were studied with the QCM to evaluate the effect of TMPTGE on dissolution and swelling rates of aqueous base developer. When unexposed, a PNB-A film with 20 pphr PAC4 quickly swelled with developer. The coupled mass quickly increased until the resistance to oscillation in the film was large enough to completely stop the oscillation of the QCM. The ability of this film to take up developer is due to the uninhibited carboxylic acids which can readily be deprotonated by TMAH, creating ionic pathways for water and base uptake. When 10 pphr TMPTGE was added to the formulation, the uptake of developer was slowed substantially.

When exposed, both films with 0 and 10 pphr TMPTGE became soluble in developer. Both films exhibited a linear decrease in mass when developer was introduced, indicating a steady state penetration of developer and dissolution of the film instead of first swelling and then dissolving. The film with 10 pphr TMPTGE had a lower dissolution rate, consistent with the addition of TMPTGE to PNB-C as measured previously. The film with 10 pphr TMPTGE also exhibited a noticeably longer period before dissolution begins. The two films were of different thicknesses, bringing about the difference in final mass between the two traces.

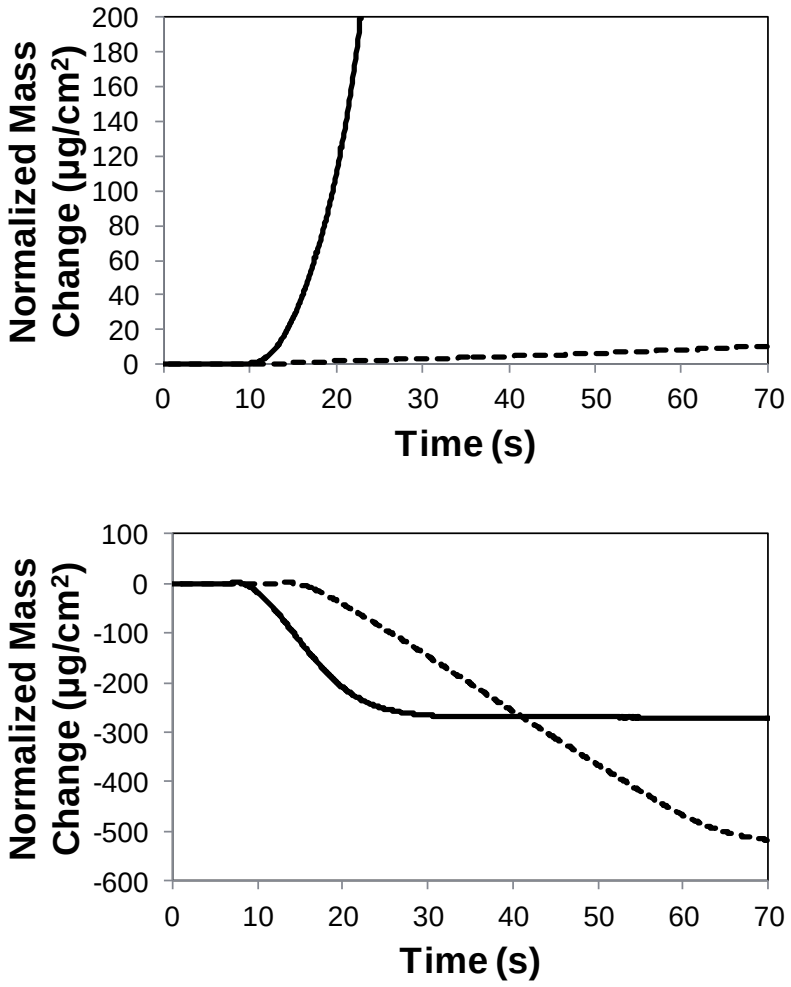

Figure 4.11: QCM traces of unexposed (top) and exposed (bottom) PNB-A formulations without TMPTGE (solid) and with 10 pphr TMPTGE (dashed)

There are several possible reasons for the dissolution slowing in TMPTGE-containing films. First, the TMPTGE may thermally react with CBANB or HFANB during the soft bake step at 100°C. This reaction is not likely to be extensive at 100°C, as Shechter et al. observed reactions times of approximately 4 hours at 125°C .[109] Films containing TMPTGE were baked and studied by FTIR to confirm the decrease of the glycidyl ether peaks at 862 and 920 cm^{-1}, however, no measurable decrease was

observed.[110] It is noted that even a small amount of cross-linking could substantially lower the dissolution rate because entanglement increases rapidly with cross-linking.

A second explanation is that TMPTGE reacts during dissolution. TMAH readily deprotonates CBANB and HFANB functionalities, and the resulting carboxyl and alkoxy anions, respectively, can readily initiate ring opening of the glycidyl ether on TMPTGE. An excess of TMAH could even directly ring open the glycidyl ether. The base catalyzed ring opening results in an alkoxy anion that can either be protonated by CBANB or HFANB, or it can ring-open another glycidyl ether group.

4.6 Lithographic Properties

The contrast, sensitivity, and maximum obtainable aspect ratio were evaluated for two different PNB/PAC formulations, Formulations X and Y. Formulation X contained PNB-A, 20 pphr PAC4, and 10 pphr TMPTGE. Formulation Y was the same as Formulation X, except the PAC4 loading was 25 pphr. The contrast and sensitivity of these two formulations were evaluated after development in 0.26 and 0.195 N TMAH. Samples were developed for 5 s longer than the time required to remove all film in the region of highest exposure dose. The regions of the film exposed to a dose > D_{100} dissolved at the same rate. Contrast curves of both formulations developed in 0.26 N TMAH is shown in Figure 4.12. The sensitivity of these two formulations, as given by the D_{100} value for Formulations X and Y, were 408 and 617 mJ cm^{-2}, respectively. The sensitivity is a function of the PAC loading, but it is not directly proportional to the PAC loading because of inefficient absorption of light (the quantum efficiency of DNQ is less than unity) and photobleaching in thick films.[111] Photobleaching is a decrease in absorption coefficient because of the chemical reaction of a DNQ after exposure to UV radiation. The D_0 values are almost identical for the two formulations. The contrast values of Formulations X and Y were calculated to be 2.3 and 1.5, respectively, in 0.26 N

TMAH. The decrease in contrast with increased PAC4 loading is a result of a higher D_{100} value for Formulation Y.

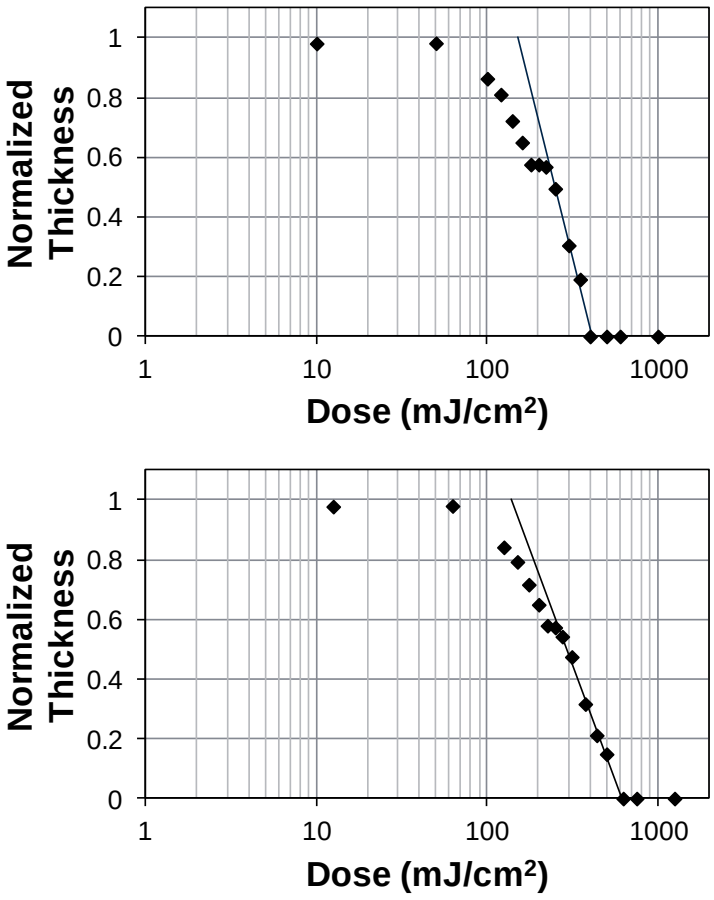

Figure 4.12: Contrast curves of Formulations X (top) and Y (bottom), developed in 0.26 N TMAH

The contrast values for Formulations X and Y in 0.195 and 0.26 N TMAH are tabulated in Table 4.2. At the lower developer concentration, 0.195 N TMAH, the contrast value for Formulation X dropped slightly to 2.0 whereas the contrast of Formulation Y remained unchanged at 1.5. The D_{100} value of each formulation was independent of the base concentration in the developer. This result shows that at the D_{100} dose, a critical fraction of the DNQ moieties in the deepest regions within the film, that

is, near the polymer–substrate interface, have been converted to ICA. This critical fraction is the amount of DNQ conversion required for the film to be soluble in aqueous base. These results indicate that this critical level of conversion of DNQ to ICA was not dependent on the base concentration over the range of concentrations used here.

Table 4.2: Contrast and sensitivity values of DNQ-based PNB

Formulation	DNQ (pphr)	Base Normality	Develop Time (s)	Contrast	D_0 (mJ cm^{-2})	D_{100} (mJ cm^{-2})
X	20	0.26	76	2.3	153	408
X	20	0.195	105	2	131	408
Y	25	0.26	79	1.5	138	618
Y	25	0.195	141	1.5	139	616

Figure 4.13 shows SEM images of Formulation Y developed in 0.26 N TMAH. The film thickness in Figure 4.13 was 9.2 μm. A dark field exposure showing line and space features in the film are shown in the top image of Figure 4.13. This formulation exhibited slight rounding at the corners of the structures and somewhat sloped sidewall profiles. The smallest features that showed no loss of the fidelity of the lines were the 12 μm pitch trenches. Almost no material remains for the 6 μm pitch features. The bottom image in Figure 4.13 shows the light field image where freestanding structures were formed on the substrate. The rounded edges and sloped sidewalls of the structures are more apparent in the light field exposure. The 12 μm pitch structures were the smallest features resolved in the light field sample. The maximum aspect ratio (height-to-width) achieved was 1.5-to-1. The next smallest feature size, which was not fully resolved, was the 10 μm pitch structures. These features had rounded tops, indicating erosion of the unexposed resin at the top of the line features.

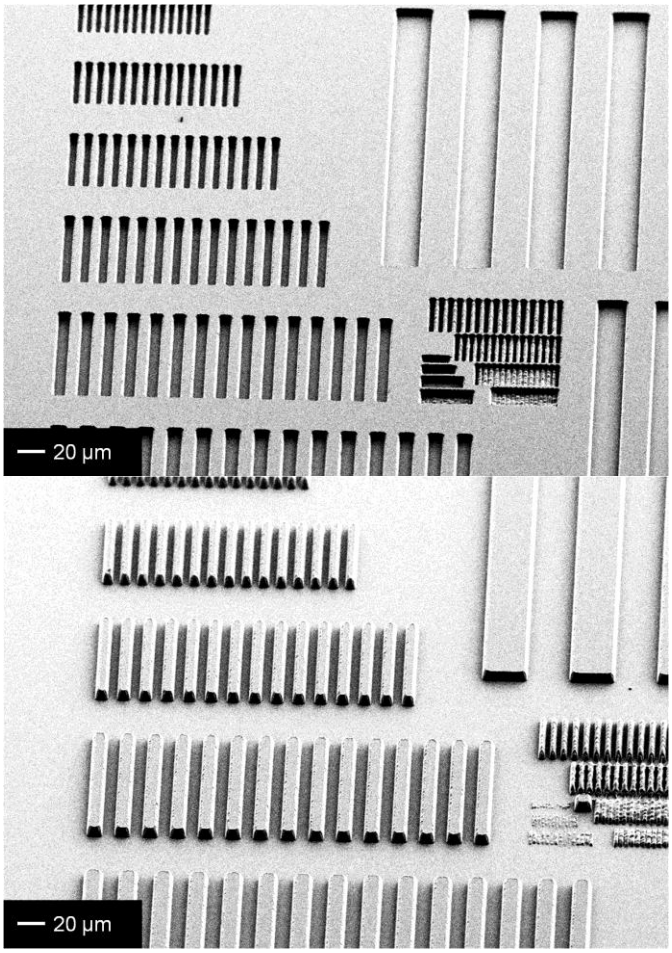

Figure 4.13: Scanning electron micrographs of Formulation X trenches (top) and hills (bottom)

4.7 Conclusions and Recommendations

A new positive tone, aqueous developable, permanent dielectric was developed. This dielectric was a copolymer of HFANB and CBANB which utilized DNQ-based photochemistry to effect the photolithographic solubility change. The structure of the PAC was found to greatly affect its miscibility in the PNB resin. Additionally, a brown residue was observed during the develop step. This was hypothesized to be a base-induced reaction of DNQ, and it was mitigated with lower DNQ loadings and slower

dissolution rates. Of the available PACs, PAC4 was selected for further experiments due to its high miscibility and slow formation of brown residue.

The effects of the monomer ratio on the dissolution characteristics of the film were studied in detail by QCM analysis. The PNB polymers were found to have unique dissolution characteristics, as the exposed curve of their Meyerhofer plots had a negative slope. A polymer with 25 mol% CBANB was found to swell significantly in developer, even in the inhibited (unexposed) state. Dissolution of polymers with 10 and 0 mol% CBANB were too slow to achieve good photolithographic patterning. The amount of free hydroxyl groups before and after exposure were measured by FTIR, and no observable increase was found. This was a possible explanation for the slow dissolution rate of exposed films.

The effect of TMPTGE on the dissolution characteristics was measured, and it was found to decrease the dissolution rate significantly. Hypotheses were made as to the cause of this effect, but no attempts to prove them were conclusive. Finally, an optimal formulation of PNB-A, 20 pphr PAC4, and 10 pphr TMPTGE was demonstrated. This formulation exhibited a D_{100} of 408 mJ cm^{-2} and constrast of 2.3, which is reasonable for the DNQ-based photochemistry.

Future work should focus on the unique dissolution characteristics of these PNB polymers, especially with regard to additives. The lowering of the dissolution rate by ICA and TMPTGE is non-trivial, and the mechanism for these effects should be found. This could enable higher sensitivity and higher contrast by tuning these additive loadings. Swelling of the unexposed regions is also an issue. Though this was decreased significantly with 10 pphr TMPTGE, work should be done to decrease this further. This would allow for flexibility in dissolution times and higher contrast.

CHAPTER 5

DNQ-BASED POLYNORBORNENE DIELECTRIC: CURING

5.1 Epoxide Cross-Linking Reactions

The previously studied Avatrel 8000P was partially cross-linked during lithography to achieve negative tone photo-definability. Cross-linking was induced by exposing a PAG to UV irradiation to create a strong acid and then heating the sample to initiate the ring-opening reaction of the epoxide functionality. The epoxide could react with CBANB, HFANB, or other epoxides. M. Raeis-Zadeh et al. showed that little-to-no cross-linking occurred before the post exposure bake step, indicating that the reaction does not proceed quickly at room temperature, even with the acid catalyst present.[112] After heating to 100°C for 5 min, approximately 50% of the epoxide had reacted as measured by IR spectroscopy. The sample was then cured three times at 160°C for 1 hour each time. After the first cure, most of the epoxide rings had reacted, and the reaction had gone to completion after the second cure. This gives an indication of the reaction kinetics when catalyzed by a strong acid.

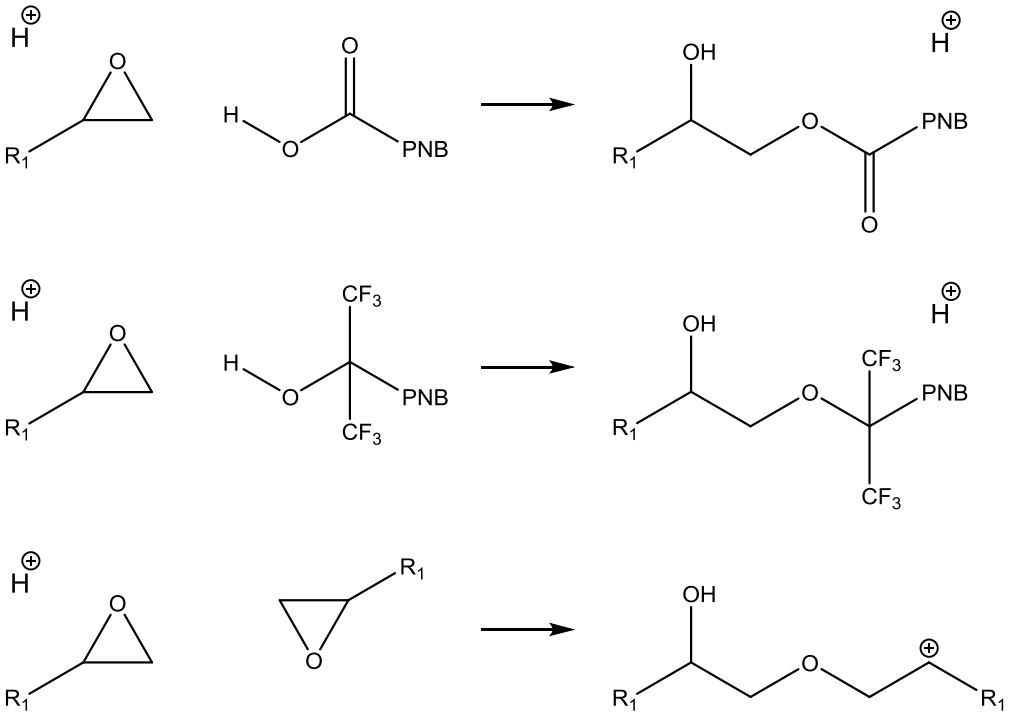

Figure 5.1: Acid-catalyzed cross-linking reactions of Avatrel 8000P

The positive tone PNB dielectric does not have a strong acid to catalyze the cross-linking reaction. Therefore, it would likely require a higher cure temperature to achieve the same level of cross-linking as Avatrel 8000P without a catalyst. Formulations of positive tone PNB-A, PAC4, and TMPTGE were cured at 180°C for 2 hours.

5.2 Composition Considerations

5.2.1 Molar Composition

Though it is unlikely that every CBANB, HFANB, and epoxide moiety will find a reactive site with which to cross-link, the ratio between these groups will certainly affect the extent of cross-linking that is possible. Particularly of interest is the CBANB content compared to the epoxide content on a molar basis. If too few epoxide groups are included in the formulation, the CBANB could remain uncross-linked after the cure. The

CBANB is likely to have the largest impact on the dielectric constant of the material because of its polarity, so cross-linking this group is critical.

If PNB-A is used, which contains 25 mol% CBANB, a loading of 10.2 pphr TMPTGE corresponds to an equimolar loading of epoxide groups and carboxylic acids. It must also be considered that epoxides can react with HFANB and other epoxides. Fortunately, CBANB is the most acidic functional group, and therefore most likely to react.

5.2.2 DNQ vs. ICA

Since the PNB/DNQ dielectric is positive tone, the regions of the film being cured will not have been exposed during photolithography. There exists the option of exposing the dielectric prior to the cure to convert the DNQ to ICA. It was hypothesized that this would be beneficial for mechanical and electrical properties, since the resulting carboxylic acid would react with the epoxide cross-linkers. Unfortunately, the dose requirement to convert all of the DNQ to ICA throughout the film is high. If the film is not completely exposed, the conversion of DNQ to ICA would vary with depth into the film, leading to non-uniform properties. As found in Chapter 4, an exposure dose of approximately 95 mJ cm^{-2} um^{-1} was required for full conversion of the DNQ.

5.3 Mechanical Properties

Compressive Young's modulus was measured with a nanoindenter. Details of these measurements are provided in Chapter 3. Formulations were made with PNB-A and a fixed loading of 20 pphr PAC4. TMPTGE was added at four different loadings of 0, 2, 5, and 10 pphr. To test the difference between curing of DNQ and ICA, each formulation was tested unexposed and exposed to 2000 mJ cm^{-2} 365 nm radiation. Photobleaching experiments in Chapter 3 indicate that this dose is enough to convert all of the DNQ to ICA. Cast films were cured for 2 hr at 180°C under nitrogen.

5.3.1 Modulus

For the exposed dielectric, it can be seen from Figure 5.2 that the modulus of the dielectric without TMPTGE is 2.08 GPa. The modulus of the neat polymer film is 1.96 GPa, so the inclusion of ICA does not significantly change the modulus. As the TMPTGE loading is increased, the modulus also increases. This is expected since more available epoxy would increase the cross-link density (i.e. decrease the molecular weight between cross-links). The modulus and the molecular weight between cross-links (M_c) are inversely proportional, so increased TMPTGE would increase the modulus. The modulus appears to level off at 2.5 to 2.6 GPa around 10 pphr TMPTGE, indicating that the maximum cross-link density is achieved at approximately this TMPTGE loading.

When the film is unexposed, a largely different trend in the modulus is observed. Without any TMPTGE, the modulus of the film is 2.52 GPa, significantly higher than the neat polymer film or the film with ICA. This indicates that DNQ somehow interacts with PNB-A. This is discussed in the next section. The modulus is further increased with 2 pphr TMPTGE, but then decreases at 5 and 10 pphr TMPTGE.

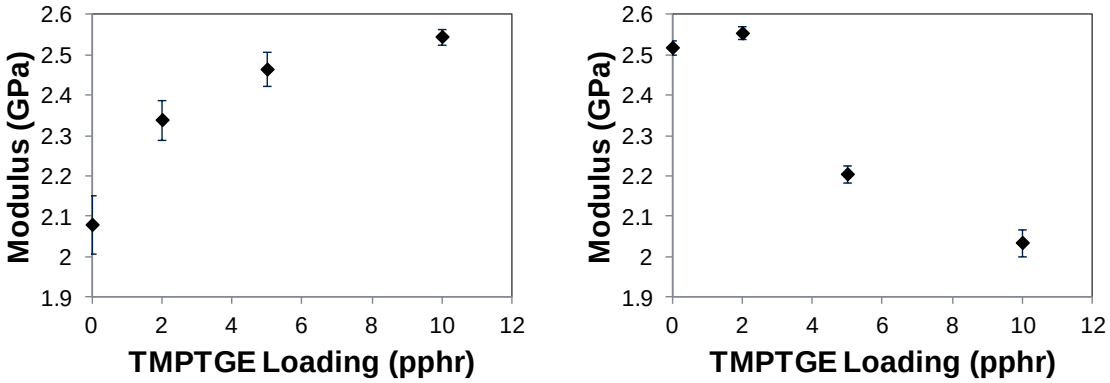

Figure 5.2: Modulus of exposed (left) and unexposed (right) PNB-A/PAC4 films

5.3.2 DNQ vs. ICA

The mechanical results show that high modulus films could be achieved with little-to-no epoxy cross-linker as long as unexposed DNQ was included in the formulation. This may enable more tailorable mechanical and electrical properties of the final dielectric by providing more parameters (additive loadings) to vary.

A possible mechanism for the DNQ reaction is shown in Figure 5.3. It is hypothesized that during the cure, DNQ undergoes the Wolff rearrangement thermally. In ambient and humid conditions, expulsion of N_2 from DNQ forms a ketene that subsequently reacts with water to form the ICA. However, at elevated temperatures in a nitrogen atmosphere, the water availability is low, so the reactive ketene does not proceed to the ICA. Figure 5.3 shows UV-Vis spectroscopy spectra for DNQ-PNB films with 20 pphr PAC4 and no TMPTGE. These films were cured at 120°C for 2 hrs under dry and humid conditions. A humid cure was achieved by placing a beaker of water in the tube furnace and flowing nitrogen at 1 LPM. Since PNB is transparent to wavelengths well below 300 nm, the absorbance peaks are from the DNQ. As seen in Figure 5.3, the spectra from the dry and humid cures differ greatly, particularly at wavelengths longer than 350 nm. This is good evidence that the thermolysis of DNQ to ICA is water-limited during the cure. With limited water available, the ketene is likely to react with CBANB or HFANB to form an anhydride or ester, respectively.

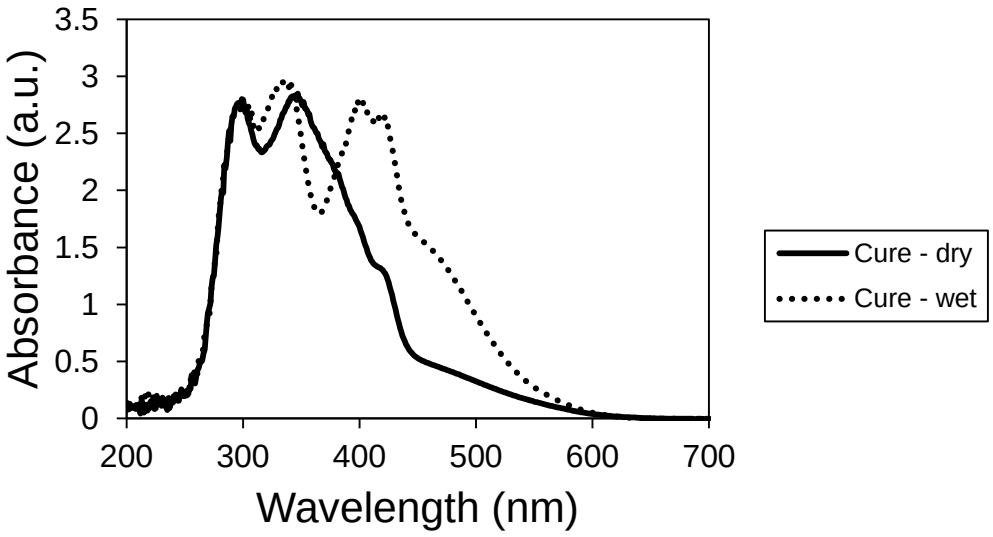

Figure 5.3: UV-Vis spectra of DNQ-PNB after dry and wet curing at 120°C for 2 hrs

The reaction of the ketene with novolac and other alcohols by the same manner has been suggested previously.[113], [114] Since PAC4 is difunctional, this reaction forms cross-links between polymer chains. The expulsion of nitrogen from DNQ can be performed photolytically, so this reaction may happen at a comparatively low temperature to the epoxy cross-linking. If the PNB-A/DNQ reaction occurs before the PNB-A/TMPTGE reaction, this could limit the number of available sites for epoxy cross-linking. It could also lower polymer mobility, hindering the PNB-A/TMPTGE reaction. If TMPTGE does not incorporate into the final structure or only reacts once, it would act as a plasticizer in the film and lower the modulus. This explains the drop in modulus when the TMPTGE loading is increased to 5 and then 10 pphr TMPTGE in the unexposed films.

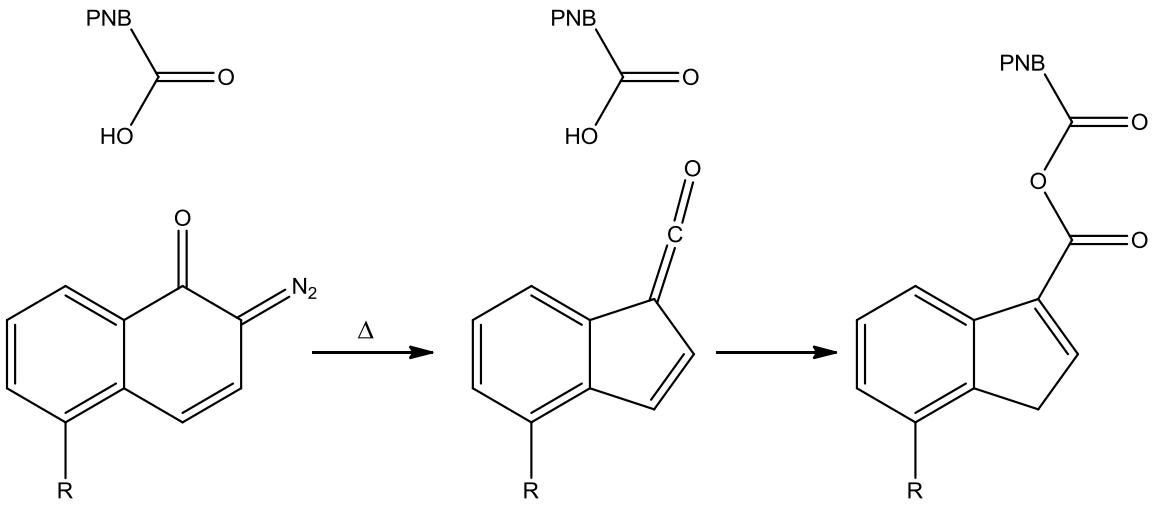

Figure 5.4: Hypothesized PNB-A/DNQ reaction

5.4 Cross-Linking Density

5.4.1 Solvent Swelling

Cross-link density is an important factor that impacts the modulus of dielectric films. To qualitatively compare the cross-link density of the eight formulations measured in Section 5.3, films were swelled with PGMEA. A higher cross-link density will allow less PGMEA to swell the polymer film. The swelling ratio is defined as the mass of solvent in the swollen film divided by the mass of the dry film.

The amount of PGMEA taken up by the films over time is shown in Figure 5.5. The exposed film without any TMPTGE dissolved in the PGMEA immediately, which is not surprising since there is no cross-linking agent. It was expected that increased TMPTGE loading would result in a lower final swelling ratio, since the cross-linking density should be higher. Although the expected trend occurred initially, a different trend evolved with a long exposure to solvent. It was seen that the swelling ratio changes over the 90 min experiment, reaching a maximum at 15 min for 2 and 5 pphr TMPTGE and slowly decreasing thereafter. It was hypothesized that uncross-linked ICA is being

leached out of the film over this time. More ICA could be leached out of films with lower TMPTGE since the cross-link density is lower, which supports the result at 90 min.

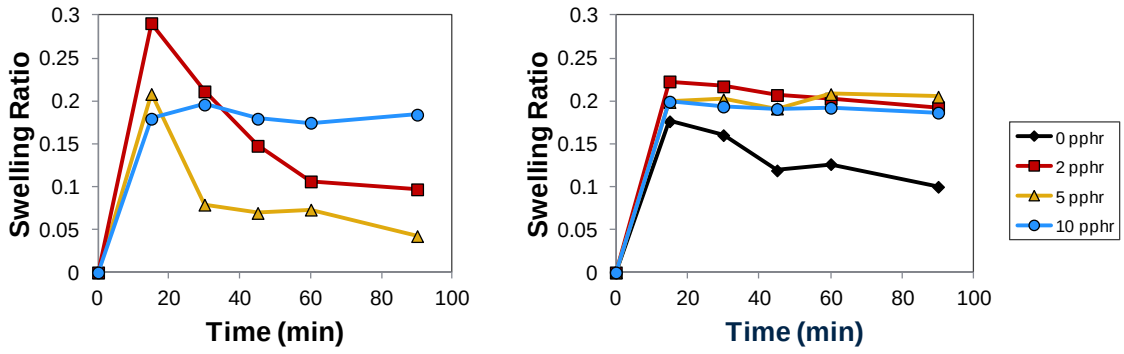

Figure 5.5: Swelling of exposed (left) and unexposed (right) PNB-A/PAC4 films

The unexposed films of PNB-A and PAC4, again, show a significantly different result. The film without any TMPTGE added does not dissolve immediately as with the exposed film. This supports the hypothesis that DNQ cross-links with PNB-A. The slight decrease in swelling ratio over time may be due to leaching of a small amount of unincorporated PAC4 from the film. No significant difference can be seen between the other three curves of 2, 5, and 10 pphr TMPTGE when unexposed. The cross-link density for these formulations must be the same, and increasing the TMPTGE loading above 2 pphr does not change the cross-linking density. An increase in TMPTGE without an increase in cross-link density further supports the plasticization trend seen in the mechanical properties. For films with 2, 5, and 10 pphr TMPTGE, no decrease in the swelling ratio was seen over time. This is not surprising since both PAC4 and TMPTGE additives are reactive and will be bound to the polymer network.

5.4.2 GPC Analysis of Non-Bound Species

To test the hypothesis of leaching ICA during the swelling experiments, exposed films were remade with the same processing conditions as previously. The samples were

swelled for 165 minutes in tetrahydrofuran (THF). The swelling solvent was then analyzed by gel permeation chromatography (GPC). THF was chosen for this experiment because it was also the eluent for GPC. The GPC traces are shown in Figure 5.6. The sample without TMPTGE dissolved into THF, and the GPC trace shows a broad peak from 12 to 22 minutes. This peak exactly matched that of the neat base polymer PNB-A. Also apparent in Figure 5.6 is a peak at 24 to 26 minutes. This would correspond to a polystyrene molecular weight of approximately 1000 to 2600 g mol^{-1}. The molecular weight of photolyzed PAC4 (i.e. converted to ICA) would be 879 g mol^{-1}. Since the technique compares hydrodynamic volume, it is possible that this peak is the more rigid, leached ICA. As the TMPTGE loading is increased, this peak decreases in intensity until it is completely gone in the 10 pphr TMPTGE sample. This supports the previous hypothesis that ICA remains in the film uncross-linked, and increased TMPTGE cross-links the ICA into the structure.

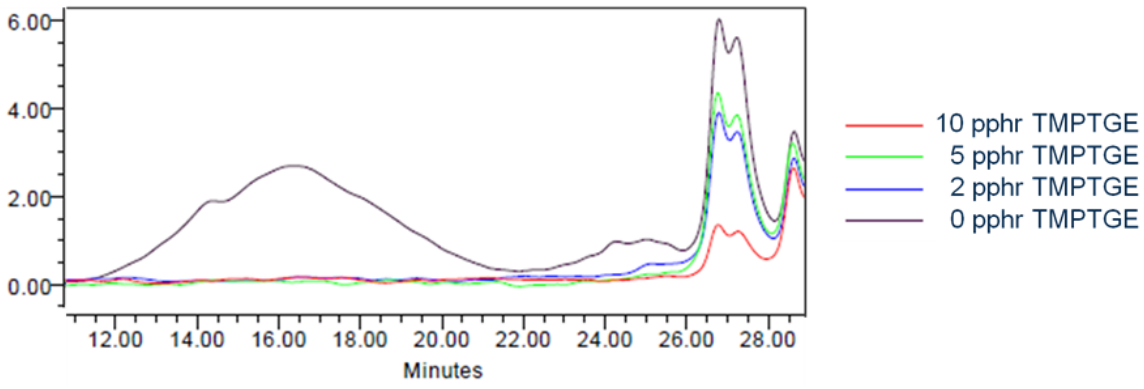

Figure 5.6: GPC analysis of leached molecules

5.5 DNQ as a Cross-Linker

The ability to use DNQ as a cross-linker is an interesting concept that could lead to new lithographic and cross-linking chemistries. This positive tone dielectric was developed with epoxy cross-linkers to impart excellent adhesion. However, epoxides can

limit the choice of photochemical reactions since they are very reactive in the presence of acids and bases. These previous results show that the multifunctional epoxy is not necessary to cross-link the dielectric. In fact, high TMPTGE loadings plasticized the film, indicating that much of the TMPTGE did not react with the base polymer. To continue evaluating the curing mechanism in these positive tone dielectrics, it was desired to understand the temperature at which thermolysis of DNQ occurred. Investigating the reaction kinetics would also provide insight on the required temperatures for DNQ-only cross-linking.

5.5.1 FTIR Kinetic Study

Attenuated total reflection Fourier transform infrared spectroscopy (ATR-FTIR) was used to measure the thermolysis of DNQ. The samples were heated *in situ* and IR spectra were recorded every 5 minutes upon reaching the desired temperature. Experiments were performed with films of PNB-C (i.e. HFANB) with 20 pphr PAC4. PNB-C was chosen so that the carboxylic acid would not be present because its carbonyl peak would overlap with a desired carbonyl peak near 1715 cm^{-1} in DNQ. The carbonyl peak is not expected to significantly change since the ester formed from reaction with HFANB will also appear in this region. A diazo peak at 2050 to 2200 cm^{-1} is also characteristic of DNQ.[115] Figure 5.7 shows these two peaks over time as the sample is held at 120°C. The carbonyl peak is shown to prove that the loss of the diazo peak was not a loss of intensity from delamination.

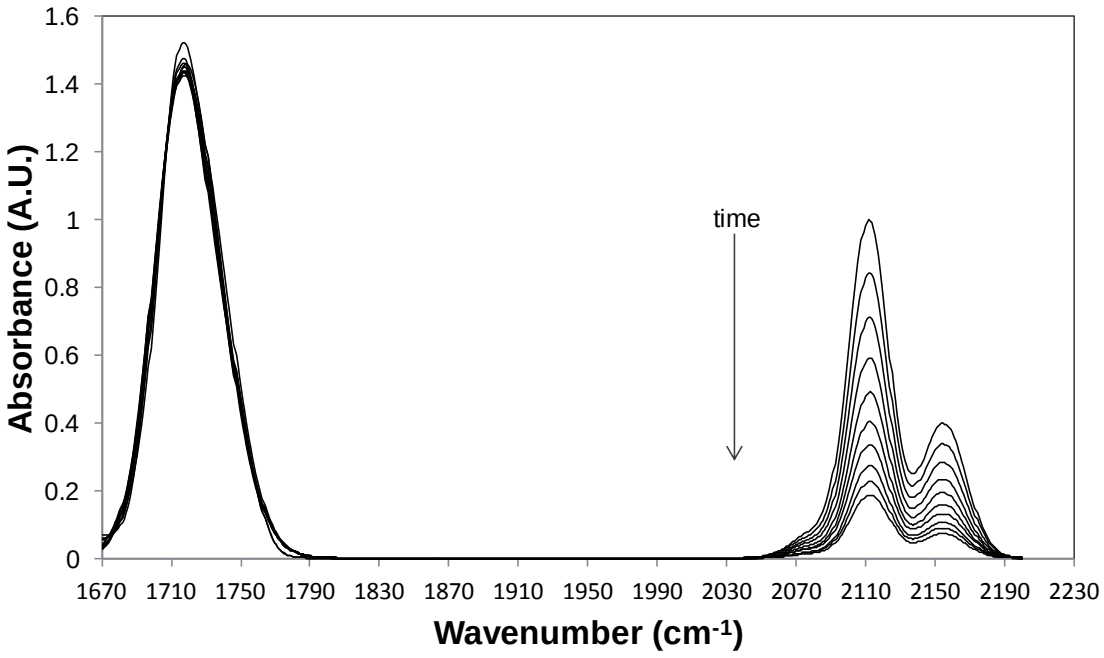

Figure 5.7: Disappearance of characteristic DNQ IR peaks at 120°C

At each time point, the diazo peaks were integrated. Since absorbance is linearly proportional to concentration, Equation 5.1 is used to determine the conversion at any measured time point. A_n is the peak area at time n, A_0 is the original peak area, C_n is the concentration at time n, C_0 is the original concentration, and ϵ is conversion.

$$\frac{A_n}{A_0} = \frac{C_n}{C_0} = 1 - \epsilon \tag{5.1}$$

Since the reaction is unimolecular, it was first assumed that the reactions could be modeled with first-order, irreversible reaction kinetics. The relationship between concentration and rate constant (k) for this type of reaction is given in Equation 5.2. As seen in Figure 5.8, the relationship between $\ln(C/C_0)$ and t is linear, and k is the slope of these curves. As the cure temperature is increased, the slope of the curve becomes more

negative, so the rate is higher at an elevated temperature. The rate constant was calculated by a linear least squares fit of the data in Figure 5.8.

$$\ln\left(\frac{C_n}{C_0}\right) = -kt_n \tag{5.2}$$

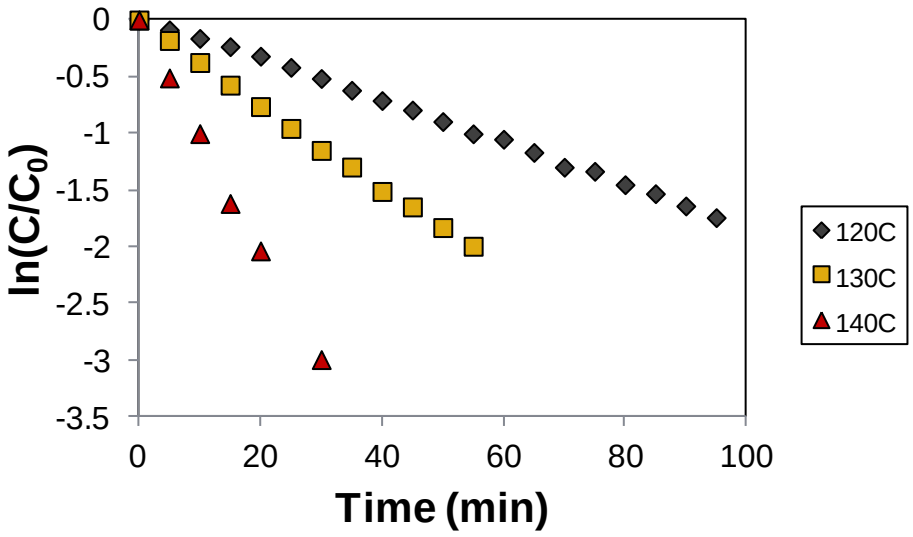

Figure 5.8: $\ln(C/C_0)$ of DNQ plotted with respect to time

To evaluate the experimental error, four experiments were run at 140°C. Unfortunately, the standard deviation of the reaction rate was calculated to be ± 21%. This high variation may be a result of inconsistent film thicknesses from the doctor blade coating process. Due to this variation, it was deemed inappropriate to calculate activation energy from the IR results. The measurement of DNQ thermolysis gives an idea of the temperatures required to cure a film with DNQ as a cross-linker. It is clear from Figure 5.8 that temperatures ≥ 140°C are sufficient for achieving high conversion of DNQ in relatively short cure times of 2 hrs or less. Additionally, this supports the hypothesis that DNQ is reacting at lower temperatures than the epoxy cross-linkers.

5.6 Property Comparisons

Properties for the DNQ-PNB dielectric developed in Chapters 4 and 5 are listed in Table 5.1. These properties are compared to existing positive tone dielectrics. As seen in the table, the DNQ-PNB has higher contrast, lower dark erosion, lower volume change, a lower cure temperature, and a lower CTE than HD-8820 or BCB. These are all positive attributes. Unfortunately, the dielectric constant and tanδ are higher than those of HD-8820 and BCB. These two properties limit the use of DNQ-PNB in low loss and/or high frequency applications.

Table 5.1: Properties of DNQ-based PNB and other positive tone dielectrics[83], [87], [116], [117] (**not reported)

Property	Unit	HD-8820	BCB	DNQ-PNB
D_{100}	mJ/cm^2	280	810	408
Contrast	-	**	1.02	2.3
Dark Erosion	%	20 - 25	19	2
Volume Change	%	20	17.4	8
T_d (1% Loss)	°C	399	**	305
T_{cure}	°C	320	250	180
CTE (xy)	ppm/K	64	60	30
Modulus	GPa	2	3.6	2 – 2.6
Dielectric Constant	-	2.94	2.9	3.7 – 3.9
tanδ	-	0.0089	0.009	0.029 – 0.031
Water Uptake	%	< 0.5	1.2 @ 50% RH	not measured

5.7 Conclusions and Recommendations

Mechanical properties of a DNQ-based, PNB dielectric were evaluated. Exposed films exhibited an increase in modulus with increased TMPTGE loading, whereas unexposed films showed an unexpected decrease in modulus. This was attributed to the ability of unexposed DNQ to react with the PNB resin via the ketene intermediate of the thermally induced Wolff rearrangement. Swelling experiments were performed that

support this conclusion and indicate that 2 pphr TMPTGE and 20 pphr PAC4 are sufficient to achieve the maximum cross-link density under these curing conditions. Swelling measurements of the exposed films revealed that ICA was not fully cross-linked into the dielectric structure and could be leached out at TMPTGE loadings less than 10 pphr.

Thermal FTIR studies were performed to evaluate the thermolysis of DNQ. It was observed that DNQ readily degrades at temperatures above 120°C, which sets a lower limit for the curing temperature. The reaction was determined to exhibit first order, irreversible reaction kinetics by fitting IR data over time. Finally, the lithographic, mechanical, and electrical properties of this dielectric were compared to those of existing positive tone dielectrics. In many cases, the DNQ-based PNB dielectric outperformed those existing dielectrics.

For future research, the DNQ cross-linking reaction should be studied in more detail as it could be an enabling reaction for other photochemistries. While the degradation of the DNQ compound was studied in this work, the rates of cross-linking to an alcohol or carboxylic acid are still unknown. In addition to the evidence here, Schwartz, et al. showed strong evidence for this reaction via NMR of model compounds.[117] The possibility of using this cross-linking reaction to enable lower curing temperatures should be studied. This would result in dielectrics with lower residual stress.

CHAPTER 6

CHEMICALLY AMPLIFIED, CROSS-LINKABLE POLYMER

Chemical amplification is a well-studied, positive tone photochemistry for photoresists, as discussed in Chapter 1. CA materials have the benefits of high sensitivity and high contrast, which allow for high throughput and densely packed features. The goal of this project was to develop a permanent dielectric with greatly improved lithographic properties.

6.1 Challenges

While CA resists have been used for decades, there is good reason as to why the photochemistry has not been translated to a permanent, cross-linkable material; the necessity of a PAG for chemical amplification catalyzes many cross-linking chemistries. Epoxy-based cross-linking cannot be used with chemical amplification for this reason. Creating a strong acid in an epoxy-based, positive tone dielectric will ring open the epoxy and cause cross-linking that lowers the solubility, which is the opposite solubility switch for a positive tone dielectric. Another possible issue is that the cross-linker could react with the strong photoacid and trap the cation. BCB cross-linkers cannot be used because the strong acid can be trapped on the BCB moiety.[118] Without the strong acid, there is no catalyst for the photochemical reaction and no solubility switch occurs. Thus, the

cross-linking chemistry must be specifically picked so that it does not interfere with the photochemistry and vice versa.

6.2 Lithographic and Cross-Linking Mechanisms

In this chapter, the chemical functionalities and mechanism to enable positive tone, aqueous-developable, CA, cross-linkable dielectrics are disclosed. The experimental results demonstrating the CA, aqueous development used a model polymer backbone. While this backbone is not suitable for use as a permanent dielectric, it nevertheless serves the purpose during this phase of the research to show that CA photo-definability is possible. The cross-linking mechanism disclosed is compatible with the traditional CA solubility switching mechanism. Also, the cross-linking mechanism does not interfere with the acid-activated deprotection and subsequent development of polymers with pendent TBOC, TBE, or other protected functionalities.[63], [64] The cross-linking is enabled by the inclusion of an alcohol and a carboxylic acid as the organic pendent groups on a polymer backbone. The carboxylic acid and/or alcohol can be on the original polymer or can be produced via the acid-catalyzed deprotection. After the exposed portions of the film are removed by an aqueous base developer, the film can be cross-linked via the Fischer esterification of an alcohol and carboxylic acid, as shown in Figure 6.1. This cross-linking mechanism does not interfere with the photo-patterning, because the esterification reaction is slow compared to the deprotection of the polymer at normal processing temperatures. The final cure should involve the continuous removal of water from the film since it is a product of the esterification. This can be done under an inert atmosphere at low temperatures or under normal atmospheric conditions at higher temperature (> 100°C).

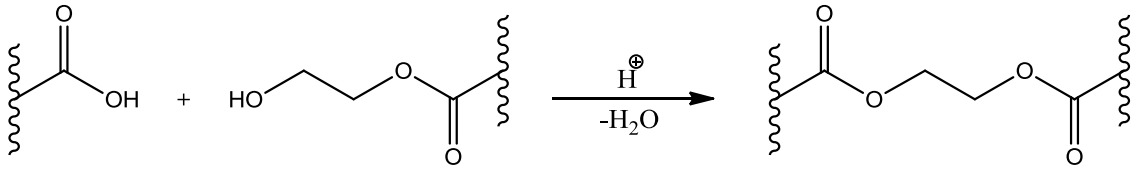

Figure 6.1: Acid-catalyzed Fischer esterification

The patternability and subsequent cross-linking of this system were demonstrated in this work on a random copolymer of tert-butyl methacrylate (TBMA) and 2-hydroxyethyl methacrylate (HEMA), shown in Figure 6.2. Unexposed films were insoluble in aqueous base. Incorporation of a PAG into the formulation and exposure to 248-nm radiation caused the aqueous base solubility switch. Films were effectively patterned at exposure doses characteristic of CA systems and then cross-linked during an extended cure at an elevated temperature.

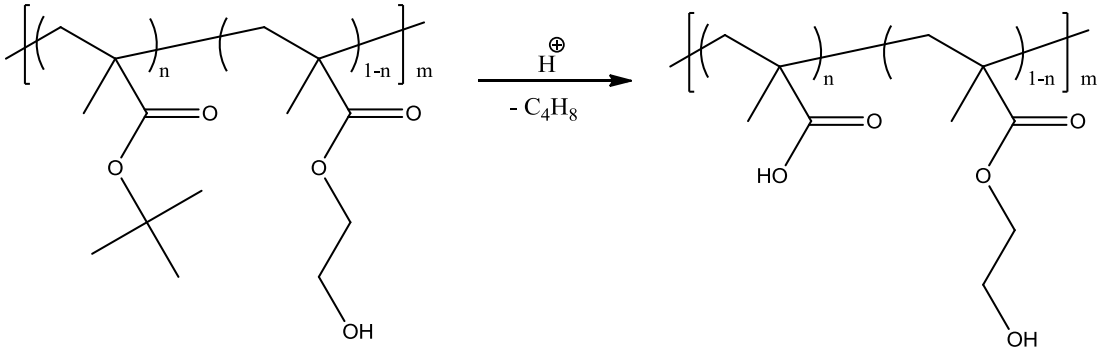

Figure 6.2: Acid-catalyzed deprotection of poly(TBMA-co-HEMA)

6.3 Poly(TBMA-co-HEMA)

A TBMA:HEMA random copolymer was synthesized for use in a CA, aqueous-developable, cross-linkable system. The polymethacrylate backbone was chosen as a model backbone for exploring the CA patterning and cross-linking reactions.

6.3.1 Poly(TBMA-co-HEMA) Synthesis

A 100 mL round bottom flask was loaded with THF (25.5 mL), TBMA (5 g, 35.2 mmol), HEMA (2.29 g, 17.6 mmol), AIBN (31.9 mg, 0.194 mmol), and a stir bar. The flask was purged with dry nitrogen gas for 30 min, and the clear solution was stirred at 60°C for 23 hrs. The polymer was precipitated in H_2O (700 mL) from THF and collected on filter paper. The polymer was then precipitated in hexanes (750 mL) from THF, collected on filter paper, and dried *in vacuo* at 50 °C to yield a white powder in good yield (6.13 g, 83.8%).

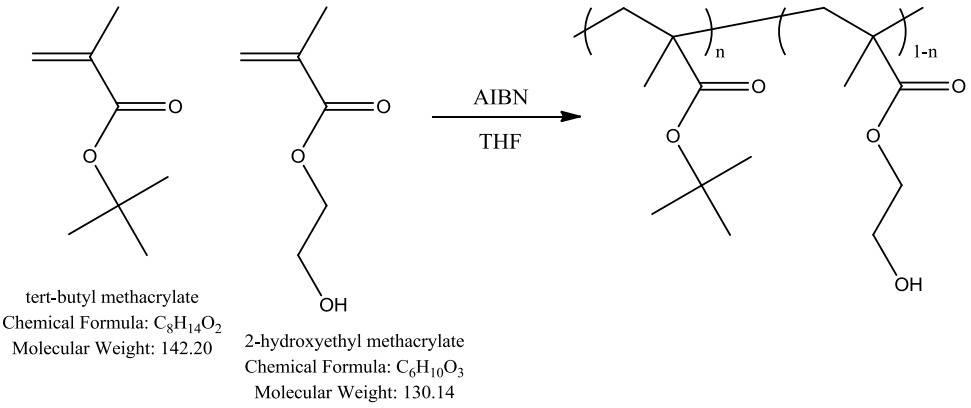

Figure 6.3: Synthesis of poly(TBMA-co-HEMA)

6.3.2 Polymer Characterization

The polymer composition was found to be 69:31 TBMA:HEMA via ^{1}H-NMR peak integration. This composition was found to be insoluble in 0.26 N TMAH. The polymer was characterized by GPC and molecular weights were compared to polystyrene standards. The synthesized polymer had a M_n of 54,400 g mol^{-1}, M_w of 151,100 g/mol, and a polydispersity of 2.78. This polydispersity is characteristic of free radical polymerization reactions.[119] The T_g of the poly(TBMA-co-HEMA) copolymer was found to be 123°C as measured by differential scanning calorimetry (DSC). This T_g is

adequate for film processing as it is above the PEB temperature at 100 to 110°C for the acid-catalyzed deprotection of TBMA. Reflow of the exposed films could degrade the spatial distribution of the photo-acid and degrade the lithographic critical dimensions. The TGA of the neat polymer revealed two decomposition temperatures. The first decomposition temperature (T_{d1}) at 214.2°C corresponds to the deprotection of the TBMA group. The mass percent decrease at T_{d1} was measured to be 28.1%, which agrees well with the theoretical value of 27.9% for the loss of isobutylene at this polymer composition. A second decomposition temperature (T_{d2}) was observed at 378.7°C due to of backbone degradation. TGA measurements were also performed on PAG-loaded formulations after spin coating, post apply bake, and blanket exposure. The presence of a photoacid caused a shift in T_{d1} to a lower temperature, 71.8°C, as shown in Figure 6.5.

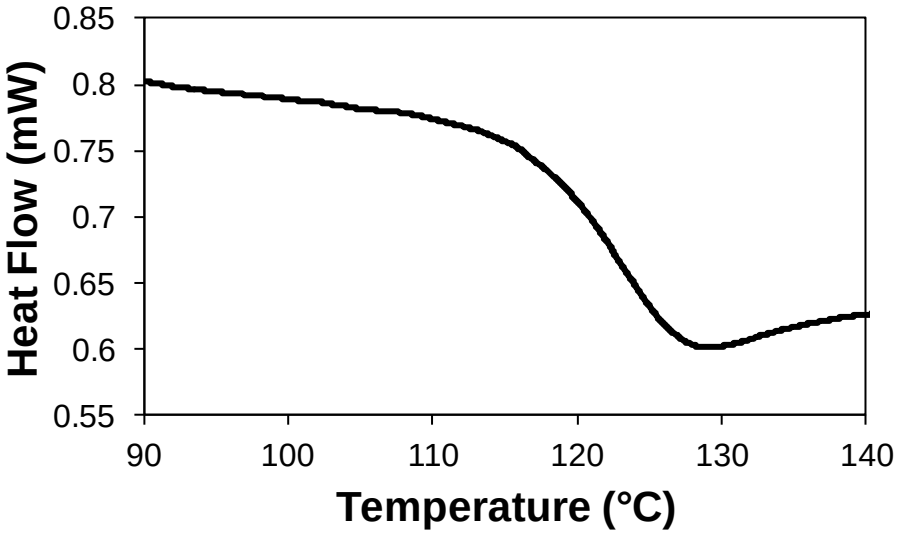

Figure 6.4: DSC analysis of poly(TBMA-co-HEMA)

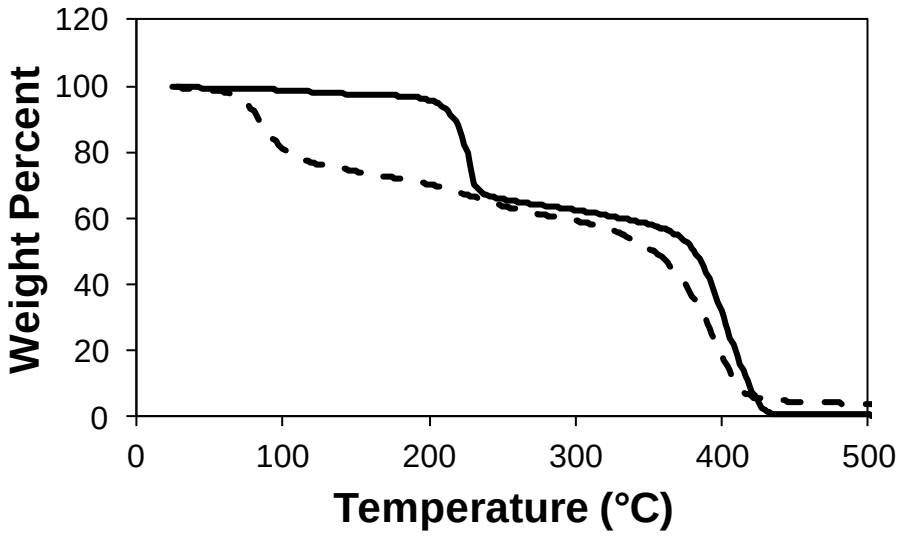

Figure 6.5: TGA of neat poly(TBMA-co-HEMA) (solid) and poly(TBMA-co-HEMA) with PAG, exposed (dashed)

6.3 Formulation and Processing Considerations

Contamination of the spin-cast film by ambient organic base in the atmosphere can interfere with the CA mechanism of positive tone resists. Trace amounts of base in the atmosphere can absorb at the solid/air interface and neutralize the acid photo-product.[120], [121] The atmospheric base can have a profound effect because of the catalytic nature of the deprotection reaction. A base-insoluble surface layer was observed on patterned films in the exposed regions because of organic base contamination in the ambient air, even though carbon filtering of the air was implemented. The surface layer was easily removed by mechanical agitation of the film in the developer. Base contamination can be further reduced by additional filtration of the air through activated carbon and limiting the exhaust of volatile bases into the air.

The contrast and sensitivity for two formulations of poly (TBMA-co-HEMA) were evaluated. Formulation A contained 1 pphr Rhodorsil FABA PAG, and Formulation B contained 3 pphr Rhodorsil FABA PAG, as listed in Table 6.1. The contrast curves for

these formulations are shown in Figure 6.6. In both cases, an insoluble layer was seen at doses above the conventional D_{100} value, and the thickness of this layer decreased at higher doses. It is hypothesized that this layer is due to organic base adsorbed at the wafer surface. It was also observed that pre-rinsing the wafer in an acid solution can have a significant effect on the thickness of this layer. This technique was not optimized.

Table 6.1: Contrast experiment conditions

Formulation	A	B
PAG Loading (pphr)	1	3
Thickness (μm)	9.07	9.87
PEB Time (s)	120	120
Developing Time (s)	120	150

6.4 Lithographic Properties

Formulation A was found to have a thick film contrast of 12.7 and a D_{100} of 50.2 mJ cm^{-2}. These are good values for positive tone, thick film formulations as D_{100} values are typically 100s of mJ cm^{-2} and contrast values are typically ~1. In Formulation B, the increased PAG loading caused the contrast to decrease to 5.2 and the D_{100} to decrease to 32.4 mJ cm^{-2}. The decrease in contrast is not desirable and can be attributed to the higher absorption coefficient of the film. Since the radiation intensity drops off exponentially with respect to distance into the film, increasing the absorbance also makes this intensity gradient larger. The increase in sensitivity, however, is a favorable trait of Formulation B. Figure 6.7 shows a SEM image of the patterned trenches in a Formulation A film. In Figure 6.7, the half-pitch of the trenches from bottom-to-top are 16, 12.5, and 10 μm. It can be seen that the high contrast of Formulation A produced a vertical sidewall profile.

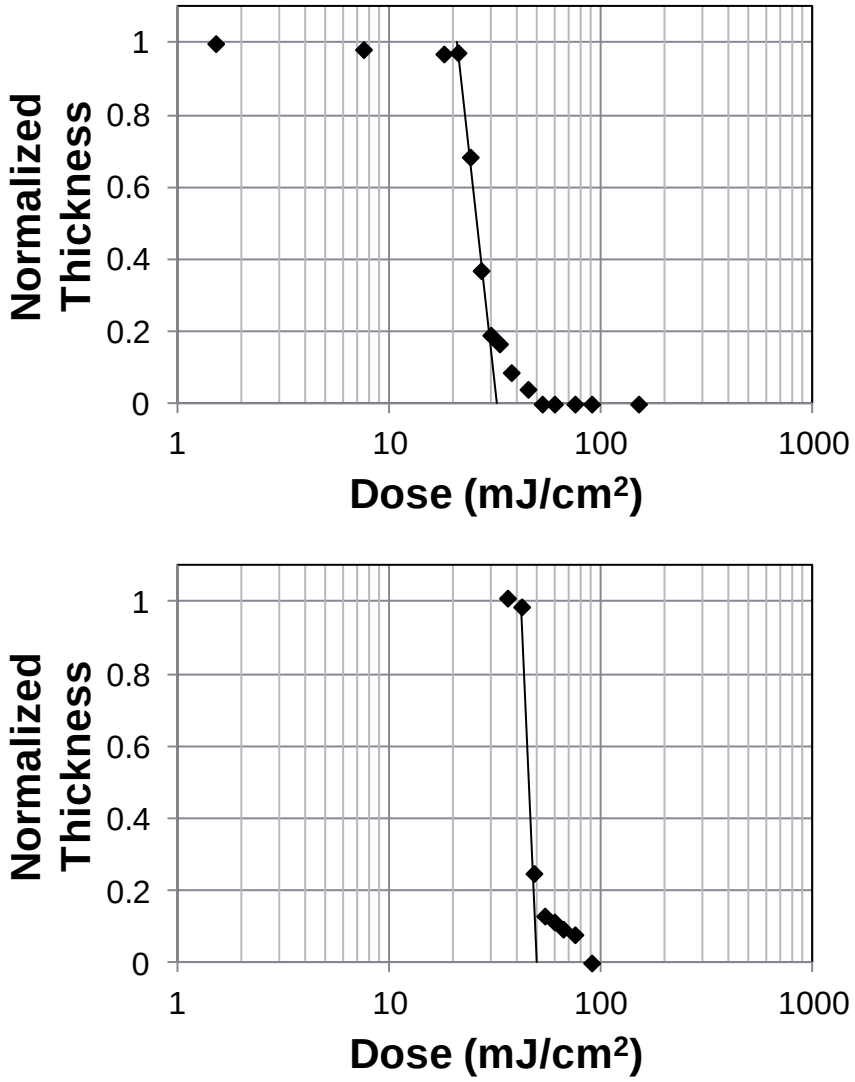

Figure 6.6: Contrast curves for Formulation A (top) and Formulation B (bottom)

The chemical amplification mechanism can be demonstrated by comparing the number of chemical reactions to the number of photons absorbed. Assuming a density of 1.0 g cm^{-3}, a 9.8-µm-thick film of Formulation A contains approximately 4.8 x 10^{-6} mol of the TBMA moiety and 9.7 x 10^{-10} mol of PAG per square centimeter. A dose of 50.2 mJ cm^{-2} of 248 nm radiation had a maximum incident dose of 1.04 x 10^{-7} mol of protons per square centimeter. This means that less than one photon is required for every 46.3 TBMA moieties at these processing conditions. Although it is not expected that 100% of

TBMA groups need to be deprotected for aqueous base solubility, the number of deprotections caused by a non-catalytic photoreaction would be insufficient to cause the observed photopatterning. This shows that the solubility switching reaction must be chemically amplified.

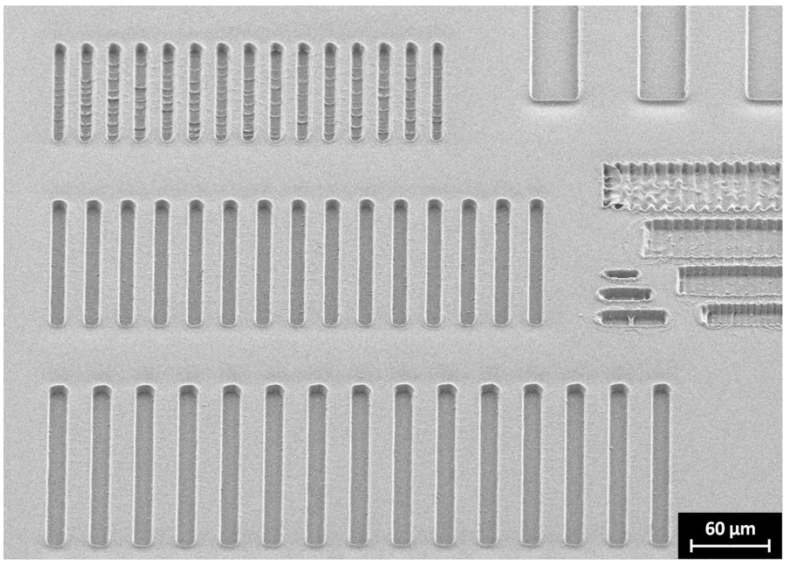

Figure 6.7: Developed trenches in film of Formulation A

The lithographic properties for other positive tone, thick film, permanent dielectrics are presented in Table 6.2. The CA system presented here has a much smaller D_{100} value than photo-patternable PI or BCB dielectrics because of the reuse of the photogenerated acid catalyst. The DNQ-based dielectrics are less efficient, because each photon can produce at most one chemical reaction. In addition, the absorption coefficient of DNQ makes exposure of thick films difficult because the radiation intensity decreases exponentially with depth into the film. This also causes the measured contrast of these dielectrics to decrease with film thickness. Low loadings of the PAC are necessary in the poly(TBMA-co-HEMA) system so that radiation can penetrate the entire depth of the film resulting in an exposure dose on the order of 10s of mJ cm^{-2} and high contrast > 5.

Table 6.2: Lithographic property comparison of poly(TBMA-co-HEMA) to reported positive tone, permanent dielectrics[87], [122], [123]

Dielectric	Film Thickness (μm)	D_{100} (mJ cm^{-2})	Contrast
Polyimide[122]	7.5	350	1.2
BCB[87]	16.4	810	1.02
Formulation A	9.07	50.2	12.7
Formulation B	9.87	32.4	5.2

6.5 Esterification Cross-Linking

After developing, the patterned films were given a blanket exposure of 1000 mJ cm^{-2} at 248 nm irradiation to activate the PAG in the undeveloped portions of film. This dose was chosen to ensure that all of the PAG is activated, however, a much smaller dose would suffice. The film was then cured at 120°C for 10 hours in a nitrogen atmosphere to carry out the Fischer esterification reaction. These conditions were chosen to ensure full cross-linking of the film and continuous removal of water. After curing, the films were insoluble in 0.26 N TMAH, which is a good indication that the carboxylic acid and alcohol functionalities on the base polymer underwent the acid-catalyzed Fischer esterification reaction. Films coated at thicknesses greater than ~4 μm cracked during the cure step. This could be due to the large volume change during cross-linking, a mismatch between the coefficients of thermal expansion for the film and the substrate, or the brittleness of the film. Films thinner than 4 μm were crack-free and had good film quality after curing.

Cross-linking was confirmed by measuring the film stress before and after a thermal cure. A formulation of poly(TBMA-co-HEMA) with 5 pphr PAG was coated to a thickness of 3.94 μm, baked at 100°C for 60 s, and given an exposure dose of 1000 mJ cm^{-2} oat 248 nm radiation. A postexposure bake of 110°C for 60 s caused the film

thickness to decrease to 3.01 μm. The stress of the coated wafer was calculated to be 6.2 MPa by measuring the curvature of the uncoated and coated Si wafer. The sample was then cured at 120°C for 10 h under ambient atmosphere. The thickness after cure was measured to be 2.77 μm. The final stress was 17.9 MPa. The large increase in stress during the cure is a result of film cross-linking at the elevated temperature followed by cooling of the film with a CTE mismatch from the Si substrate. A separate sample was processed under the same conditions through the PEB step. After this, the sample was developed in 0.26 N TMAH to verify that these processing conditions did not result in cross-linking prior to the cure.

6.6 Conclusions and Recommendations

A new, high sensitivity and contrast, permanent polymer was developed based on poly(TBMA-co-HEMA) and a CA photochemistry. The copolymer was synthesized via free radical polymerization with a monomer ratio of 69 mol% TMBA and 31 mol% HEMA. The synthesized polymer had a T_g of 123°C and a T_{d1} of 214.2°C, which were both appropriate for its use as a photo-definable, permanent polymer. Acid catalyzed deprotection of TMBA was shown by a shift in T_{d1} to 71.8°C.

The polymer was cast into a film from PGMEA and the lithographic properties were measured. A formulation with 3 pphr PAG had a D_{100} of 32.4 mJ cm^{-2} and contrast of 5.2. Lowering the PAG loading to 1 pphr shifting the D_{100} to 50.2 mJ cm^{-2} and contrast to 12.7. The photoreaction was further shown to be catalytic by the quantum efficiency of one photon per every 46.3 TBMA functional groups. SEMs revealed nearly vertical side-wall profiles of the patterned films. Cross-linking of the film was shown by two methods. First, the thermal cure at 120°C increased the residual stress of the film substantially from 6.2 MPa to 17.9 MPa. Second, the cure resulted in a film that was completely insoluble in both aqueous base and PGMEA.

The low decomposition temperature of polymethacrylate precluded this material from being used as a conventional permanent dielectric material. Thus, the mechanical and electrical properties of the film were not measured in this work. The low cure temperature and remarkable lithographic properties of this material merit further investigation into its materials properties, especially for applications that do not require a solder reflow. The monomer ratio of TBMA and HEMA should be studied to evaluate its effect on the mechanical and electrical properties. Further, different variations on this type of cross-linking can be considered with a TBOC protected group instead of the TBE used here.

CHAPTER 7

CHEMICALLY AMPLIFIED, POLYNORBORNENE DIELECTRIC

The CA patterning and subsequent cross-linking of a permanent material were successfully demonstrated on p(TBMA-co-HEMA). This model polymer was not suitable for use as a permanent dielectric because of its poor thermal stability. After demonstrating a CA proof of concept, it was desired to use the same photochemistry on a more suitable dielectric polymer. The previous work with PNB, as well as its excellent properties made PNB a good polymer with which to move forward. Additionally, the synthesis of PNB was well-suited for making random copolymers with the desired pendent groups.

7.1 Polymers for Chemical Amplfication

The two necessary functional groups for the CA, permanent dielelctric were a TBE entity for photopatterning and an alcohol entity for cross-linking. In the p(TBMA-co-HEMA) polymer, the HEMA hydroxyl group likely contributed little to the overall solubility of the polymer in aqueous base. Unfortunately, PNBs have much lower solubilities, so a more acidic alcohol monomer was desired. The polymer chosen was a copolymer of tert-butyl ester norbornene (TBENB) and HFANB. After TBENB was deprotected by the photoacid, the resulting polymer structure would be almost identical to the polymers studied in Chapters 4 and 5.

Four polymers were donated by Promerus LLC in support of this project. PNB-C, as in previous chapters, was a homopolymer of HFANB. PNB-D and PNB-E were 70/30 and 35/65 mol% random copolymers of HFANB/TBENB, respectively. PNB-F was a homopolymer of TBENB. The structure of these four polymers is shown in Figure 7.1.

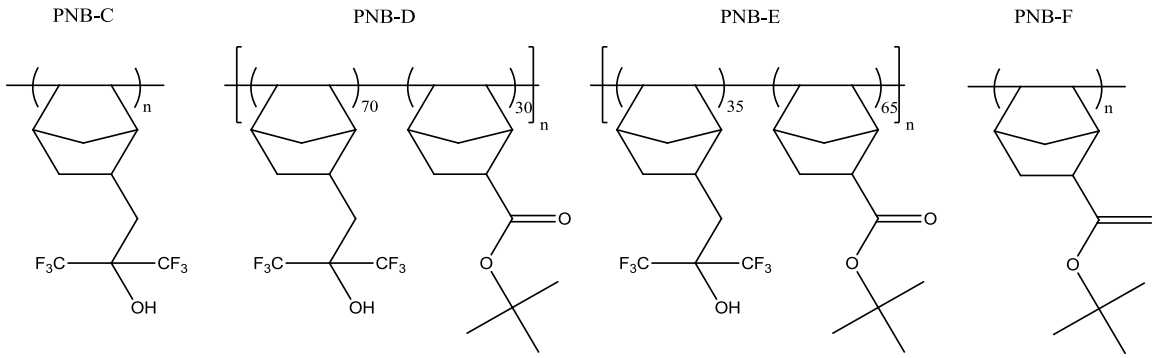

Figure 7.1: Structure and monomer ratios of PNB-C, D, E, and F

To study the effect of the PAG loading, formulations 1 through 4 were prepared using PNB-E and 0.1, 0.5, 1.0, and 3.0 pphr PAG, respectively. To study the effect of monomer ratio, formulations 5 through 9 were prepared as mixtures of homopolymers and/or copolymers with 3 pphr PAG. The tested formulations are listed in Table 7.1.

Table 7.1: Monomer ratios in CA PNB formulations

Formulation	PNB Polymers	NBFA:TBENB
1, 2, 3, 4	PNB-E	35:65
5	PNB-D	70:30
6	PNB-D, PNB-E	60:40
7	PNB-D, PNB-E	50:50
8	PNB-D, PNB-E	40:60
9	PNB-E, PNB-F	30:70

7.2 Effect of PAG Loading

7.2.1 Lithography

Acid is a catalyst for both the deprotection of the TBENB and the esterification of HFANB and TBENB. The effect of the PAG loading on sensitivity, and contrast were measured for formulations 2, 3, and 4. The contrast curves for these formulations are

shown in Figure 7.2. These films were much more sensitive than common positive tone dielectric materials.[87], [122], [116] Positive tone PI and BCB dielectrics require 100s of mJ cm^{-2} to pattern due to the high concentration of DNQ needed to inhibit the dissolution of the films in aqueous base. The sensitivity and contrast of the CA PNB were found to be higher than the previously reported poly(TBMA-co-HEMA) polymer, which were 32.4 mJ cm^{-2} and 5.2, respectively.[123] This is likely due to the higher acidity of the hexafluoroisopropanol in the case of the PNB, which renders this polymer more readily dissolved in aqueous base developer.

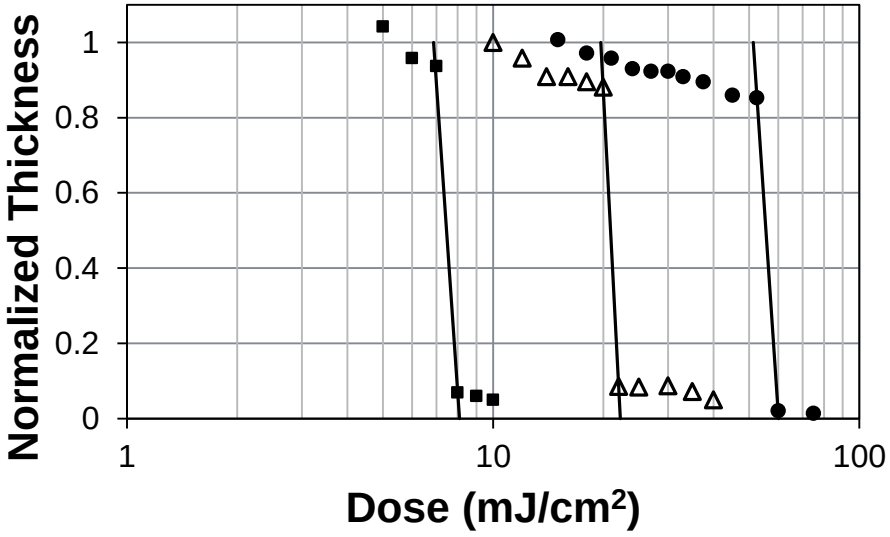

Figure 7.2: Contrast curves of PNB-C with 0.5 (●), 1.0 (Δ), and 3.0 (▪) pphr PAG

It was found that increasing the PAG loading increased the sensitivity, which was expected due to the increased absorbance at 248 nm and higher photoacid concentration within the film at higher PAG loading. For all formulations, scumming was observed at doses above D_{100}, which is likely due to adsorbed water or base on the wafers before processing.[120] The hydronium cation (H_3O^+) that formed by the acid catalyst in the presence of water is less acidic than the photogenerated acid decreasing the rate of the

deprotection reaction. The D_{100} values for formulations 2, 3, and 4 are 60.2, 22.2, and 8.09 mJ cm^{-2}, respectively. The contrast was calculated with only two points. Since the contrast was high it was difficult to expose at doses which produce partial dissolution of the film. Thus, the contrast values are only minimum contrast values with the true value at least as great as the ones reported here. The calculated contrast values for formulations 2, 3, and 4 are ≥ 14.3, ≥ 18.9, and ≥ 14.2, respectively. These lithographic properties show promise for the potential patterning of high aspect ratio or thick film dielectrics. Optical micrographs of patterned trenches in a 4.09 μm PNB film are shown in Figure 7.3. Features of 4 μm half-pitch were resolved, though line-and-space dimensions were not equal. Rounding of the features can be seen near the feature corners, which is a result of the high sensitivity and contrast of these PNB dielectrics. Light diffraction through the mask results in lower light intensity at the corners of the features. High contrast dielectrics exhibit rounding since the change from insoluble to soluble is sharp. Low contrast dielectrics would exhibit partial solubility and sloping of feature corners. This is generally fixed by biasing the mask with optical proximity correction to offset the diffracted light. The aspect ratio and feature quality are sufficient for packaging applications, and these are expected to improve with better lithographic techniques. These films were exposed in soft contact with the photomask, so diffraction under the mask limited the minimum feature size, especially in a line and space pattern.

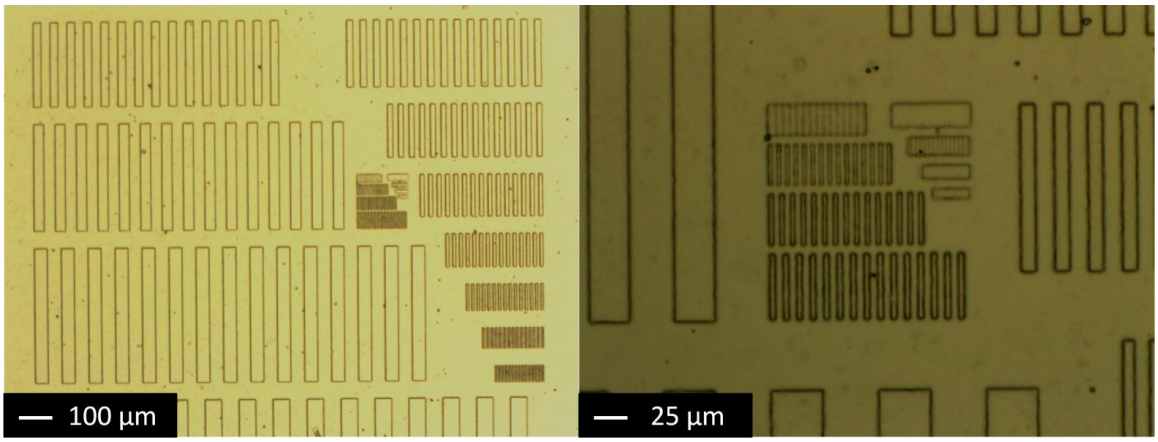

Figure 7.3: Optical micrographs of patterned 4.09 µm PNB film

7.2.2 Mechanical Properties

Modulus and hardness values were measured for formulations of PNB-E with different PAG loadings after cure by indentation. Due to the acid participation in the cross-linking reaction, it is possible that higher PAG loading would increase the reaction rate and total amount of cross-linking. This increased cross-linking could then result in higher values for the mechanical properties. However, no measurable difference was found in modulus or hardness for the films with the PAG loadings investigated here. This suggests that the films were fully cross-linked at all conditions due to the catalytic nature of the Fischer esterification cross-linking reaction. A small concentration of PAG will cause cross-linking until the film is stabilized so that mobility of functional groups is suitably inhibited. This raises the T_g of the film above the cure temperature. In addition, the non-catalyzed esterification can occur with enough thermal energy, which likely occurs at the 250°C cure temperature. Thus, cross-linking can occur even with a low concentration of PAG at elevated temperature and time. The polymer films cured without PAG were found to be insoluble in PGMEA and TMAH, which is a good indication that thermal cross-linking occurred.

7.2.3 Permittivity

The complex permittivity was also measured as a function of PAG loading. A low dielectric constant and low tanδ are desirable for interconnect applications. Figure 7.4 shows the dielectric constant vs composition with one standard deviation error bars. Eight capacitors were measured for each loading of PAG. Although the values fall within the uncertainty of each other, there is a general trend of decreasing dielectric constant with increasing PAG loading. This shows that the excess PAG is not by itself making a significant contribution to the dielectric constant. Since the films are likely fully cured, it appears that the effect of the small concentration of PAG is offset by other factors, such as the density change or esterification of polar functional groups.

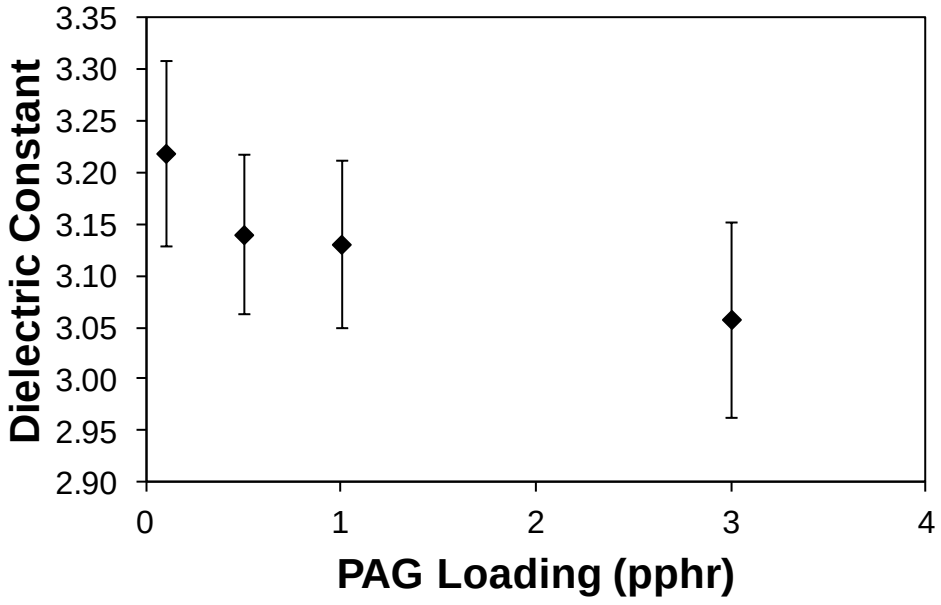

Figure 7.4: Dielectric constant of PNB-E with various PAG loadings

7.3 Effect of Monomer Ratio

The synthesis of PNB through vinyl addition polymerization allows for an easy modification of the monomer mole ratio of HFANB to TBENB.[94] For photopatterning,

the polymer must initially be insoluble in aqueous base. A formulation with too high HFANB content will be soluble because the hexafluoroisopropanol has an acidic proton that can be deprotonated by aqueous base. Further, there is likely a range of monomer ratios that are sufficiently insoluble in aqueous base but still swell during the develop. This is undesirable because swelling can distort the patterned features and affect the curing reaction, yielding poor mechanical and electrical properties. Further, a polymer with an excessively high HFANB content may require fewer TBENB to be deprotonated to engender the solubility switch. This would likely affect the sensitivity and contrast. If the patterning required fewer deprotection reactions, this would generally lead to higher sensitivity since less time and/or radiant energy would be required. However, the resulting carboxylic acid leads to higher solubility in aqueous base, compared to HFANB.

To measure the effect of monomer ratio in the copolymer on the final film properties, mixtures of the different homopolymers and copolymers were made. In every case, the copolymer formulations were well-mixed, and high quality films could be cast. Formulations 5 through 9 were made with varying amounts of the four PNB polymers to achieve specific monomer ratios of HFANB to TBENB. Each formulation had 3 pphr PAG.

7.3.1 Shrinkage

Film shrinkage of 30% or less was observed due to mass loss and densification during the cure reactions. This also results in widening of the patterned features at the surface of the film. Two different mechanisms contribute to volume change: (i) the deprotection of the TBENB group to form gaseous isobutylene and (ii) the formation and evolution of water by the formation of the ester or anhydride cross-links. Curing at an elevated temperature vaporizes the produced water, which adds to the irreversibility of the reaction. Since the film is constrained to the substrate in the in-plane dimensions, the volume change of the film is mainly reflected as a thickness decrease, as plotted in Figure

7.5. A decreasing mole ratio of the TBENB monomer results in a smaller overall volume change. The smallest volume change was measured for the 70 mol% HFANB / 30 mol% TBENB, which exhibited a change of 12.2% during cure.

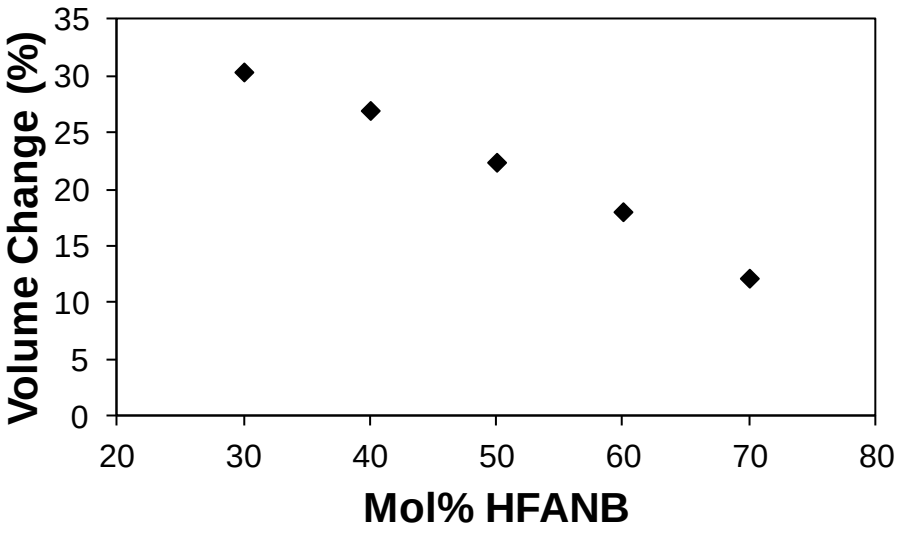

Figure 7.5: Volume change during thermal cure

7.3.2 Modulus

The reduced modulus and hardness of each formulation were measured after cure. As seen in Figure 7.6, both the reduced modulus and hardness decreased with decreasing HFANB content. This is most likely due to the ability of the carboxylic acid formed from the TBENB to participate in two cross-linking reactions. First, it can react with HFANB to form an ester. Second, it can react with another carboxylic acid to form an anhydride. The formation of the anhydride was confirmed by FTIR measurements. The measurement was performed on the TBENB homopolymer after reaction. Prior to cure, only one FTIR peak was observed in the region from 1850 to 1650 cm^{-1}. The peak at 1725 cm^{-1} is due to the carbonyl stretch of TBENB. However, it is noted that residual PGMEA may contribute to this peak slightly. After curing at 250°C for 2 hours, the original peak split into three peaks in the same spectral region. The broad peak centered

at 1810 cm^{-1} is consistent with anhydride carbonyl stretching along with one of the peaks between 1750 and 1700 cm^{-1}.[105] The other peak is most likely due to the carbonyl stretching of the unreacted carboxylic acid. Even though the carboxylic acid can theoretically react to completion in the TBENB homopolymer, the mobility of the polymer chain segments decreases as the cross-linked covalent network is formed. Formation of the anhydride in the copolymers is possible, however, the ester is the rate-favored product. The same FTIR experiment was performed on a film with 30 mol% of the HFANB. Although a clear anhydride peak was found, the peak height was lower than that of the TBENB homopolymer discussed above.

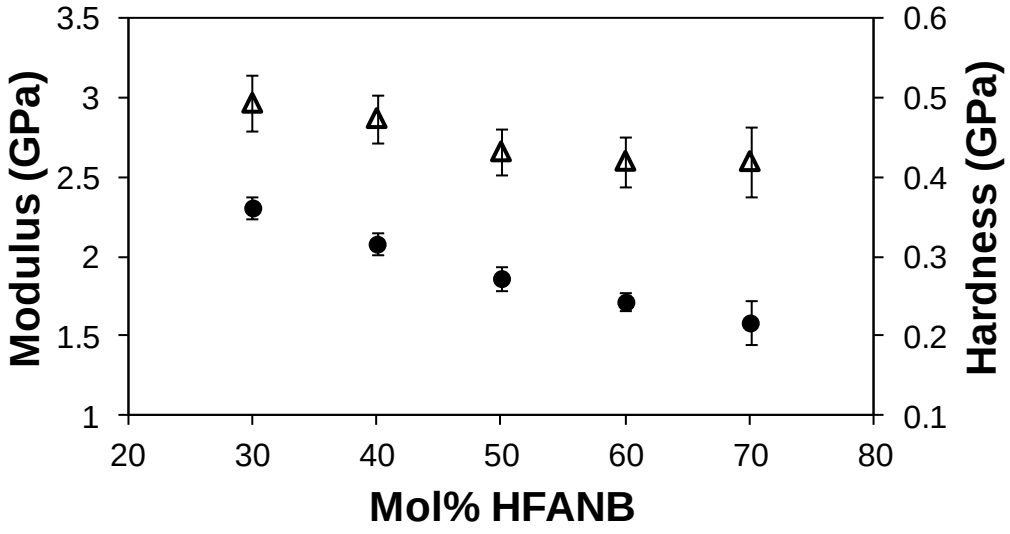

Figure 7.6: Elastic modulus (Δ) and hardness (●) of PNB films

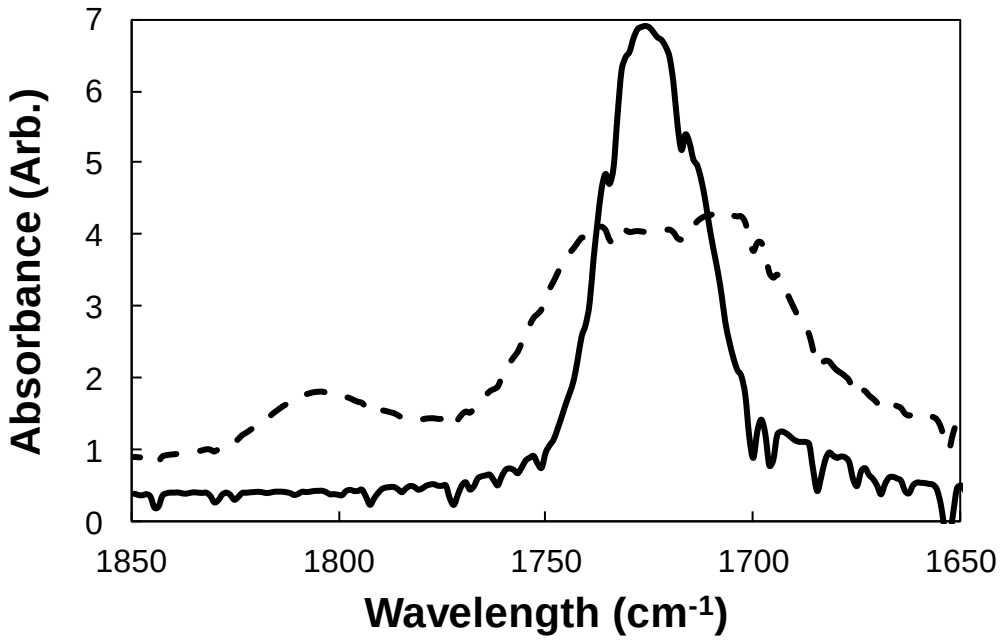

Figure 7.7: Emergence of anhydride IR peak from pre-cure (solid) to post-cure (dashed)

7.3.3 Coefficient of Thermal Expansion

Cooling the film to room temperature after curing induces a thermal strain in the polymer as a result of the mismatch in CTE between the film and the Si substrate. In addition, a lower Young's modulus contributes to lower stress. The in-plane and through-plane CTEs of these PNB films were measured and are shown in Figure 7.8. The in-plane CTE decreased with increasing HFANB content with a value of 32.6 ppm K^{-1} for pure HFANB homopolymer. The through-plane CTE shows the opposite trend, with a higher through-plane CTE when the HFANB concentration increased, as shown in Figure 7.8. This anisotropy can be a result of chain orientation within the polymer film. The helical conformation of PNB forms a near-linear chain which lends itself to stacking of polymer chains, especially when the PNB is functionalized with hexafluoroisopropanol groups because they extensively hydrogen bond with one another. This results in an in-plane orientation of the polymer along the hydrogen-bonded

domains.[92] The stacked, linear assembly of the polymer is consistent with the low in-plane CTE (i.e. axial direction of the polymer backbone) because of the limited ability of the carbon-carbon bonds to expand. In the through-plane direction, the thermal expansion occurs by increasing the void space between polymer strands. When HFANB is substituted with TBENB, the driving force to form chain-chain ordered domains is lower because the TBE and carboxylic acid do not form long-range hydrogen bonds like the hexafluoroisopropanol. This results in a more random configuration of the polymer strands and a more isotropic CTE.

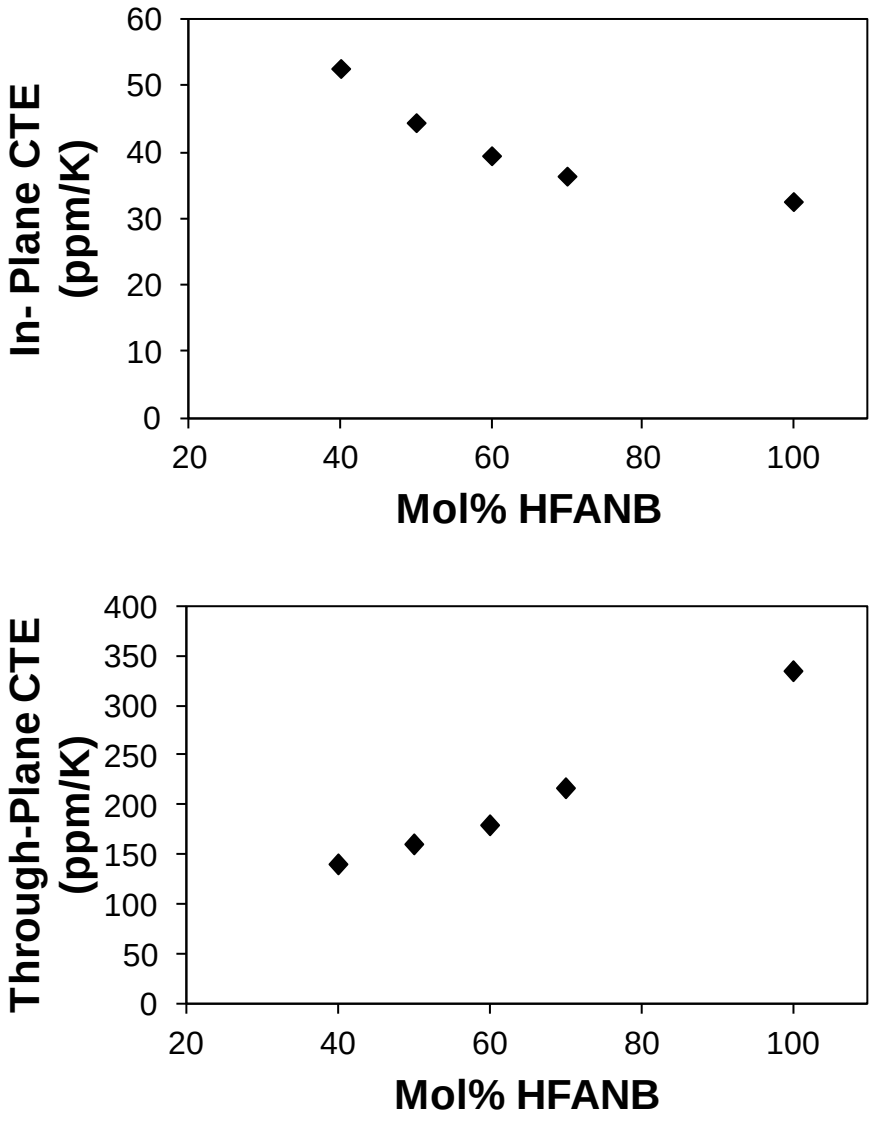

Figure 7.8: CTE of PNB films measured in-plane (top) and through-plane (bottom)

7.3.4 Permittivity

The complex permittivitiy of formulations 5 through 9 were measured at 200 kHz, where the dielectric constant is reported in Figure 7.9 and tanδ in Figure 7.10. As seen in Figure 7.9, the dielectric constant (i.e. real part of the permittivity) decreased with increasing HFANB content. The lowest dielectric constant was for the 70 mol% HFANB / 30 mol% TBENB, which had a value of 2.23. The dielectric constant at very high

frequency, as measured by squaring the index of refraction determined by ellipsometry, is also plotted in Figure 7.9. At the an optical frequency of 500 THz (600 nm), the same 70 mol% HFANB / 30 mol% TBENB exhibits a value of 1.95. The trend of lower permittivity with increasing HFANB content is confirmed by these optical measurements. At the high frequency used for ellipsometric measurements, dipolar and atomic contributions to the dielectric constant are not seen.[79] Tanδ was measured for formulations 5 through 9 at 200 kHz. As with the dielectric constant, tanδ generally decreased with increasing HFANB.

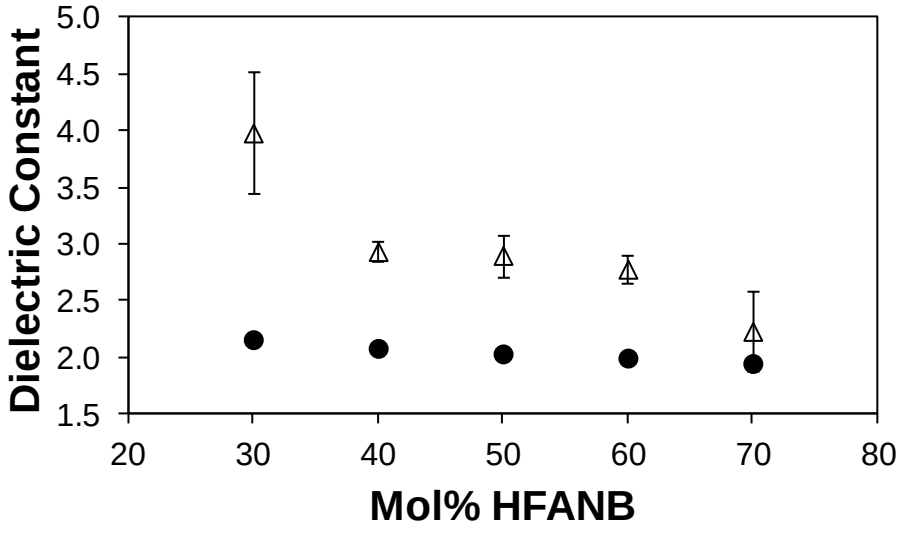

Figure 7.9: Dielectric constant of PNB films at 200 kHz (Δ) and 500 THz (●)

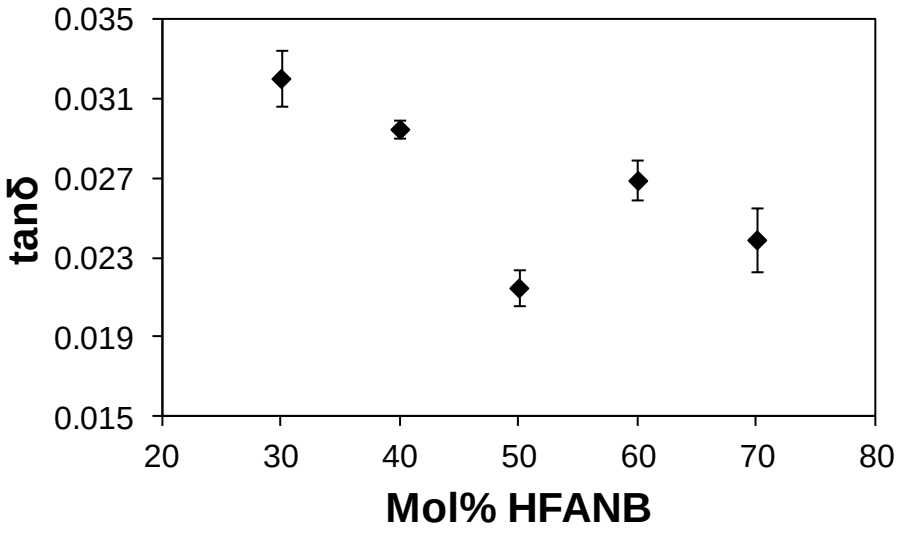

Figure 7.10: Dielectric loss of PNB films measured at 200 kHz

The increasing concentration of less-polarizable carbon-fluorine bonds with HFANB content contributes to lower permittivity and loss. Since the minimum dielectric constant did not occur with the 50 mol% HFANB / 50 mol% TBENB mixture, but rather with the 70 mol% HFANB / 30 mol% TBENB mixture, it appears that the contribution of the carbon-fluorine content (i.e. low polarizability and low affinity for water) outweighs the higher polarizability of the uncross-linked carboxylic acid and alcohol groups. In addition, density differences can contribute to the dielectric constant changes by adding free volume to the cured polymer film.

7.4 Property Comparisons

Table 7.2 lists properties of the CA PNB dielectrics in comparison to the previously discussed HD-8820, BCB, and DNQ-based PNB (Chapters 4 and 5). Lithographic properties are reported for formulation 4 (35/65 mol% HFANB/TBENB with 3 pphr PAG) as it would have been inappropriate to measure the dissolution properties of the blended formulations. Lithographic properties of other monomer ratios were expected to be similar due to the catalytic nature of the photoreaction. All other

properties are reported for formulation 6. As seen in Table 7.2, the D_{100} and contrast of the CA-PNB are orders of magnitude better than any other positive tone dielectric. Additionally, thermal and mechanical properties are appropriate for use as a permanent dielectric, and the dielectric constant is lower than other positive tone materials. The tanδ is lower than the previously measured DNQ-PNB (Chapter 5), but it is not as low as HD-8820 or BCB.

Table 7.2: Properties of CA PNB and other positive tone dielectrics[83], [87], [117], [124] (**not reported)

Property	Unit	HD-8820	BCB	DNQ-PNB	CA-PNB
D_{100}	mJ/cm^2	280	810	408	8
Contrast	-	**	1.02	2.3	> 14.2
Dark Erosion	%	20 - 25	19	2	
Volume Change	%	20	17.4	8	18
T_d (1% Loss)	°C	399	**	305	307
T_{cure}	°C	320	250	180	250
CTE (xy)	ppm/K	64	60	30	40
Modulus	GPa	2	3.6	2 – 2.6	2.6
Dielectric Constant	-	2.94	2.9	3.7 – 3.9	2.78
tanδ	-	0.0089	0.009	0.029 – 0.031	0.0269
Water Uptake	%	< 0.5	1.2 @ 50% RH	not measured	not measured

7.5 Conclusions

A highly light-sensitive, positive tone, permanent dielectric was developed. This dielectric utilized the same CA photochemistry shown in Chapter 6, but the polymer backbone was replaced with copolymer of HFANB and TBENB. This dielectric exhibited excellent lithographic properties, with 8.09 mJ cm^{-2} being the highest sensitivity achieved. At PAG loadings of 0.5 to 3.0 pphr, the contrast could not be measured as it was too high, but it was ≥ 14.2 at all loadings. The PAG loading was found to have negligible effects on the mechanical and electrical properties, likely due to the catalytic nature of the Fischer esterification curing reaction.

The monomer ratio of the copolymer was studied and found to have profound effects on the final film properties. Film shrinkage, elastic modulus, hardness, dielectric constant, and tanδ all decreased with increased HFANB content. IR spectra showed the emergence of an anhydride functional group during the thermal cure. The decreases in elastic modulus and hardness with increasing HFANB are attributed to this, since the anhydride indicates TBENB-to-TBENB cross-linking. The CTE was measured with respect to the monomer ratio, and anisotropy was observed in all films. This was attributed to stacking of PNB chains, which is increased with HFANB due to hydrogen bonding.

The dielectric constant and tanδ vary greatly with the monomer content, which was attributed to the low polarizability of the HFANB functional group. Finally, the lithographic, mechanical, and electrical properties of the CA PNB dielectric were compared to existing positive tone dielectrics. This dielectric outperformed existing dielectrics in all categories except T_d and tanδ. The lithographic properties of this photo-definable dielectric were 10x greater than existing materials. This work is continued in Chapter 7, and recommendations for future work will be discussed there.

CHAPTER 8

ENABLING THICK FILM, CHEMICALLY AMPLIFIED, POLYNORBORNENE DIELECTRICS

The PNB dielectric developed in Chapter 7 has excellent lithographic properties that enable dense patterning of features at low doses. The dielectric also exhibited a low dielectric constant appropriate for use in packaging applications. However, for use in electronics packaging, two more properties must be demonstrated: the ability to coat and pattern a crack-free thick film (> ~5 μm) and sensitivity to 365 nm irradiation.

8.1 Thick Film Considerations

The HFANB/TBENB copolymers cracked after soft baking or after curing when coated to thicknesses above ~3 μm on silicon. This was likely due to a combination of phenomena. First, the in-plane CTE of these polymers was measured to be 36 to 53 ppm K^{-1} depending on the monomer ratio. The CTE of silicon is 3 ppm K^{-1}, so there is a large mismatch between these two materials. This mismatch induces a large stress upon cooling of the film from the cure temperature. For instance, curing a 60/40 mol% HFANB/TBENB copolymer at 250°C would result in a residual stress of 32.6 MPa upon cooling to room temperature. This assumes that the cure temperature is the stress-free temperature (confirmed by experiments) and that deformation is elastic. A film of 40/60 mol% HFANB/TBENB would exhibit a residual stress of 48.9 MPa, because it has a higher elastic modulus and CTE.

Another issue with the CA PNB polymers is the molecular weight. During synthesis the inclusion of the polar TBENB interacts with the catalyst in such a way that it slows down the polymerization. This lowers the polymer molecular weight since termination still occurs at the same rate. Additionally, TBENB contains tert-butyl

acrylate impurities that destroy the catalyst. These effects limit the molecular weight of the polymer to ~50 kg mol^{-1}. The low entanglement at this molecular weight leads to low toughness of the film.

8.2 Formulation Modifications

8.2.1 Sensitizer

Rhodorsil FABA, the PAG used in this PNB dielectric, is sensitive at a range of wavelengths around 248 nm. Unfortunately, its absorbance does not extend into the i-line region. One option to impart 365 nm patternability is to substitute Rhodorsil FABA with a PAG that is sensitive at 365 nm. The available selection of PAGs, however, is limited. Most iodonium and sulfonium PAGs are not sensitive at the higher wavelengths desired.

Another option is to add a sensitizing molecule. This molecule must absorb light at 365 nm and transfer the absorbed energy to the PAG. Thioxanthones are common sensitizers as they have maxima in their absorption at wavelengths between 333 and 416 nm.[125] To sensitize Rhodorsil FABA in this case, a thioxanthone derivative, 1-chloro-4-propoxy-9H-thioxanthen-9-one (CPTX), was added to the formulations. This sensitizer was used previously by Raeis-Zadeh, et al. to increase i-line absorbance for negative tone Avatrel 8000P (PNB). CPTX exhibited excellent solubility in the formulations, and it was added at a loading of 1 pphr. The PAG loading was maintained at 3 pphr.

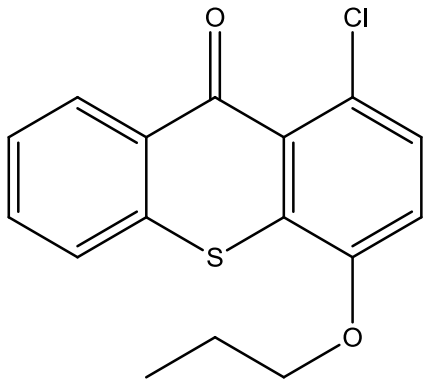

Figure 8.1: Chemical structure of CPTX

8.2.2 ButylNB

One method to improve the mechanical properties of the dielectric is to modify the polymer composition. Non-functional alkyl side chains may serve the purpose of increasing the toughness. To study this, terpolymers were synthesized with HFANB, TBENB, and a third monomer, ButylNB. The chemical structure of this terpolymer is shown in Figure 8.2. In addition to increasing toughness, this butyl side-chain was expected to lower the dielectric constant because of its non-polar nature. A homopolymer of ButylNB is expected to have a dielectric constant of approximately 2.31.[88]

Three polymers were synthesized by Promerus, LLC to study the effect of the butyl pendent group. Similar to PNB-D and PNB-E, PNB-G was a random copolymer of HFANB and TBENB, except PNB-G had a 50/50 molar ratio between the two monomers. PNB-H and PNB-I were terpolymers of HFANB/TBENB/ButylNB with molar ratios of 43/47/10 and 38/38/24.

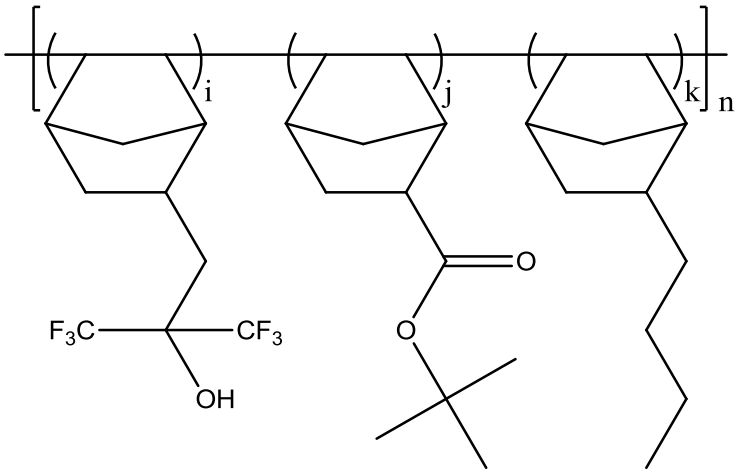

Figure 8.2: Chemical structure of HFANB/TBENB/ButylNB terpolymer

Two potential issues arise with the introduction of the ButylNB monomer. The first is the decrease in solubility. The HFANB and the deprotected TBENB are acidic functional groups that contribute to solubility in aqueous base. ButylNB cannot be deprotonated by TMAH, so adding this monomer lowers the solubility. This lowers the sensitivity since more TBENB must be deprotected to impart solubility. Another issue is the inability of the ButylNB to cross-link. Lowering the density of functional cross-linking pendent groups lowers the final cross-link density.

8.2.3 Low Molecular Weight Additives

A second method to prevent cracking is to add low molecular weight additives to the formulation. These additives lower the modulus of the material and lower the yield strain. In looking at possible additives, two factors were considered: functionality and molecular weight. The functionality of the additive refers to its ability to cross-link into the final structure. To study this, additives were selected with varying numbers of alcohol moieties, as this group could cross-link to carboxylic acids (deprotected TBENB) in the dielectric. The studied additives are listed in Table 8.1 along with their molecular weight and the number of alcohol moieties per molecule.

Table 8.1: Studied plasticizing additives

Additive	Abbreviation	# of Alcohols	Molecular Weight (g mol^{-1})
Poly(ethylene glycol) dimethyl ether	PEGME	0	500
Trimethylolpropane	TMP	3	134.17
Trimethylolpropane ethoxylate	TMPEO	3	450
Pentaerythritol	PE	4	136.15
Pentaerythritol ethoxylate	PEEO	4	270

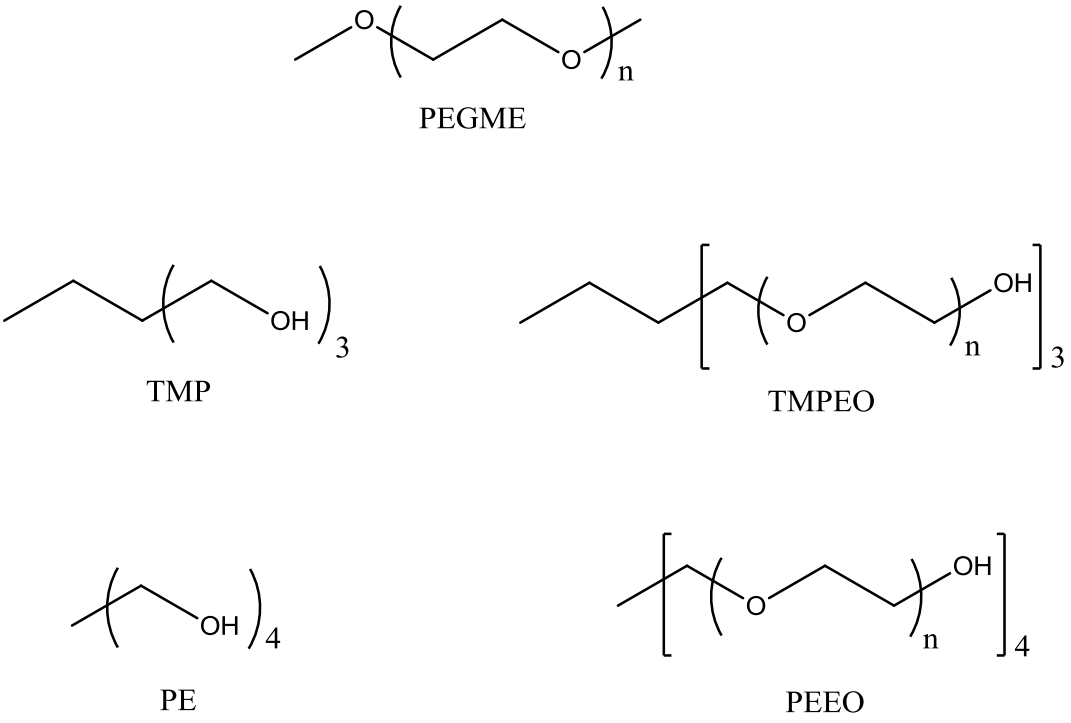

Figure 8.3: Chemical structures of plasticizing additives

8.3 Effect of ButylNB

8.3.1 Mechanical Properties

The elastic moduli and hardness of CA PNB terpolymers were measured by indentation. In Figure 8.4, the modulus of PNB-G, PNB-H, and PNB-I are plotted with respect to the ButylNB mole fraction holding the HFANB/TBENB ratio constant at approximately 1:1 on a molar basis. It can be seen that the introduction of the ButylNB monomer into the terpolymer lowers the modulus and hardness, and this change in mechanical properties is a function of the amount of ButylNB substituted. For the 50/50 mol% copolymer of HFANB/TBENB, the modulus and hardness are 2.64 GPa and 0.287 GPa, respectively. The terpolymer of 24 mol% ButylNB HFANB/TBENB polymer resulted in a lower modulus and hardness, 2.35 GPa and 0.205 GPa, respectively. This result may be due to several factors. First, the ButylNB could exhibit a low modulus due to the oily, butyl pendent groups. The inclusion of ButylNB into the polymer shifts the modulus closer to that of the ButylNB homopolymer. Second, HFANB and TBENB are functional pendent groups that can result in cross-linking of the polymer whereas the butyl substituent cannot participate in cross-linking. Thus, the inclusion of ButylNB likely results in lower cross-link density and lower elastic modulus since the modulus increases with cross-linking.

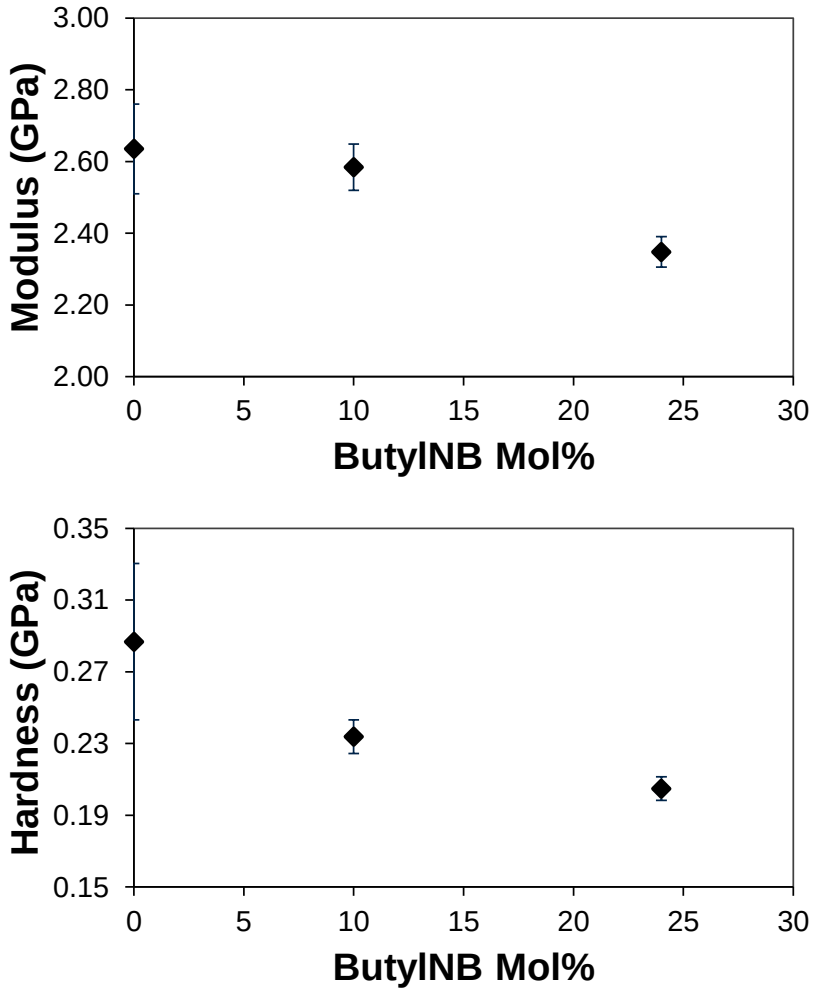

Figure 8.4: Modulus (top) and hardness (bottom) as a function of ButylNB content

8.3.2 Electrical Properties

The dielectric constant of PNB terpolymers was measured in order to evaluate the effect of the ButylNB content on the electrical properties. Although ButylNB has a lower polarity than the other two monomers in the terpolymer, the dielectric constant increased with the inclusion of the ButylNB monomer in the terpolymer, as shown in Figure 8.5. Previous work showed that increasing the HFANB mol% in the copolymer decreased the dielectric constant, likely due to the low polarizability of the CF_3 moieties. It is possible that replacement of the HFANB with ButylNB may increase the dielectric constant

because HFANB has a lower polarizability than ButylNB. The substitution led to an overall increase in the dielectric constant from 2.78 to 3.48. In addition, decreasing the concentration of the cross-linkable pendent groups (HFANB and TBENB) with ButylNB could result in a lower cross-link density after cure affecting the final film properties. Also, uncross-linked acidic groups would increase the dielectric constant because they have high polarizability. An increase in density could also cause the increase in dielectric constant. However, to achieve the observed dielectric constant increase, the density would have to increase by 20 to 30%. This was not supported by refractive index measurements. The refractive index (measured at 638 nm) only increased from 1.467 for the polymer with 0 mol% ButyNB to 1.470 for the polymer with 24 mol% ButyNB. Since the refractive index was relatively unaffected by the inclusion of ButylNB, the dielectric constant increase was likely not a density effect. The unaffected refractive index also suggests that the increase in dielectric constant at 200 kHz was due to an increase in dipolar or atomic polarizability. Electronic contributions are captured in the index of refraction.

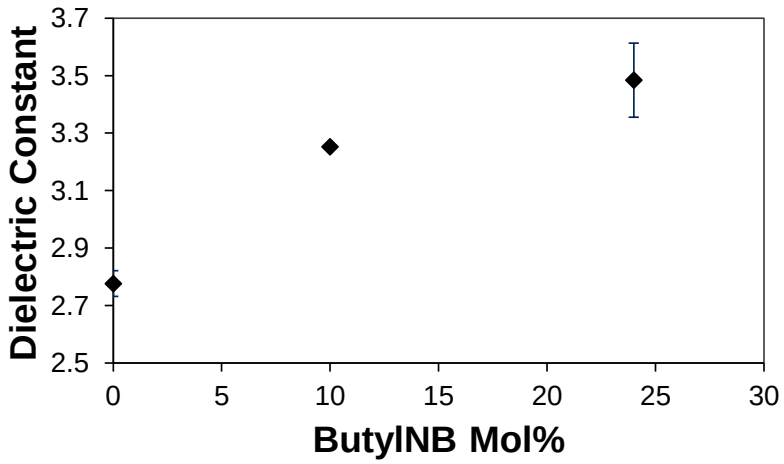

Figure 8.5: Dielectric constant as a function of ButylNB content

8.3.2 Lithographic Properties

The lithographic properties of PNB-H with 3 pphr PAG and no CPTX were measured at 248 nm to evaluate the effect of ButylNB. As seen in Figure 8.6, the resulting contrast curve looked very similar to contrast curves of the HFANB/TBENB copolymer. Even though the number of protected TBENB groups is very different, the catalytic photoreaction results in a sharp onset of solubility near the same dose. The D_{100} of this formulation was measured to be 15 mJ cm^{-2}, and the contrast was $\geq$ 16.8.

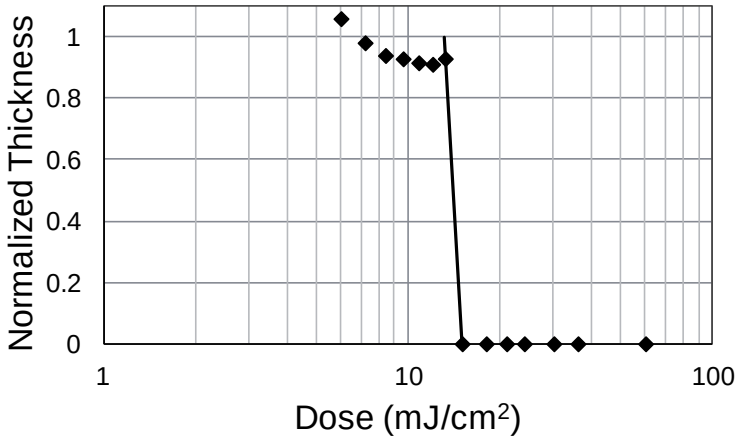

Figure 8.6: Contrast curve of PNB-H

The same lithographic experiments were performed on a formulation of PNB-I, which had 24 mol% ButylNB. This formulation, however, was insoluble in developer at any exposure dose. This indicates that the ButylNB decreased the solubility of the polymer in TMAH, and the solubility limit is somewhere between 10 and 24 mol%, holding the other two monomers to a 1:1 molar ratio.

8.4 Effect of Low Molecular Weight Additives

8.4.1 Miscibility of Additives

The addition of low molecular weight plasticizing additives to the polymers can be used to improve the thick-film mechanical properties. In evaluating potential additives, it was desired to understand how the ability of the additive to cross-link into the final structure and molecular weight affect the material properties. Five additives were chosen for this purpose. PEGME was chosen as a nonfunctional additive that cannot cross-link. TMP and TMPEO were two trifunctional additives of different molecular weight. Pentaerythritol and pentaerythritol ethoxylate were tetrafunctional additives of different molecular weight. Five different formulations of PNB-E (35/65 mol% HFANB/TBENB) were made, each with a different additive. Formulations were mixed at 20 pphr of each additive. It was found that only PEGME, TMP, and TMPEO were visibly miscible with the PNB base polymer. Pentaerythritol and pentaerythritol ethoxylate are likely too hydrophilic for high miscibility with the hydrophobic polymer. However, it was undetermined whether these additives were completely immiscible or if a miscibility limit had been reached, so films were cast with each formulation and cured.

Films prepared with pentaerythritol ethoxylate were of poor quality after spin coating due to the immiscibility of the additive with the base polymer. Films prepared with PEGME produced good quality films after spinning and soft bake, but upon curing, an oily layer was observed on the surface of these samples. Later attempts to evaporate aluminum on PEGME-containing films proved difficult as the aluminum did not adhere to thie oily film. It is likely that PEGME diffused out of the film to the surface at the elevated cure temperature. Curing of TMPEO-loaded films, on the other hand, produced high quality films with no oily film. This suggests that the alcohol groups on TMPEO participate in the cross-linking polymer reaction and are no longer mobile after curing.

The polymer films made with TMP, TMPEO, and pentaerythritol produced high quality films without cracks. The elastic modulus of the high quality films are compared to a control film with no additive. The modulus of the control film was 3.27 GPa, whereas films with TMP and pentaerythritol had a modulus of 3.38 GPa and 3.34 GPa, respectively. These are slightly higher than the value without additives, though the standard deviation of the measurement was measured to be ~0.9 GPa. This indicates that TMP and pentaerythritol had little influence on the mechanical properties, likely due to immisciblity. A film with TMPEO was measured to have an elastic modulus of 2.69 GPa, which is a clear decrease from the value without additives. Additional testing was performed on TMPEO containing films since it was the only additive to lower the elastic modulus, completely dissolve into the starting mixtures, and produce high quality films.

8.4.2 Mechanical Properties

Polymer formulations were prepared with PNB-D (70/30 mol% HFANB/TBENB) with various TMPEO loadings. The 70/30 polymer produced the lowest modulus and dielectric constant of the copolymers investigated in a previous work.[124] Mechanical properties of the TMPEO-loaded films were measured by nanoindentation. As seen in Figure 8.7, the elastic modulus of the film decreased from 2.47 to 1.80 GPa and the hardness decreased from 0.20 to 0.14 GPa with the addition of 20 pphr TMPEO. Films with 10 pphr TMPEO were coated to 4.8 μm thickness without cracks. Minor cracking was seen at 5.7 um. Films with 15 and 20 pphr TMPEO did not exhibit cracking at any thicknesses attempted, up to 7.5 um. Without TMPEO, cracks were observed in all films greater than 3 μm thick.

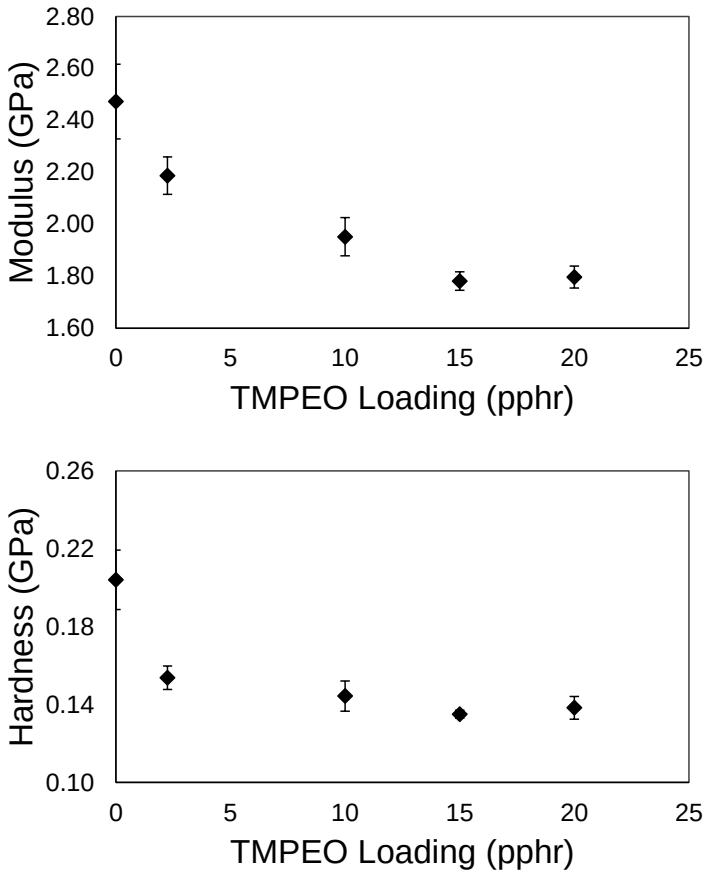

Figure 8.7: Effect of TMPEO on modulus (top) and hardness (bottom) of CA PNB dielectric

8.4.3 Electrical Properties

The dielectric constant of the PNB-D formulations with TMPEO was measured. The addition of 5 pphr TMPEO to PNB-D resulted in a slight decrease in the dielectric constant, however, the dielectric constant increased at higher TMPEO concentrations. Without TMPEO, cross-linking proceeds via the esterification reaction until the mobility of the polymer is sufficiently low so as to prevent further reaction. The presence of TMPEO increases the mobility of reactive groups within the polymer matrix. The polarizability of the resulting ester is lower than that of the carboxylic acid reactant giving the ester product a lower dielectric constant. Increasing the loading of TMPEO shifts the alcohol-to-carboxylic acid ratio. When the ratio of alcohol-to-acid becomes too

high, by addition of excess TMPEO, the unreacted alcohol adds to the dielectric constant. Unreacted TMPEO can also act as mobile charge carriers in the dielectric if they are not bound to the cross-linked matrix. The dielectric losses of TMPEO-containing films were also measured. As seen in Figure 8.9, these values do not vary significantly at loadings of ≤ 15 pphr. Poor cross-linking of excess TMPEO groups could cause the high variation measured at 20 pphr TMPEO.

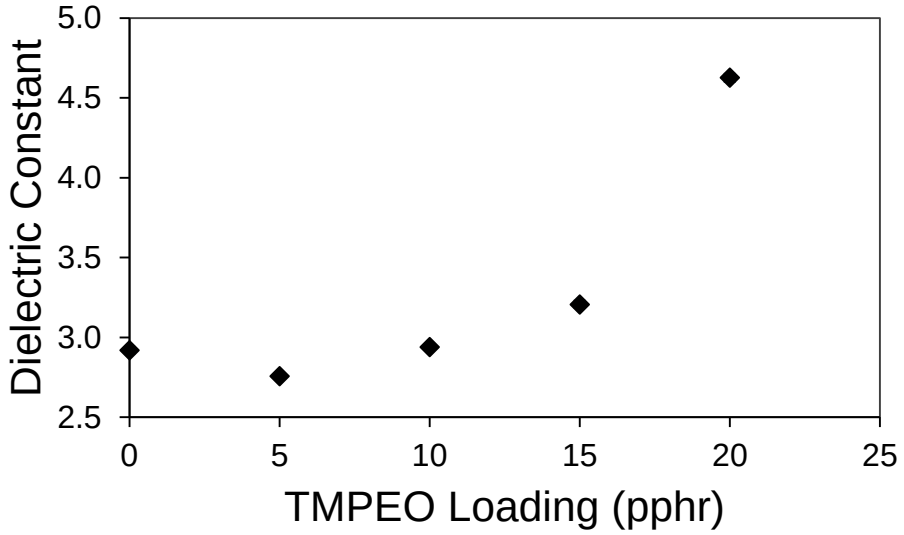

Figure 8.8: Effect of TMPEO on dielectric constant of CA PNB dielectric

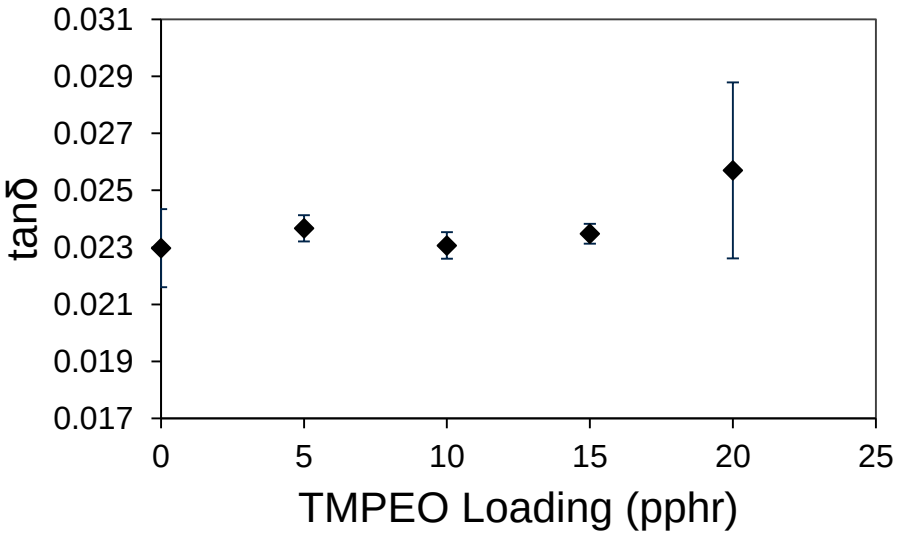

Figure 8.9: Dielectric loss of CA PNB dielectric with TMPEO

8.4.4 Lithographic Properties

The positive results from the mechanical and electrical measurements by the TMPEO to the films merited a detailed study of the lithographic properties. QCM experiments were performed to evaluate the swelling behavior of the PNB films. Previous results showed that non-CA, positive tone PNB dielectrics readily swelled when exposed to aqueous base developer.[116] The presence of aqueous base in the film before curing can negatively impact the acid-catalyzed cross-linking reaction, so minimal swelling is desired. Formulations of PNB-E with 10 pphr TMPEO were coated onto QCM crystals and processed in the same way as described above. The unexposed films were baked at 140°C (the PEB temperature) for various times and developed in a QCM flow cell for 90 s with aqueous base. Figure 8.10 shows the QCM traces of normalized mass change with respect to time. Prior to the experiment, water flowed through the flow cell so that a sharp air-to-liquid transition was not seen when the sample was exposed to the developer. At time zero, a valve in the flow path was switched from water to TMAH. This resulted in TMAH reaching the sample at approximately the 10 s mark. As seen in

Figure 8.10, the samples baked for 30 and 60 s exhibited little or no mass change as a result of the TMAH. However, samples baked for 120 s and 240 s slowly dissolved (the mass decreases) upon exposure to TMAH. For reference, fully exposed samples developed within 15 s of contact with TMAH. This dark erosion (i.e. development of the unexposed regions) is unusual since the 140°C bake temperature should not be hot enough to cause thermal degradation of the TBE or the PAG. Similar QCM experiments were performed with a PNB-E formulation without any TMPEO. It was found that this formulation exhibited no dark erosion even when baked for 240 s at 140°C. This shows that TMPEO affects the solubility of the protected polymer. The effect of the PEB time on the solubility of the polymer suggests that a reaction is occurring.

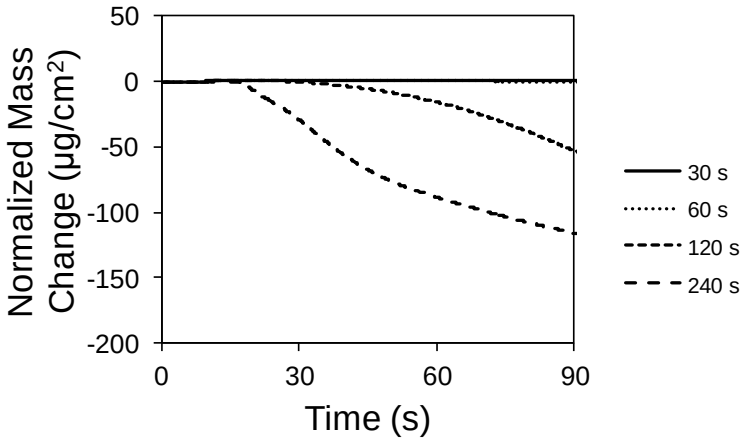

Figure 8.10: QCM traces of PNB-E with 10 pphr TMPEO baked at 140°C for various times

The thermal stability of the PNB-E with various loadings of TMPEO and PAG was investigated using TGA. The base polymer without any additives decomposed at 212°C. This is an appropriate temperature for the thermal deprotection of TBENB. Additionally, the loss of 15% to 20% of the overall mass was expected based on the mass of isobutylene released during the deprotection of TBENB. When TMPEO was added to

the PNB-E, no change in the deprotection temperature was observed. Next, a film of PNB-E was analyzed that had 3 pphr PAG. In this film, the deprotection occurred at 176°C, which is approximately the temperature at which the PAG thermally decomposes. Once PAG decomposition occurs, a strong acid is generated that can catalyze the deprotection reaction. When 3 pphr PAG and 5 pphr TMPEO were added to PNB-E, the deprotection temperature shifted to 160°C, a lower temperature than PAG or TMPEO alone. Finally, a film of PNB-E with 3 pphr PAG and 10 pphr TMPEO exhibited a deprotection temperature at 145°C.

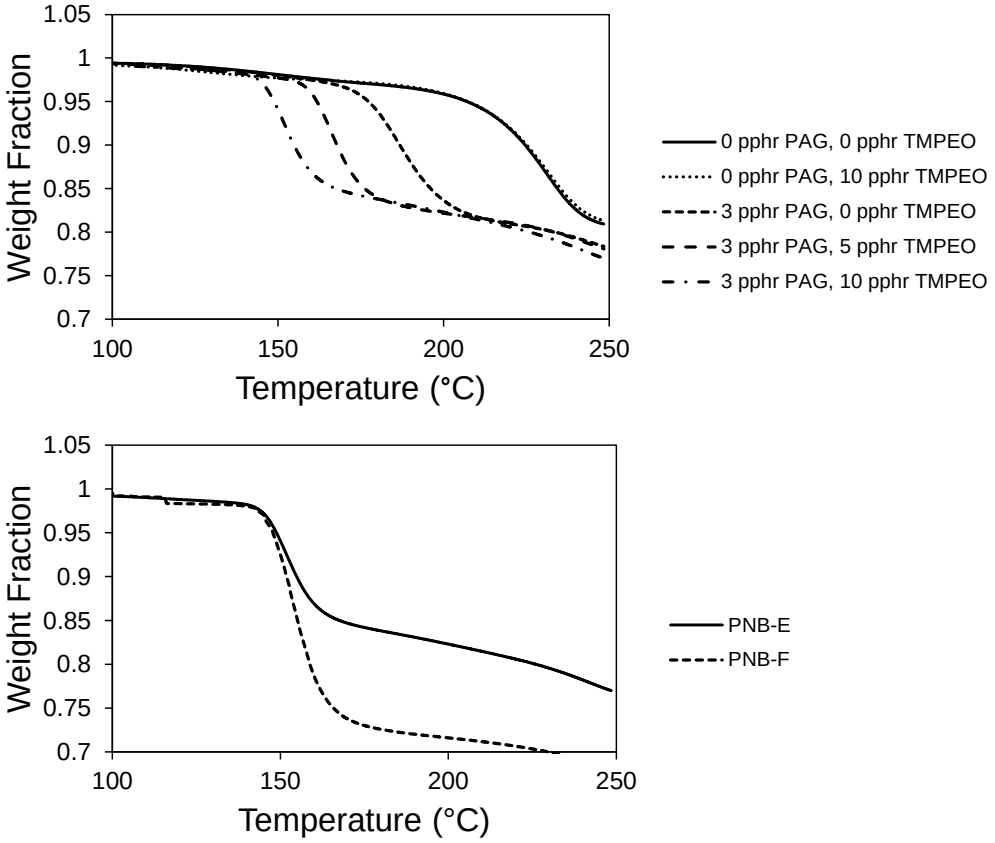

Figure 8.11: TGA traces of (top) PNB-E films with various additive loadings and (bottom) PNB-E and PNB-F with 3 pphr PAG and 10 pphr TMPEO

The same TGA experiment was performed with a film of PNB-F loaded with 3 pphr PAG and 10 pphr TMPEO. This film exhibited the same deprotection temperature as the PNB-C film with the same loadings, indicating that HFANB is not participating in the reaction. It is hypothesized from these QCM and TGA results that the TMPEO lowers the decomposition temperature of the PAG. Crivello et al. found that the diaryl iodonium PAG is reduced during the decomposition reaction, and the products can lower the energy required for the deprotection reaction.[126], [127] It is likely that TMPEO acts as a reducing agent in this system, and the decomposition temperature of the PAG depends on the concentration of TMPEO. The QCM and TGA results correlate well for formulations with 3 pphr PAG and 10 pphr TMPEO. Even though there is a slight temperature discrepancy between the hot plate and the TGA, the 140°C PEB is very close to the observed deprotection temperature. It is likely that the 140°C PEB causes a small amount of deprotection of the PNB-E that imparts solubility in the aqueous base developer.

Based on the results given above, the PEB time was kept at 60 s. It is noted that dark erosion could also be mitigated by lowering the PEB temperature or reducing the amount of TMPEO, but these were not explored. The contrast and sensitivity of PNB-E with 3 pphr PAG, 10 pphr TMPEO, and 1 pphr CPTX were measured using a 1.48 µm film. The films were exposed at 365 nm and the resulting contrast curve is plotted in Figure 8.12. The sensitivity (D_{100}) of this formulation was measured to be 175 mJ cm^{-2}, which is significantly higher than the same PNB dielectric without plasticizer at 248 nm (8.09 mJ cm^{-2}).[124] This can be attributed to two factors. First, 248 nm radiation directly activates the PAG, whereas exposure at 365 nm requires an inefficient energy transfer between the CPTX and PAG. The second, the TMPEO introduces excess water into the film before exposure. The excess water forms a hydrated hydronium ion rather than the strong acid which would exist in the absence of excess water. These hydronium ions catalyze the deprotection reaction at a slower rate, resulting in a loss of sensitivity.

The water from the film could be baked out at an elevated temperature, but the above mentioned PAG/TMPEO reaction limited the temperature excursion. The contrast of this formulation was 4.36. It is noted that both the sensitivity and contrast are better than existing positive tone dielectrics.[87], [122]

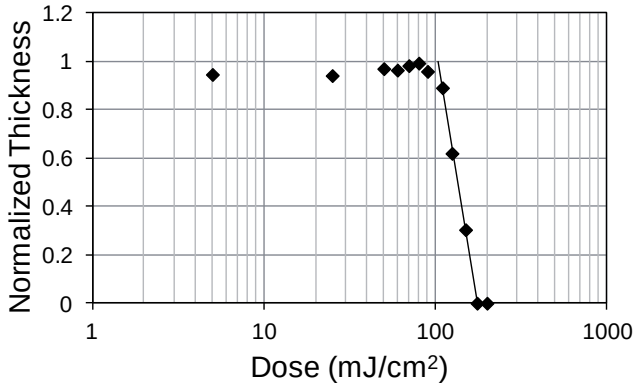

Figure 8.12: Contrast curve of PNB-E with 3 pphr PAG, 10 pphr TMPEO, and 1 pphr CPTX

SEM micrographs of patterned films are shown in Figure 8.13. Since soft contact photolithography was employed, diffraction limited the minimum feature size achievable. The top and middle images in Figure 8.13 show 50 µm and 16 µm half-pitch trenches, respectively, in a 4.5 µm film, exposed at 360 mJ cm^{-2}. The bottom image shows 16 µm half-pitch hills in the same 4.5 µm film, exposed at 225 mJ cm^{-2}. It can be seen that both hills and trenches have nearly vertical side-wall profiles. Exposure of this film with an appropriate photolithography tool could enable very high aspect ratio features.

Figure 8.13: SEMs of 50 µm trenches (top), 16 µm trenches (middle), and 16 µm hills (bottom)

8.5 Conclusions and Recommendations

Two methods were employed to improve the mechanical properties of the dielectric developed in Chapter 7. First, ButylNB was added as a third monomer to the polymer backbone. The substitution of HFANB/TBENB with ButylNB resulted in a lower modulus and hardness. However, this substitution also increased the dielectric constant, which is undesirable. A terpolymer with 10 mol% ButylNB exhibited similar lithographic properties to the HFANB/TBENB copolymer, with a D_{100} of 15 mJ cm^{-2} and contrast of $\geq$ 16.8. When the ButylNB content was increased to 24 mol%, the terpolymer was no longer soluble in aqueous base.

The second method employed was to add small molecular weight, plasticizing additives to the HFANB/TBENB copolymer formulations. Five additives were initially evaluated which varied in cross-linking functionality and molecular weight. Of the five, only TMPEO was fully miscible, produced high quality films, and remained in the film

during the cure. The effect of TMPEO on the mechanical properties was measured, and it lowered the elastic modulus and hardness significantly. This allowed enabled ≥ 4.8 μm films with 10 pphr TMPEO and ≥ 7.5 μm films with ≥ 15 pphr TMPEO.

At low loadings, it was found that TMPEO improved the dielectric constant, likely by reacting with carboxylic acids to produce the less-polarizable ester. At loadings of ≥ 15 pphr, TMPEO was found to significantly increase the dielectric constant. Partial solubility of the films in TMAH was observed when baked at 140°C for ≥ 120 s, and this was attributed to a TMPEO-PAG interaction whereby the degradation temperature of the PAG is decreased. This was supported with TGA experiments.

Finally, an optimum formulation of 10 pphr TMPEO, 3 pphr PAG, and 1 pphr CPTX (for 365 nm sensitivity) was set along with the processing conditions to minimize the thermal conversion of the PAG. This formulation exhibited a D_{100} of 175 mJ cm^{-2} and contrast of 4.36. Both of these properties are worse than the formulation evaluated in Chapter 7 but better than existing positive tone dielectrics. SEM of these patterns showed nearly vertical side-wall profiles.

There exist many area in which these materials may be further evaluated. First, optimization of the polymer synthesis may enable higher molecular weight and adequate entanglement for thick film dielectrics. Additionally, adding other miscible PNB polymers of high molecular weight could induce entanglement without having to improve the TBENB polymerization. In addition to increasing the molecular weight, other additives should be evaluated and in more detail. It is anticipated that these copolymers will exhibit the same unique dissolution characteristic as seen in Chapter 3. If so, this could be used advantageously to affect the lithographic properties. QCM analysis should be performed with other additives to evaluate these effects. Finally, work should be performed to lower the cure temperature of the CA PNB system. This could be done by lowering the T_g of the polymer with additives; however, the measurement of T_g in PNB polymers in non-trivial, so this was not pursued in this work.

REFERENCES

[1] Intel Corporation, “Intel’s Newest Microarchitecture and 14nm Manufacturing Process,” *Intel Newsroom*, 2014. [Online]. Available: http://newsroom.intel.com/docs/DOC-5677. [Accessed: 05-Nov-2014].

[2] R. R. Tummala and M. Swaminathan, *Introduction to System-on-Package*. New York: McGraw-Hill, 2008.

[3] P. A. Kohl, “Low-dielectric constant insulators for future integrated circuits and packages,” *Annu. Rev. Chem. Biomol. Eng.*, vol. 2, pp. 379–401, Jan. 2011.

[4] P. E. Garrou, W. B. Rogers, D. M. Scheck, A. J. G. Strandjord, Y. Ida, K. Ohba, and S. Member, “Stress-Buffer and Passivation Processes for Si and GaAs IC’s and Passive Components Using Photosensitive BCB: Process Technology and Reliability Data,” *IEEE Trans. Adv. Packag.*, vol. 22, no. 3, pp. 487–498, 1999.

[5] X. J. Fan, B. Varia, and Q. Han, “Design and optimization of thermo-mechanical reliability in wafer level packaging,” *Microelectron. Reliab.*, vol. 50, no. 4, pp. 536–546, Apr. 2010.

[6] P. N. An and P. A. Kohl, “Modeling Simplification for Thermal Mechanical Analysis of High Density Chip-to-Substrate Connections,” *J. Electron. Packag.*, vol. 133, no. 4, p. 041004, 2011.

[7] W. W. Flack, G. E. Flores, L. D. Christensen, and G. Newman, “An Investigation of the Properties of Photosensitive Polyimide Films,” *Proc. SPIE*, vol. 2726, no. 75, pp. 169–185, Jun. 1996.

[8] D. Frear, *Springer Handbook of Electronic and Photonic Materials*. 2007, pp. 1267–1285.

[9] Intel Corporation, “Ball Grid Array (BGA) Packaging,” in *Packaging Databook*, 2000, pp. 14–4.

[10] M. Huang, O. G. Yeow, C. Y. Poo, and T. Jiang, “Intermetallic Formation of Copper Pillar With Sn–Ag–Cu for Flip-Chip-On-Module Packaging,” *IEEE Trans. Components, Packag. Manuf. Technol.*, vol. 31, no. 4, pp. 767–775, 2008.

[11] E. D. Blackshear, M. Cases, E. Klink, S. R. Engle, R. S. Malfatt, D. N. de Araujo, S. Oggioni, L. D. LaCroix, J. a. Wakil, N. H. Pham, G. G. Hougham, and D. J. Russell, “The evolution of build-up package technology and its design challenges,” *IBM J. Res. Dev.*, vol. 49, no. 4.5, pp. 641–661, Jul. 2005.

[12] W. W. Flack, S. Kulas, and C. L. Franklin, “Characterization Study of an Aqueous Developable Photosensitive Polyimide on 300 mm Wafers,” *SPIE*, vol. 4346–96, pp. 1–11, Sep. 2001.

[13] S. K. Bhattacharya, K. S. Moon, R. R. Tummala, and G. S. May, “Meniscus Coating : A Low-Cost Polymer Deposition Method for System-on-Package (SOP) Substrates,” *IEEE Trans. Electron. Packag. Manuf.*, vol. 26, no. 2, pp. 110–114, 2003.

[14] B. N. J. Trujillo, Q. Wu, and K. K. Gleason, “Ultralow Dielectric Constant Tetravinyltetramethylcyclotetrasiloxane Films Deposited by Initiated Chemical Vapor Deposition (iCVD),” *Adv. Funct. Mater.*, vol. 20, pp. 607–616, 2010.

[15] A. Grill and V. Patel, “Interaction of Hydrogen Plasma with Extreme Low-k SiCOH Dielectrics,” *J. Electrochem. Soc.*, vol. 151, no. 6, p. F133, 2004.

[16] E. T. Ryan, S. M. Gates, A. Grill, S. Molis, P. Flaitz, J. Arnold, M. Sankarapandian, S. a. Cohen, Y. Ostrovski, and C. Dimitrakopoulos, “Property modifications of nanoporous pSiCOH dielectrics to enhance resistance to plasma-induced damage,” *J. Appl. Phys.*, vol. 104, no. 9, p. 094109, 2008.

[17] R. D. Allen, G. M. Wallraff, R. A. Dipietro, and D. C. Hofer, “193 nm Single Layer Positive Resists Building Etch Resistance Into a High Resolution Imaging System,” *Proc. SPIE*, vol. 2438, no. Advances in Resist Technology and Processing XII, pp. 474–485, 1995.

[18] S. F. Wanat, R. R. Plass, and M. D. Rahman, “Novolak resins and the microelectronic revolution,” *J. Micro/Nanolithography, MEMS MOEMS*, vol. 7, no. 3, pp. 033008–1–033008–11, 2008.

[19] F. A. Vollenbroek, W. P. M. Nijssen, C. M. J. Mutsaers, M. J. H. J. Geomini, M. E. Reuhman, and R. J. Visser, “The chemistry of g-line photoresist processes,” *Polym. Eng. Sci.*, vol. 29, no. 14, pp. 928–936, Aug. 1989.

[20] M. W. Davidson, “Fundamentals of Mercury Arc Lamps,” *Education in Microscopy and Digital Imaging*. [Online]. Available: http://zeiss-campus.magnet.fsu.edu/articles/lightsources/mercuryarc.html. [Accessed: 05-Nov-2014].

[21] T. Ito and S. Okazaki, “Pushing the limits of lithography,” *Nature*, vol. 406, no. August, pp. 1027–1031, 2000.

[22] C. A. Mack, “PROLITH: a comprehensive lithography model,” *Proc. SPIE*, vol. 538, no. Optical Microlithography, pp. 207–220, 1985.

[23] S. Angaluri and K. Vidimce, “Fresnel Diffraction, Single Slit: Theory.” [Online]. Available: http://webtop.msstate.edu/singleslit/theory/2.html. [Accessed: 05-Nov-2014].

[24] C. J. Lawrence, “The mechanics of spin coating of polymer films,” *Phys. Fluids*, vol. 31, no. 10, pp. 2786–2795, 1988.

[25] Y. Bai, “Photodefinition and Structure-Property Relations for Polynorbornene Based Dielectric,” Georgia Institute of Technology, 2001.

[26] R. Rubner, “Innovation via Photosensitive Polyimide and Poly(benzoxazole) Precursors - a Review by Inventor,” *J. Photopolym. Schience Technol.*, vol. 17, no. 5, pp. 685–691, 2004.

[27] N. Fritz, R. Saha, S. A. B. Allen, and P. A. Kohl, “Photodefinable Epoxycyclohexyl Polyhedral Oligomeric Silsesquioxane,” *J. Electron. Mater.*, vol. 39, no. 2, pp. 149–156, Dec. 2009.

[28] M. Raeis-zadeh, E. Elce, B. Knapp, and P. A. Kohl, “Cross-linking of Aqueous Base-Developable , Photosensitive Polynorbornene,” *J. Appl. Polym. Sci.*, vol. 120, pp. 1916–1925, 2011.

[29] V. Rajarathinam, C. H. Lightsey, T. Osborn, B. Knapp, E. Elce, S. A. Bidstrup Allen, and P. A. Kohl, “Aqueous-Develop, Photosensitive Polynorbornene Dielectric: Properties and Characterization,” *J. Electron. Mater.*, vol. 38, no. 6, pp. 778–786, Mar. 2009.

[30] L. W. Flanagin, C. L. McAdams, W. D. Hinsberg, I. C. Sanchez, and C. G. Willson, “Mechanism of Phenolic Polymer Dissolution: Importance of Acid−Base Equilibria,” *Macromolecules*, vol. 32, no. 16, pp. 5337–5343, Aug. 1999.

[31] Y.-K. Han and A. Reiser, “Length of Phenolic Strings in Dissolution Inhibition Resists,” *Macromolecules*, vol. 31, no. 25, pp. 8789–8793, Dec. 1998.

[32] Y.-K. Han, Z. Yan, and A. Reiser, “Mechanism of the Trefonas Effect (Polyphotolysis) in Novolak−Diazonaphthoquinone Resists,” *Macromolecules*, vol. 32, no. 25, pp. 8421–8426, Dec. 1999.

[33] M. Hanabata, F. Oi, and A. Furuta, “Novolak design concept for high performance positive photoresists,” *Polym. Eng. Sci.*, vol. 32, no. 20, pp. 1494–1499, Oct. 1992.

[34] M. Hanabata, Y. Uetani, and A. Furuta, “Design concept for a high-performance positive photoresist,” *J. Vac. Sci. Technol. B*, vol. 7, no. 4, pp. 640–650, 1989.

[35] R. Hanawa, Y. Uetani, and M. Hanabata, “Design of PACs for High-Performance Photoresists (I) Role of Di-esterified PACs having hindered -OH groups,” *Proc.*

SPIE, vol. 1672, no. Advances in Resist Technology and Processing IX, pp. 231–241, 1992.

[36] R. Hanawa, Y. Uetani, and M. Hanabata, "Design of PACs for High-Performance Photoresists (II) Effect of number and orientation of DNQs and -OH of PACs on lithographic performances," *Proc. SPIE*, vol. 1925, pp. 227–234, 1992.

[37] C. L. Henderson, P. C. Tsiartas, L. L. Simpson, K. D. Clayton, S. Pancholi, A. R. Pawloski, and C. G. Wilison, "Factors Affecting the Dissolution Rate of Novolac Resins II: Developer Composition Effects," *Proc. SPIE*, vol. 2724, no. Advances in Resist Technology and Processing XIII, pp. 481–490, 1996.

[38] S. Jha, A. Reiser, L. Sruobkova, and R. Zahradnı, "A New Design Principle for the Photoactive Components (PACs) of Dissolution Inhibition Resists," *Macromolecules*, vol. 31, no. 19, pp. 6549–6553, 1998.

[39] M. S. Kim and A. Reiser, "Effect of Salt on the Dissolution of Novolak in Base," *Proc. SPIE*, vol. 3049, no. Advances in Resist Technology and Processing XIV, pp. 528–534, 1997.

[40] M. S. Kim and A. Reiser, "Percolation View of Novolak Dissolution. 7. The Effect of Salts," *Macromolecules*, vol. 30, no. 13, pp. 3860–3866, Jun. 1997.

[41] H.-Y. Shih and A. Reiser, "Dissolution Promotion in Novolak-Diazoquinone Resists," *Proc. SPIE*, vol. 3049, no. Advances in Resist Technology and Processing XIV, pp. 340–344, 1997.

[42] H.-Y. Shih and A. Reiser, "Percolation View of Novolak Dissolution. 5. The Dissolution of Exposed Resist Films," *Macromolecules*, vol. 29, no. 6, pp. 2082–2087, Jan. 1996.

[43] H.-Y. Shih and A. Reiser, "Percolation View of Novolak Dissolution. 6. The Acceleration of Novolak Dissolution by Phenolic Additives," *Macromolecules*, vol. 30, no. 13, pp. 3855–3859, Jun. 1997.

[44] H.-Y. Shih, H. Zhuang, A. Reiser, I. Teraoka, J. Goodman, and P. M. Gallagher-Wetmore, "Percolation View of Novolak Dissolution . 10 . Effect of Resin Molecular," *Macromolecules*, vol. 31, no. 4, pp. 1208–1213, 1998.

[45] H.-Y. Shih and A. Reiser, "A Percolation View of Novolak Dissolution. 4. Mechanism of Inhibitor Action," *Macromolecules*, vol. 28, no. 16, pp. 5595–5600, Jul. 1995.

[46] H. Shih and A. Reiser, "Percolation View of Novolak Dissolution . 8 . Effect of the Base Cation on Dissolution Rate," *Macromolecules*, vol. 30, no. 15, pp. 4353–4356, 1997.

[47] H.-Y. Shih, T. F. Yeh, A. Reiser, R. R. Dammel, H. J. Merrem, and G. Pawlowski, "A Percolation View of Novolak Dissolution. 3. Dissolution Inhibition," *Macromolecules*, vol. 27, no. 12, pp. 3330–3336, 1994.

[48] Z. Yan and A. Reiser, "Effect of Hydrogen Acceptors on pKa of Phenolic Resins: Link to Dissolution Inhibition," *Macromolecules*, vol. 31, no. 22, pp. 7723–7727, 1998.

[49] J. J. M. Vleggaar, A. H. Huizer, P. A. Kraakman, W. P. M. Nijssen, R. J. Visser, and C. A. G. O. Varma, "Photoinduced Wolff-Rearrangement of 2-Diazo- 1 - naphthoquinones : Evidence for the Participation of a Carbene Intermediate," *J. Am. Chem. Soc.*, vol. 116, no. 26, pp. 11754–11763, 1994.

[50] P. Trefonas III and B. K. Daniels, "New Principle for Image Enhancement in Single Layer Positive Photoresists," *SPIE*, vol. 771, no. Advances in Resist Technology and Processing IV, pp. 194–210, 1987.

[51] D. Meyerhofer, "Photosolubility of diazoquinone resists," *IEEE Trans. Electron Devices*, vol. 27, no. 5, pp. 921–926, May 1980.

[52] C. G. Wilisona, A. Reiserc, C. G. Willson, R. A. Dammel, and A. Reiser, "Photoresist Materials: A Historical Perspective," *Proc. SPIE*, vol. 3048, no. Emerging Lithographic Technologies, pp. 28–41, 1997.

[53] J. Frechet, E. Eichler, H. Ito, and C. Willson, "Poly (p-tert-butoxycarbonyloxystyrene): a convenient precursor to p-hydroxystyrene resins," *Polymer (Guildf).*, vol. 24, pp. 995–1000, 1983.

[54] H. Ito, "Chemical amplification resists : History and development within IBM," *IBM J. Res. Dev.*, vol. 44, no. 1, pp. 119–130, 2000.

[55] E. Reichmanis, F. M. Houlihan, O. Nalamasu, and T. X. Neenan, "Chemical Amplification Mechanisms for Microlithography," *Chem. Mater.*, vol. 3, no. 3, pp. 394–407, 1991.

[56] R. Ichikawa, M. Hata, N. Okimoto, S. Oikawa-Handa, and M. Tsuda, "Acid-Catalyzed Deprotection Mechanism of tert-Butyloxycarbonyloxy Polymers in Chemically Amplified Resists," *J. Polym. Sci. Part A Polym. Chem.*, vol. 36, pp. 1035–1042, 1998.

[57] J. Cameron, J. Thackeray, J. W. Sung, S. M. Coley, V. Jain, O. Ongayi, M. D. Wagner, P. LaBeaume, A. Kwok, D. Valeri, M. Hellion, B. Icard, B. Dal'zotto, C. Sourd, and L. Pain, "Comparison of EUV and e-Beam Lithographic Technologies for Sub 22nm Node Patterning," *Proc. SPIE*, vol. 8322, no. Extreme Ultraviolet (EUV) Lithography III, pp. 1–12, Mar. 2012.

[58] R. D. Allen, W. Conley, P. P. Naulleau, C. J. Progler, C. J. Raymond, M. L. Rieger, M. H. Somervell, W. M. Tong, B. Lin, C. A. Mack, and C. G. Willson, *Technical Abstract Summaries : 7636 Extreme Ultraviolet (EUV) 7637 Alternative Lithographic 7639 Advances in Resist Materials and Processing Technology XXVII 102 – 134 7641 Design for Manufacturability through*, no. February. 2010, pp. 21–25.

[59] M. D. Stewart, D. J. Becker, T. B. Stachowiak, G. M. Schmid, T. B. Michaelson, H. V. Tran, and C. G. Willson, "Acid Mobility in Chemically Amplified Photoresists," *Proc. SPIE*, vol. 4690, no. Advances in Resist Technology and Processing XIX, pp. 943–951, 2002.

[60] P. L. Zhang, A. R. Eckert, C. G. Willson, S. E. Webber, and J. Byers, "Acid Diffusion through Polymer Films," *Proc. SPIE*, vol. 3049, no. Advances in Resist Technology and Processing XIV, pp. 898–909, 1997.

[61] H. Ito and C. G. Willson, "Chemical Amplification in the Design of Dry Developing Resist Materials," *Polym. Eng. Sci.*, vol. 23, no. 18, pp. 1012–1018, 1983.

[62] S. A. Macdonald, H. Ito, C. G. Willson, and S. Jose, "Advances in the design of organic resist materials," *Microelectron. Eng.*, vol. 1, no. 4, pp. 269–293, 1985.

[63] G. M. Waliraff, W. D. Hinsberg, F. Houle, J. Opitz, D. Hopper, and J. M. Hutchinson, "Kinetics of Chemically Amplified Resists," *Proc. SPIE*, vol. 2438, no. Advances in Resist Technology and Processing XII, pp. 182–190, 1995.

[64] R. D. Allen, R. Sooriyakumaran, J. Opitz, G. M. Wallraff, R. A. Dipietro, G. Breyta, D. C. Hofer, R. R. Kunz, S. Jayaraman, R. Shick, B. Goodall, U. Okoroanyanwu, and C. G. Willson, "Protecting Groups for 193-nm Photoresists," *Proc. SPIE*, vol. 2724, no. Advances in Resist Technology and Processing XIII, pp. 334–343, 1996.

[65] H. Ito, R. D. Allen, J. Opitz, T. I. Wallow, H. D. Truong, D. C. Hofer, P. R. Varanasi, G. M. Jordhamo, S. Jayaraman, R. Vicari, and R. Vicaric, "Dissolution/swelling behavior of cycloolefin polymers in aqueous base," *Proc. SPIE*, vol. 3999, no. Advances in Resist Technology and Processing XVII, pp. 2–12, 2000.

[66] W. Li, R. Varanasi, M. C. Lawson, R. W. Kwong, K. Chen, H. Ito, H. Truong, R. D. Allen, M. Yamamotoc, E. Kobayashi, and M. Slezak, "Rational Design in Cyclic Olefin Resists for Sub-lOOnm Lithography," *Proc. SPIE*, vol. 5039, no. Advances in Resist Technology and Processing XX, pp. 61–69, 2003.

[67] S. Yamada, J. Owens, T. Rager, M. Nielsen, J. D. Byers, and C. G. Wilison, "The design and study of aqueous-processable positive tone photoresists," *Proc. SPIE*,

vol. 3999, no. Advances in Resist Technology and Processing XVII, pp. 569–578, 2000.

[68] H. Ito, G. Breyta, D. Hofer, T. Fischer, and B. Prime, “Influence of acid generator structure on T-top formation in high temperature bake processes for environmental stabilization,” *Proc. SPIE*, vol. 2438, no. Advances in Resist Technology and Processing XII, pp. 53–60, 1995.

[69] C. A. Mack, “Resolution enhancement technologies,” *Microlithogr. World*, vol. 12, no. 2, pp. 14–20, 2003.

[70] N. Jakatdar, J. Bao, C. J. Spanos, R. Subramanian, B. Rangarajan, and A. Romano, “A Physically Based Model for Predicting Volume Shrinkage in Chemically Amplified Resists,” *Proc. SPIE*, vol. 3743, pp. 16–24, 1999.

[71] G. M. Schmid, S. D. Burns, M. D. Stewart, and C. G. Willson, “Mesoscale simulation of positive tone chemically amplified photoresists,” *Proc. SPIE*, vol. 4690, no. Advances in REsist Technology and Processing XIX, pp. 381–390, Jul. 2002.

[72] G. Maier, “Low dielectric constant polymers for microelectronics,” *Prog. Polym. Sci.*, vol. 26, pp. 3–65, 2001.

[73] K. A. Mauritz, “Dielectric responses,” *Permittivity*. [Online]. Available: http://en.wikipedia.org/wiki/Permittivity. [Accessed: 05-Nov-2014].

[74] X. J. Fan and E. Suhir, Eds., *Moisture Sensitivity of Plastic Packages and IC Devices*. New York: Springer, 2010.

[75] D. L. Dunson, “Synthesis and Characterization of Thermosetting Polyimide Oligomers for Microelectronics Packaging,” Virginia Polytechnic Institute, 2000.

[76] K. Feng, M. Tsushima, T. Matsumoto, and T. Kurosaki, “Synthesis and Properties of Novel Photosensitive Polyimides Containing Chalcone Moiety in the Main Chain,” *J. Polym. Sci. Part A Polym. Chem.*, vol. 36, pp. 685–693, 1998.

[77] T. Omote, “Photosensitive Polyimides: Molecular Design and Synthesis,” in *Polyimides Fundamentals and Applications*, M. K. Ghosh and K. L. Mittal, Eds. New York: Marcel Dekker, 1996, pp. 121–150.

[78] DuPont, “Kapton summary of properties,” *2009 International Conference on Information and Automation*. Ieee.

[79] J. O. Simpson and A. K. St. Clair, “Fundamental insight on developing low dielectric constant polyimides,” *Thin Solid Films*, vol. 308–309, pp. 480–485, Oct. 1997.

[80] R. Rubner, H. Ahne, E. Kuhn, and G. Kolodziej, “No Title,” *Photogr. Sci. Eng.*, vol. 23, no. 303, 1979.

[81] M. T. Pottiger, D. L. Goff, and W. J. Lautenberger, “Photodefinable polyimides. II. The characterization and processing of photosensitive polyimide systems,” *Electron. Components Conf.*, no. Proceedings of the 38th, pp. 315–321, 1988.

[82] L. Minnema and J. M. van der Zande, “Pattern Generation in Polyimide Coatings and Its Application in an Electrophoretic Image Display,” *Polym. Eng. Sci.*, vol. 28, no. 12, pp. 815–822, Jun. 1988.

[83] HD MicroSystems, “HD-8820 Process Guide,” no. September. 2009.

[84] DuPont, “Aqueous Developer Systems - Positive.” [Online]. Available: http://www2.dupont.com/WLP/en_US/uses_apps/RDL/hd8800_hd8900.html. [Accessed: 10-Nov-2014].

[85] A. K. Schrock, “Addition polymerization, coatings, adhesives,” US4812588 A, 1989.

[86] Y. So, S. F. Hahn, Y. Li, and M. T. Reinhard, “Styrene 4-Vinylbenzocyclobutene Copolymer for Microelectronic Applications,” *J. Polym. Sci. Part A Polym. Chem.*, vol. 46, pp. 2799–2806, 2008.

[87] Y. So, E. J. Stark, Y. Li, S. Kisting, A. Achen, K. Baranek, D. Scheck, J. Hetzner, J. J. Folkenroth, M. Töpper, and T. Baumgartner, “Aqueous-Base-Developable Benzocyclobutene (BCB)-Based Material Curable in Air,” *IEEE Trans. Adv. Packag.*, vol. 29, no. 4, pp. 741–750, 2006.

[88] N. R. Grove, P. A. Kohl, S. A. Bidstrup Allen, S. Jayaraman, and R. Shick, “Functionalized Polynorbornene Dielectric Polymers: Adhesion and Mechanical Properties,” *J. Polym. Sci. Part B Polym. Phys.*, vol. 37, pp. 3003–3010, 1999.

[89] R. J. Hung, H. V. Tran, B. C. Trinque, T. Chiba, S. Yamada, D. Sanders, E. F. Connor, R. H. Grubbs, J. M. Klopp, J. M. J. Frechet, B. H. Thomas, G. J. Shafer, D. D. DesMarteau, W. Conley, and C. G. Willson, “Resist Materials for 157 nm Microlithography: An Update,” *Proc. SPIE*, vol. 4345, no. Advances in Resist Technology and Processing XVIII, pp. 385–395, Aug. 2001.

[90] S. Ahmed, S. A. Bidstrup, P. A. Kohl, and P. J. Ludovice, “Development of a New Force Field for Polynorbornene,” *J. Phys. Chem. B*, vol. 102, no. 49, pp. 9783–9790, Dec. 1998.

[91] S. Ahmed, P. J. Ludovice, and P. Kohl, “Microstructure of 2,3 erythro di-isotactic polynorbornene from atomic simulation,” *Comput. Theor. Polym. Sci.*, vol. 10, pp. 221–233, 2000.

[92] W. J. Chung, C. L. Henderson, and P. J. Ludovice, “RIS Model of the Helix-Kink Conformation of Erythro Diisotactic Polynobornene,” *Macromol. Theory Simulations*, vol. 19, no. 7, pp. 421–431, Aug. 2010.

[93] T. Hoskins, W. J. Chung, A. Agrawal, P. J. Ludovice, C. L. Henderson, L. D. Seger, L. F. Rhodes, and R. A. Shick, “Bis(trifluoromethyl)carbinol-Substituted Polynorbornenes: Dissolution Behavior,” *Macromolecules*, vol. 37, no. 12, pp. 4512–4518, Jun. 2004.

[94] U. Okoroanyanwu, T. Shimokawa, J. Byers, and C. G. Willson, “Alicyclic Polymers for 193 nm Resist Applications: Synthesis and Characterization,” *Chem. Mater.*, vol. 10, no. 11, pp. 3319–3327, Nov. 1998.

[95] Y. Bai, P. Chiniwalla, E. Elce, R. A. Shick, J. Sperk, S. Ann, B. Allen, and P. A. Kohl, “Photosensitive Polynorbornene Based Dielectric. I. Structure – Property Relationships,” *J. Appl. Polym. Sci.*, vol. 91, pp. 3023–3030, 2004.

[96] Y. Bai, P. Chiniwalla, E. Elce, S. Ann, B. Allen, and P. A. Kohl, “Photosensitive Polynorbornene Based Dielectric. II. Sensitivity and Spatial Resolution,” *J. Appl. Polym. Sci.*, vol. 91, pp. 3031–3039, 2004.

[97] B. J. Briscoe, L. Fiori, and E. Pelillo, “Nano-indentation of polymeric surfaces,” *J. Phys. D Appl. Phys*, vol. 31, pp. 2395–2405, 1998.

[98] W. C. Oliver and G. M. Pharr, “An improved technique for determining hardness and elastic modulus using load and displacement sensing indentation experiments,” *J. Mater. Res.*, vol. 7, no. 6, pp. 1564–1583, 1992.

[99] American Society for Testing and Materials, “D150-11 Standard Test Methods for AC Loss Characteristics and Permittivity (Dielectric Constant) of Solid Electrical Insulation.”

[100] M. Toriumi, T. Itam, J. Yamashita, T. Sekine, and K. Nakatani, “Dissolution characteristics of resist polymers studied by Quartz Crystal Microbalance transmission-line analysis and PKa acidity analysis,” *Proc. SPIE*, vol. 4690, no. Advances in Resist Technology and Processing XIX, pp. 904–911, 2002.

[101] J. Dicarlo, O. B. Evans, J. Fedyk, S. Ficner, M. Khadim, and R. R. Dammel, “Identification of Diazonaphthoquinone Esters of Polyhydroxybenzophenone Compounds,” *Proc. SPIE*, vol. 2195, no. Advances in Resist Technology and Processing XI, pp. 696–706, 1994.

[102] J. J. M. Vleggaar, A. H. Huizer, C. A. G. O. Varma, P. A. Kraakman, W. P. M. Nijssen, and R. J. Visser, “Vleggaar - Fluorescence behavior of diazonaphthoquinone-type photoresist materials.pdf,” *J. Vac. Sci. Technol. B Microelectron. Nanom. Struct.*, vol. 11, no. 3, pp. 688–698, 1993.

[103] K. Tanigaki, T. Honda, and T. W. Ebbesen, “Photochemical Reactions of 1-oxo-2-diazo-1,2-dihydronaphthalenes and Reactivity of their Products,” *Polym. Mater. Sci. Eng.*, vol. 61, pp. 291–295, 1989.

[104] M. Koshiba, M. Murata, M. Matsui, and Y. Harita, “Thermally induced and base catalyzed reactions of naphthoquinone diazides,” *Proc. SPIE*, vol. 920, no. Advances in Resist Technology and Processing V, pp. 364–371, 1988.

[105] W. Hinsberg, S.-W. Lee, H. Ito, D. Hornea, and K. Kanazawa, “Experimental approaches for assessing interfacial behavior of polymer films during dissolution in aqueous base,” *Proc. SPIE*, vol. 4345, no. Advances in Resist Technology and Processing XVIII, pp. 1–9, 2001.

[106] W. Hinsberg, F. A. Houle, S.-W. Lee, H. Ito, and K. Kanazawa, “Characterization of Reactive Dissolution and Swelling of Polymer Films Using a Quartz Crystal Microbalance and Visible and Infrared Reflectance Spectroscopy,” *Macromolecules*, vol. 38, no. 5, pp. 1882–1898, Mar. 2005.

[107] H. Ito, W. D. Hinsberg, L. F. Rhodes, and C. Chang, “Hydrogen bonding and aqueous base dissolution behavior of hexafluoroisopropanol-bearing polymers,” *Proc. SPIE*, vol. 5039, no. Advances in Resist Technology and Processing XX, pp. 70–79, 2003.

[108] R. C. Daly, T. DoMinh, R. A. Arcus, and M. J. Hanrahan, “Effect of Additives on Positive Photoresist Development,” in *ACS Symposium Series*, 1987.

[109] L. Shechter and J. Wynstra, “Glycidyl Ether Reactions with Alcohols, Phenols, Carboxylic Acids, and Acid Anhydrides,” *Ind. Eng. Chem.*, vol. 48, no. 1, pp. 86–93, 1956.

[110] G. C. Stevens, “Cure Kinetics of a Low Epoxide/Hydroxyl Group-Ratio Bisphenol A Epoxy Resin-Anhydride System by Infrared Absorption Spectroscopy,” *J. Appl. Polym. Sci.*, vol. 26, no. 12, pp. 4259–4278, 1981.

[111] C. A. Mack, “Absorption and exposure in positive photoresist,” *Appl. Opt.*, vol. 27, no. 23, pp. 4913–9, Dec. 1988.

[112] M. Raeis-Zadeh, N. D. Melendez, Y. Chen, and P. A. Kohl, “Aqueous-Develop, Photosensitive Polynorbornene Dielectric: Optimization of Mechanical and Electrical Properties,” *J. Electron. Mater.*, vol. 40, no. 10, pp. 2126–2138, Jul. 2011.

[113] W. D. Hinsberg, C. G. Willson, and K. K. Kanazawa, “Use of a QCM rate monitor to examine photoproduct effects on resist dissolution,” *Proc. SPIE*, vol. 539, no. Advances in Resist Technology and Processing II, pp. 6–13, 1985.

[114] F. Rice, J. Greenberg, C. E. Waters, and R. E. Vollrath, “Ketene. I. Preparation and Reactions,” *J. Am. Chem. Soc.*, vol. 56, pp. 1760–1765, 1934.

[115] B. T. J. Beauchemin and P. R. Brown, “Quantitative Analysis of Diazonaphthoquinones by Thin-Layer Chromatographic/Diffuse Reflectance Infrared Fourier Transform Spectrometry,” *Anal. Chem.*, vol. 61, pp. 615–618, 1989.

[116] B. K. Mueller, E. Elce, A. M. Grillo, and P. A. Kohl, “Positive-tone, aqueous-developable, polynorbornene dielectric: Lithographic, and dissolution properties,” *J. Appl. Polym. Sci.*, vol. 127, no. 6, pp. 4653–4661, Jun. 2012.

[117] J. M. Schwartz, B. K. Mueller, E. Elce, Z. D. Pritchard, H. W. Li, A. M. Grillo, S. Y. Lee, and P. A. Kohl, “Positive Tone, Polynorbornene Dielectric Crosslinking,” *ECS J. Solid State Sci. Technol.*, vol. 4, no. 1, pp. N3008–N3014, Aug. 2014.

[118] G. A. Olah, N. J. Head, G. Rasul, and G. K. S. Prakash, “Protonation of Benzocyclobutene with Superacid: Cram’s Phenonium Ion (Spiro[5.2]octa-5,7-diene-4-yl Cation) Revisited,” *J. Am. Chem. Soc.*, vol. 117, no. 3, pp. 875–882, 1995.

[119] G. Odian, *Principles of Polymerization*, 4th ed. Hoboken, NJ: John Wiley & Sons, 2004.

[120] S. A. MacDonald, N. J. Clecak, H. R. Wendt, C. G. Willson, C. D. Snyder, C. J. Knors, N. B. Deyoe, J. G. Maltabes, J. R. Morrow, A. E. McGuire, and S. J. Holmes, “Airborne Chemical Contamination of a Chemically Amplified Resist,” *Proc. SPIE*, vol. 1466, no. Advances in Resist Technology and Processing VIII, pp. 2–12, 1991.

[121] R. R. Kunz, R. D. Allen, W. D. Hinsberg, and G. M. Waliraff, “Acid-catalyzed single-layer resists for ArF lithography,” *Proc. SPIE*, vol. 1925, no. Advances in Resist Technology and Processing X, pp. 167–175, 1993.

[122] X. Z. Jin and H. Ishii, “Novel positive-type photosensitive polyimide with low dielectric constant,” *J. Appl. Polym. Sci.*, vol. 98, pp. 15–21, Oct. 2005.

[123] B. K. Mueller and P. A. Kohl, “Chemically amplified, positive tone, cross-linkable thick-film polymer,” *J. Appl. Polym. Sci.*, vol. 130, no. 2, pp. 759–765, Oct. 2013.

[124] B. K. Mueller, J. M. Schwartz, A. E. Sutlief, W. K. Bell, C. O. Hayes, E. Elce, C. G. Willson, and P. A. Kohl, “Chemically Amplified, Positive Tone, Polynorbornene Dielectric for Microelectronics Packaging,” *ECS J. Solid State Sci. Technol.*, vol. 4, no. 1, pp. N3001–N3007, 2015.

[125] K. Meier and H. Zweifel, “Thioxanthone ester derivatives: efficient triplet sensitizers for photopolymer applications,” *J. Photochem.*, vol. 35, no. 3, pp. 353–366, Dec. 1986.

[126] V. Crivello and W. Lam, “Redox Cationic Polymerization: The Diaryliodonium Salt/Ascorbate Redox Couple,” *J. Polym. Sci. Part Polym. Chem. Ed.*, vol. 19, pp. 539–548, 1981.

[127] J. V. Crivello, T. P. Lockhart, and J. L. Lee, “Diaryliodonium Salts as Thermal Initiators of Cationic Polymerization,” *J. Polym. Sci. Polym. Chem. Ed.*, vol. 21, pp. 97–109, 1983.